Evaluation of Seismic Assessment Procedures for Existing Reinforced Concrete Structures Damaged in the 2016 Meinong Earthquake

Jakob Sumearll

A thesis
submitted in partial fulfillment of the
requirements for the degree of

Master of Science in Civil Engineering

University of Washington

2019

Committee:

Dawn E. Lehman, Chair

Laura N. Lowes, Chair

Paolo M. Calvi

Program Authorized to Offer Degree:
Civil and Environmental Engineering

University of Washington

Abstract

Evaluation of Seismic Assessment Procedures for Existing Reinforced Concrete Structures Damaged in the 2016 Meinong Earthquake

Jakob Sumearll

Co-Chairs of the Supervisory Committee:

Professor Dawn E. Lehman
Civil and Environmental Engineering

Professor Laura N. Lowes
Civil and Environmental Engineering

The magnitude 6.4 Meinong Earthquake struck the Southern region of Taiwan in February 2016. This event resulted in unexpected damage relative to the magnitude. A study was undertaken to investigate the response of the buildings using advanced analysis tools and standards of practice. Most structures had non-ductile moment framing as the primary lateral-force resisting system. The most commonly observed response mechanism was soft-story resulting from apparent shear and/or flexure-shear damage to the first story. The initial phase of the study employed triage-type procedures, including the well-established ASCE 41 Tier 1 (preliminary screening) and a new process funded by FEMA and developed by ATC for the city of Los Angeles: ATC 78-7. The second phase of the study investigated the ASCE 41 Tier 3 procedure to determine seismic vulnerability through use of linear and nonlinear dynamic analysis. Information sourced from structural drawings (with material properties) and ground-motion recording stations provided a basis to simulate the seismic response. The results were compared with the observed damage pattern to evaluate the effectiveness of different modeling approaches in order to provide recommendations for improvements for ASCE 41.

TABLE OF CONTENTS

Page

LIST OF FIGURES

LIST OF TABLES

LIST OF SYMBOLS

ABBREVIATIONS

ACI = American Concrete Institute
$ASCE$ = American Society of Civil Engineers
ATC = Applied Technology Council
BF = Bare-Frame model variation
BSE = Basic Safety Earthquake, [ASCE-41, 2017]
C = Compliant checkmark in Tier 1 screening, [ASCE-41, 2014]
$CBMR$ = Column-to-beam moment ratio
CM = Model variation with masonry infill modeled with rigid offset from joints
CP = Collapse Prevention performance state, [ASCE-41, 2017]
CSI = Computer and Structures, Inc.
CWB = Central Weather Bureau, Taiwan
DCR = Demand-to-capacity ratio
DL = Dead load
DS = Model variation with masonry infill modeled with diagonal struts
EW = East-west
$FEMA$ = Federal Emergency Management Agency
FC = Flexure-Controlled beam-column response mode
FS = Flexure-Shear beam-column response mode
HCT = Hollow clay tile, suspected infill masonry material composition
IO = Immediate Occupancy performance state, [ASCE-41, 2017]
LDP = Linear dynamic procedure, [ASCE-41, 2017]
LL = Live load
LS = Life Safety performance state, [ASCE-41, 2017]
MF = Moment framing, beam-column connection that can resist translation and rotation
NA = Not-Applicable checkmark in Tier 1 screening, [ASCE-41, 2014]
NC = Noncompliant checkmark in Tier 1 screening, [ASCE-41, 2014]
NDP = Nonlinear dynamic procedure, [ASCE-41, 2017]
$NIST$ = National Institute of Standards and Technology
NS = North-south
NSF = National Science Foundation
$OpenSees$ = Open System for Earthquake Engineering Simulation
PM = Interaction of axial force and moment in component cross-section
= Plastic mechanism defining potential collapse mode, [ATC-78, 2018]
$RAPID$ = Rapid Response Research, NSF program
RC = Reinforced concrete
RZ = Z rotational mass participation factor from SAP eigenvalue analysis
SC = Shear-Critical beam-column response mode
$SCWB$ = Strong-Column-Weak-Beam, based on ratio of column to beam moments over beam-column joint
SH = Model variation with masonry infill modeled with shell elements
TMS = The Masonry Society
T_1 = First mode natural period from eigenvalue analysis
U = Unknown checkmark in Tier 1 screening, [ASCE-41, 2014]
$USGS$ = United States Geological Survey
UX = X-direction translational mass participation factor from SAP eigenvalue analysis
UY = Y-direction translational mass participation factor from SAP eigenvalue

analysis

UW = University of Washington

LOWERCASE SYMBOL NOTATION

a = Site class factor equal to: 130 for Site Class A or B; 90 for Site Class C; 60 for Site Class D, E, or F, Equation 5.11

= Thickness of equivalent diagonal strut, Equation 6.2

= Refer to θ_a, Equation 7.1

b = Width dimension of beam-column element; for concrete columns, oriented in plan EW direction

= Strain-hardening ratio of OpenSees *Steel02*, Figure 7.6

= Refer to θ_b, Equation 7.2

b_w = Width dimension of beam-column element

= Width of 'T'-beam web

b_{eff} = Effective width of 'T'-beam flange

c = Residual moment capacity in generalized moment-rotation backbone, Equation 7.3

$cR1$ = Parameter to control the transition from elastic to plastic branches of OpenSees *Steel02*, Figure 7.6

$cR2$ = Parameter to control the transition from elastic to plastic branches of OpenSees *Steel02*, Figure 7.6

d = Effective depth to longitudinal reinforcement

d_b = Rebar diameter

$epsc0$ = Maximum compressive strain of OpenSees *Concrete01*, Figures 7.4, 7.5, and 7.8

$epsU$ = Residual crushing strain of OpenSees *Concrete01*, Figures **??**, Tables 7.4, 7.5, and 7.8

f'_c = Specified compressive strength of concrete material

$f'_{ce,E}$ = Expected concrete compressive strength

$f'_{cl,L}$ = Lower-bound, specified concrete compressive strength

$f_{col,i}$ = Fraction of gravity loads supported by column i with total sum value of 1.0, Equation 5.19

$f_{wall,i}$ = Fraction of gravity loads supported by wall i with total sum value of 1.0, [ATC-78, 2018]

f'_m = Compressive strength of masonry infill material

$f'_{me,E}$ = Expected masonry infill compressive strength

f_{pc} = Maximum compressive strength of OpenSees *Concrete01*, Figures 7.4, 7.5, and 7.8

f_{pcu} = Residual crushing strength of OpenSees *Concrete01*, Figures 7.4, 7.5, and 7.8

ft = Specified tensile strength of OpenSees *Concrete02*, Figure 7.5

f_y = Specified yield strength of steel material

= yield strength of OpenSees *Steel02*, Figure 7.6

$f_{ye,E}$ = Expected steel yield strength

$f_{yl,L}$ = Lower-bound, specified steel yield strength

f_{yt} = Specified yield strength of transverse steel reinforcement

$f_{yte,E}$ = Expected yield strength of transverse steel reinforcement

$f_{ytl,L}$ = Lower-bound, specified yield strength of transverse steel reinforcement

g = Acceleration due to gravity

h = Height dimension of beam-column element; for concrete columns, oriented in plan NS direction

h_{col} = Column height between center lines of beams, Equation 6.2

h_{inf} = Height of infill panel, Equation 6.1

h_{eff} = Effective height of the lateral force-resisting system (assumed $0.7h_n$)

h_n = Total height of the lateral force-resisting system, [ATC-78, 2018]

h_x = Height of story x, [ATC-78, 2018]

h_{sx} = Height of story x, [ATC-78, 2018]

k = represent a shear strength degradation factor based on displacement ductility demand, Equation 4.3

k = represent a shear strength degradation

factor based on displacement ductility demand, Equation 4.4

l_{inf} = taken as half of the unbraced length, l_u, Equation 4.6

l_u = Unbraced, clear height of beam-column element between joints or regions of captivity

m = Capacity modification factor to account for allowable, expected deformation ductility, [ASCE-41, 2017]

n_c = Total number of columns, Equation 4.1

n_{col} = Total number of columns in a story, Equation 5.19

n_f = Total number of frames in the direction of loading, Equation 4.1

r_{inf} = Diagonal length of infill panel, Equation 6.2

s = Vertical spacing of shear reinforcement

t = Thickness of T-beam flange

t_{inf} = Thickness of infill panel and equivalent strut, Equation 6.1

v_j^{avg} = Column average shear stress, Equation **??**

UPPERCASE SYMBOL NOTATION

A_c = Total summation of all column cross-sections, Equation 4.1

A_g = Cross-sectional area of beam-column element

A_v = Cross-sectional area of shear reinforcement

A_T = Torsional amplification factor, Equation 5.14

BR = Building Rating, [ATC-78, 2018]

C_m = Effective mass factor, Equation 5.8

COV = Standard deviation of all the column ratings at a story divided by R_{avg}, Equation 5.18

C_1 = Modification factor to relate expected maximum inelastic displacement to displacement calculated for linear elastic response, Equation 5.11

C_2 = Modification factor to represent the effect of pinched hysteresis shape, cyclic stiffness degradation, and strength deterioration on maximum displacement response, Equation 5.12

CR = Column Rating, Table 5.2

EA_{gross} = Component section axial stiffness using gross section properties

E_c = Elastic (Young's) modulus for concrete material

EI_{gross} = Component section flexural stiffness using gross section properties

E_m = Elastic (Young's) modulus for masonry infill material

E_{me} = Expected modulus of elasticity of infill material, Equation 6.1

E_{fe} = Expected modulus of elasticity of frame material, Equation 6.1

E_s = Elastic (Young's) modulus for steel material

Ets = Tensile softening stiffness of OpenSees *Concrete02*, Figure 7.5

$E0$ = Initial elastic tangent of OpenSees *Steel02*, Figure 7.6

GA_{gross} = Component section shear stiffness using gross section properties

I_{col} = Moment of inertia of adjacent columns, Equation 6.1

J = Force-delivery reduction factor calculated from the moment DCR $M_{UD}/M_{CE} \leq 1.0$, Equation 6.6

K = Knowledge factor, [ASCE-41, 2017]

M_n = Nominal moment strength of beam-column element

M_{nc} = Column moment capacity for SCWB ratio

M_{nb} = Beam moment capacity for SCWB ratio

M_{njx} = Smallest moment that can be developed at the joint, Equation 5.5

M_s = System modification factor, Equation 4.1

M_{UD} = Deformation-controlled moment demand from LDP, Equation 6.9

$M/V*d$ = Represent the largest ratio of moment to shear under design loading conditions (also $M_{UD}/V_{UD}*d$), Equations 4.3 and 4.4

N_u = Axial compressive force due to gravity,

Equations 4.2 and 4.3

N_{UG} = Axial compressive force due to gravity, Equations 4.4

P = Component axial load considering both gravity and overturning forces, Table 5.1

P_g = Axial compressive force due to gravity

P_n = Column nominal axial capacity, calculated using gross-section properties

Q_{CE} = Expected strength of deformation-controlled action, Equation 6.7

Q_{CL} = Lower-bound, specified strength of force-controlled action, Equation 6.8

Q_E = Demands resulting from time-history lateral forcing, Equations 6.5 and 6.6

Q_G = Demands caused by gravity loads (either Q_1 or Q_2) that maximizes the combination with Q_E, Equations 6.5 and 6.6

Q_{UD} = Deformation-controlled demands caused by gravity loads and earthquake forces, Equation 6.5

Q_{UF} = Force-controlled demands caused by gravity loads and earthquake, Equation 6.6

Q_1 = Load combination where the combination of gravity and lateral loading on a component yields net addition of forcing, Equation 6.3

Q_2 = Load combination where gravity loading impedes overturning forces and would otherwise act as subtractive to the net forcing demand, Equation 6.4

R_{adj} = Adjusted average column rating in the story, Equation 5.18

R_{avg} = weighted average column rating for all columns in the story, Equation 5.19

$R0$ = Parameter to control the transition from elastic to plastic branches of OpenSees *Steel02*, Figure 7.6

S_a = Magnitude of spectral acceleration sourced from response spectrum

SR = Story Rating, Equation 5.18

T_e = Building effective fundamental period, Equation 5.6

V = Recorded column internal shear force from NDP, Equation 7.6

V_j = Story shear based on a pseudo-static analysis, Equation 4.1

V_n = Nominal shear capacity of beam-column element

V_{nc1} = Lateral strength of a column in story 1, Equation 5.2

V_{nw1} = Shear strength of walls in story 1, Equation 5.3

V_p = Plastic shear demand resulting from plastic hinging of column top and bottom, Equation 4.6

V_{px} = Plastic mechanism shear strength at story x, Equation 5.13

V_{p1} = Plastic mechanism base shear strength in story 1, Equations 5.1 and 5.4

V_{Col0E} = Expected shear capacity, V_n, without modification by k_{nl}, Equation 7.1

V_{UF} = Force-controlled shear demand from LDP, Equation 6.10

V_y = Effective building yield strength, [ATC-78, 2018]

V_{yE} = Plastic shear demand, V_p, calculated using expected material strength, Equation 7.1

W = Building seismic weight

W_x = Seismic weight above story x, Equation 5.13

WR = Wall Rating, [ATC-78, 2018]

GREEK SYMBOL NOTATION

α_{Col} = reduction factor attributed to the steel contribution that depends on s/d, Equation 4.4

α_x = Coefficient to modify story drifts considering number of stories in a building, the yield mechanism, and whether story x is a critical story, Equation 5.13

γ = Drift factor representing fraction of story drift affecting the component, Equation 5.14

δ = Cumulative column and shear spring displacement from NDP, Equation 7.4

δ_{eff} = Global seismic drift demand for a single-degree-of-freedom system, Equation 5.9

δ_x = Projected story drift demand, Equation 5.10

δ_{x1} = Amplified story drift demand to account for P-Delta effects, Equation 5.13

θ = Angle with tangent equal to the infill height-to-length aspect ratio, Equation 6.1

= Recorded column end rotation from NDP, Equation 7.5

θ_a = Plastic rotation parameter in generalized moment-rotation backbone, Equation 7.1

θ_b = Plastic rotation parameter in generalized moment-rotation backbone, Equation 7.2

θ_c = Allowable plastic rotation, Table 5.1

$\theta_{c,min}$ = Minimum allowable plastic rotation, Equation 5.15

λ = Light-weight concrete adjustment factor

= Ratio between unloading slope and the initial slope of OpenSees *Concrete02*, Figure 7.5

λ_1 = Coefficient used to determine equivalent width of infill strut, Equation 6.1

$\mu_{strength}$ = Global demand-to-capacity ratio, Equation 5.8

ρ = Longitudinal, tensile steel reinforcement ratio

ρ' = Longitudinal, compression steel reinforcement ratio

ρ_t = Transverse steel reinforcement ratio

χ = Factor for adjusting per performance level, Equation 6.6

Δ_C = Component drift (displacement) capacity, Equation 5.16

Δ_D = Component adjusted drift (displacement) demand, Equation 5.14

ACKNOWLEDGMENTS

I write these acknowledgements from my desk at Chalmers, reflecting on the journey that was this Master's Degree. In particular, the following individuals hold a special place in my heart for their various roles in my life during the past three years. Ryan Kobbe has been a professor, adviser, and friend since my first year at UW (Wyoming). In many ways, he is the best role model I could have lucked into finding. Sarah Wichman is a best friend and definitely the better grad student. Also, she is the nicest and most genuine person that I've ever met, period. My time at UW has been all the better knowing that I got to see her every day. Good luck in becoming the world's smartest stay-at-home mom! (and it's okay to say "No." every once and a while). Yasmine Farhat is a best friend and the best partner for Monday b*tch sessions over lunch. She always kept life in perspective and has the best gossip, even when we had to negotiate video dates between Sweden and Cambodia during our respective ex-pat adventures. Though I know far too much about her cat, we successfully skirted department ties with our inter-disciplinary affair. Bobby Baraldi and I met day one of graduate school on an easy run with the Husky Running Club. Me, out of shape, turned early from the seven loop. I cannot express the value of mutual bonding over venting about first-year grad school (and the damn rain). I consistently admire his dedication to and unparalleled success in academia and sport. Even with him flexing on me in every workout, I'm happy to play the flamboyant foil to his apathetic, hipster nature. Tyler van Iderstein, said in the nicest way, gave me a taste of what it would have been like to meet myself in undergrad: he was (and is) always right, hands-down. This was frustrating, but forcedly humbling, as a struggling first-year. It took us sharing an office for me to come to appreciate his notorious personality. That being said, he was instrumental in my

understanding of structural mechanics (read: passing of 501), learning to code *efficiently*, and in keeping me up-to-date with whatever is happening with SpaceX. Stephanie Yamamoto has been a lovely addition to my life, at perhaps the most untimely moment. She is a wonderful embodiment of strength and confidence framed by wild hair and contagious energy. She is a friend, partner, and close love. Her support throughout this thesis (and the following nine months abroad) has been wonderfully stabilizing and is largely the reason why I smile while I write. I would like to acknowledge my advisers, Dawn Lehman and Laura Lowes, for taking me along for this journey and encouraging me each step of the way. Shout out to Team 313b: Alec Yeutter, Anne Magnus, Gloria de Zamacona, and Sarah Bergquist for having to deal with, *and accept*, my variable work hours, irregular fashion, and playing of rock and metal out loud, as I pulled rank on the speakers. And finally, a big thank you to Karin Lundgren for accepting me into the Concrete Division at Chalmers and giving me to the opportunity to spend 2019 in Göteborg. Of so many great people within the department, I had the best of times with Samanta Robuschi and Yu Xiaotong, *the better Ph.D.* This Masters was one hell of an experience.

Chapter 1
INTRODUCTION

Older reinforced concrete (RC) structures, designed without ductile detailing, represent a large percentage of the building stock both in the United States and internationally. Because these buildings do not include ductile detailing required by current building codes, they are prone to non-ductile failure modes (e.g. shear failure prior to flexural yielding, splice failure, and non-ductile flexural response) that may result in full system collapse when subject to earthquake loading. This is of significant concern in areas with high seismicity with respect to the risk of building damage leading to loss of life and/or substantial financial loss. Financial loss can be characterized as both direct (e.g. repairs or reconstruction) or indirect (e.g. downtime and non-productivity). The cost of retrofitting existing buildings to improve earthquake performance is significant; however, this price is justified with the merit to reduce the health and financial risk posed by older concrete buildings in their current condition. Thus, engineers require tools for assessing the damage and collapse potential posed by existing, non-ductile RC so that owners may make informed decisions about the need to retrofit and the resulting benefits.

Chapter 2

LITERATURE REVIEW

Numerous studies have investigated means to assess seismic performance of older RC structures. These sources range from research reports characterizing performance of individual components to community standards for full-system assessment. In the US, the American Society of Civil Engineers (ASCE) 41-17 *Seismic Evaluation and Retrofit of Existing Building* [ASCE-41, 2017] is the most commonly used methodology for building performance assessment. This document exists as the combination of previous standards ASCE 31 *Seismic Evaluation of Existing Buildings* and ASCE 41 *Seismic Rehabilitation of Existing Buildings*. ASCE 'Standards' undergo peer and committee review prior to publication, and thus the ASCE 41-17 document (or previous 41-13 edition) is considered to represent the standard of practice and is adopted by most cities, counties, and states as the legally required assessment procedure.

Though, ASCE is not unique in this endeavor. Other organizations have developed and published alternative methods for assessment. The Applied Technology Council (ATC), for example, has developed an independent provision with funding provided by the Federal Emergency Management Agency (FEMA) titled ATC 78-7 *Seismic Evaluation of Older Concrete Buildings for Collapse Potential* [ATC-78, 2018]. It utilizes plastic analysis, probabilistic concepts, and structural reliability theory to identify collapse indicators as markers of potential collapse vulnerability. The work provides a variant to the ASCE 41 Tier 1 preliminary screening processes (which makes use of checklists to provide a quick, but very crude, assessment) and to the ASCE 41 Tier 3 systematic evaluation which requires full building models and a significant investment of time and money. Outside of engineering organizations, academic research projects (commonly distributed in journal publications,

peer-reviewed or otherwise) offer a more focused and in-depth exploration into a particular structural component, structural system, and/or a particular step in the assessment process. Whereas the scope of such reports may be too limited for a complete building assessment, they offer supplemental techniques that may be substituted into more established methodologies. In performing this study on current evaluation methods, ASCE 41, ATC 78-7, and complimentary journal articles were considered and used.

2.1 ASCE 41

ASCE 41 exists to provide an approved methodology by which the practicing engineering can undertake seismic evaluation and possible retrofit measures for existing structures. ASCE 41 is separate and distinct from provisions specifying the design of new structures in that it focuses instead on the characterization of strength and deformability of components in existing structures. The assessment process first initiates with the coupling of th seismic demand with a desired set of building performance objectives. Building performance is defined by the usability of a structure following a specific seismic event and is classified as *immediate occupancy* (IO), *life safety* (LS), or *collapse prevention* (CP). The decision of the desired performance state for a given level of earthquake hazard is often at the discretion of the owner or regulatory agent, while the earthquake hazard level itself is largely independent and pertains to the geographic location. Basic performance objectives (BSE-1E and BSE-2E) and are given in Table 2.1. BSE-1E is based on a seismic hazard with 20% probability of exceedance in 50 years, and BSE-2E is 5% probability of exceedance in 50 years. Neither objective makes a statement towards the magnitude of the seismic event, but rather are two categories of likelihood that an event of such scale will not occur within the 50-year time period.

With the seismic hazard for a building defined, the bulk of ASCE 41 focuses on the determination of structural performance; this is particularly linked to methods for developing a model of the building. Analysis provisions are divided into distinct tiers for which the scope of work and analytical rigor increase with subsequent tiers. Tier 1 offers a means

Table 2.1: Standard Performance Objectives

Risk Category	BSE-1E	BSE-2E
1 and 2	Life Safety Structural Performance	Collapse Prevention Structural Performance
	Life Safety Nonstructural Performance (3-C)	Hazards Reduced Nonstructural Performance (5-D)
3	Damage Control Structural Performance	Limited safety Structural Performance
	Position Retention Nonstructural Performance (2-B)	Hazards Reduced Nonstructural Performance (5-D)
4	Immediate Occupancy Structural Performance	Life Safety Structural Performance
	Position Retention Nonstructural Performance (1-B)	Hazards Reduced Nonstructural Performance (3-D)

for a preliminary screening of main system components but does not require substantial calculations or modeling. Tiers 2 and 3 detail specific modeling practices as well as an outlined analysis scheme and result acceptance criteria. A discussion of each tier is provided in following subsections of this chapter. In all cases, ASCE 41 seeks to define the capacity and resilience of an existing building. The standard does not require the engineer to consider all of the tiers nor that they must be utilized in order. Though, a preliminary assessment using the Tier 1 screening is recommended. In the event that Tier 1 (or Tiers 2 or 3) indicate inadequate performance, the engineer may choose to 1) design a retrofit measure and iterate on the retrofit design until the building and component performance states are satisfactory, or 2) increase the sophistication of the evaluation by moving from a lower to a higher tier. Ultimately, the objective is to satisfy the acceptance criteria outlined by the chosen method. Once complete, the as-built or retrofit structure is acceptable per the ASCE 41 standard.

2.1.1 Tier 1 Screening

The ASCE 41 Tier 1 Screening provides an outline to perform a preliminary assessment to "screen out buildings that are reliably expected to comply with this standard or to quickly identify potential deficiencies" [ASCE-41, 2017] that may result in unacceptable damage and/or collapse at a certain hazard level. Chapter 4 of the standard contains the requirements for use of the Tier 1 procedure as well as designates the appropriate checklist based on building type (e.g. C1: Concrete Moment Frames) and level of seismicity (very low, low, moderate, or high). These checklists contain multiple quantities for which the evaluator determines the building features or structural components to be *compliant* (C), *noncompliant* (NC), *not-applicable* (NA), or *unknown* (U) based on information available. Separate checklist items are required at different levels of seismicity. Different checklists address structural and nonstructural categories. Chapter 4 also defines estimates of material strengths and includes equations and justification for all *Quick Check* calculations required in the evaluation. *Quick Check* are designed to give estimates of stiffness and strength of certain building components without significant time investment. In the case that the engineer has sufficient evidence that the building was designed and constructed (or retrofit) in compliance with benchmark provisions detailed in ASCE-41 [2017] *Table 3-3* (i.e. seismic evaluation considering a recent edition of ASCE 31 or 41), only the nonstructural checklist is required. Figure 2.1 provides a flowchart of the Tier 1 Screening procedure.

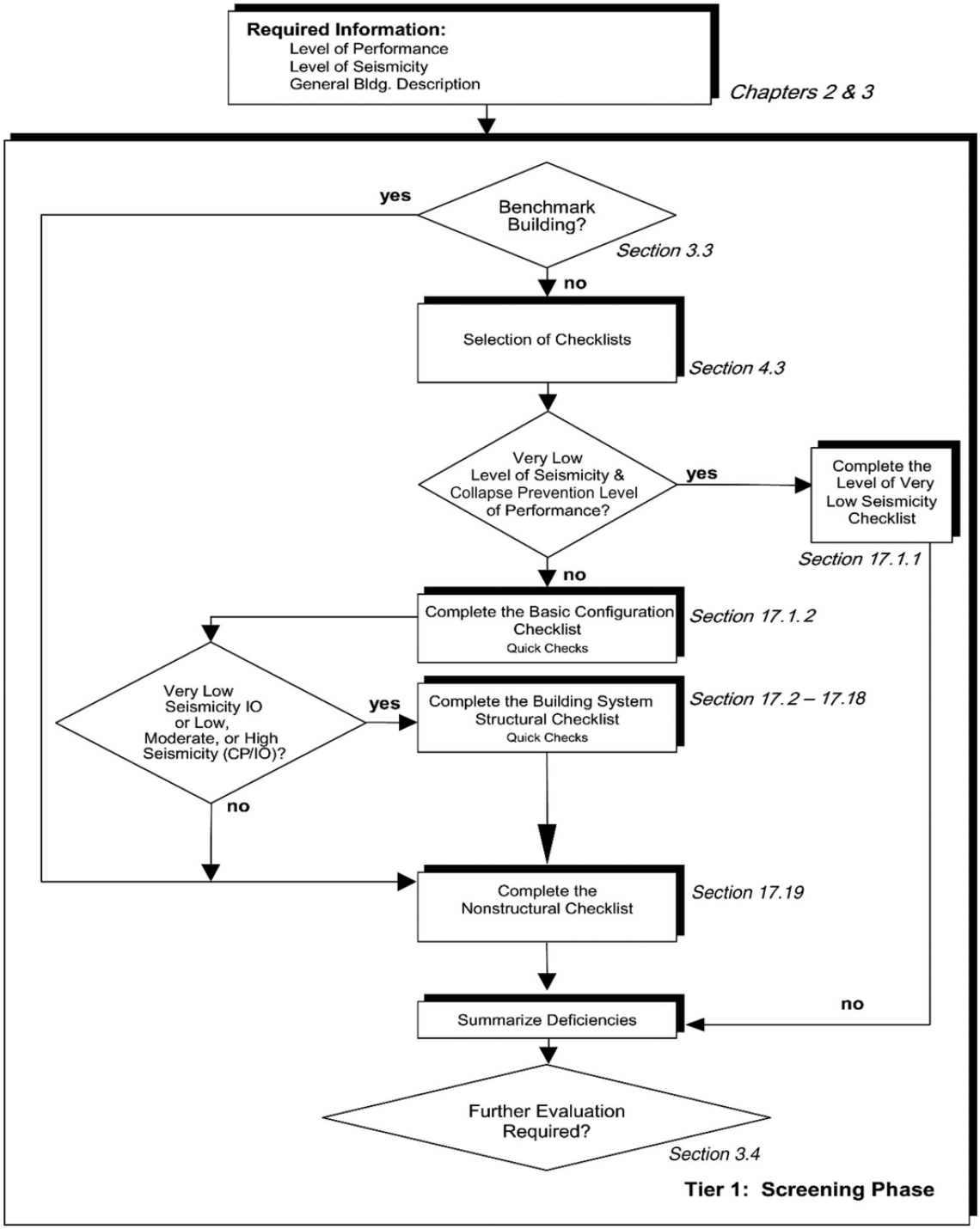

Figure 2.1: Flowchart of Tier 1 Screening Process [ASCE-41, 2017]

Outcomes of a Tier 1 Screening are the identification of "potential deficiencies in the building based on performance of similar buildings in past earthquakes" [ASCE-41, 2017]. The evaluation employs simple calculations and generalized assumptions that result in estimates of quantities that potentially determine performance. Items identified as *noncompliant* are flagged for further investigation with a more in-depth methodology. The ASCE 41 standard provides mechanisms for continuation from the Tier 1 assessment to both the Tier 2 and Tier 3 procedures depending on the type and extent of noncompliance and whether the building meetings the requirements for use of these procedures.

2.1.2 Tier 2 Deficiency-Based Evaluation and Retrofit

The Tier 2 assessment procedure represents a direct extension of the Tier 1 Screening. the purpose is to specifically address the "the potential deficiencies identified in the Tier 1 screening" through selection and iteration of a retrofit measure. This evaluation "need not expand beyond the evaluation of the potential deficiencies identified..." [ASCE-41, 2017] by the previous investigation. Chapter 5 of the standard describes the requirements for use of the Tier 2 evaluation; though, a Tier 2 evaluation was not conducted as part of this study.

2.1.3 Tier 3 Systematic Evaluation and Retrofit

The Tier 3 procedure "involves a systematic analysis of the entire building, either in its current configuration or with proposed retrofit measures...," [ASCE-41, 2017] where the end result is a full-scale performance-based analysis considering all acting components. Chapter 6 of the standard describes the requirements for use of the Tier 3 evaluation. Chapter 7 of the standard defines the approved analysis methods for linear and nonlinear analysis considering either static or dynamic loading. Linear analysis procedures, for both static and dynamic loading, are reserved for structures that are geometrically regular and have adequate strength and stiffness; nonlinear analysis procedures, for both static and dynamic loading, are applicable for all buildings. Chapters 8-11 of the standard each pertain to a single structural material (e.g. Chapter 10 for reinforced concrete) and provide reference

for material strengths, component modeling, capacity assessment, and acceptance criteria. Individual components of the lateral force-resisting system are categorized as *primary* or *secondary* based on their engagement with the structural system. Primary components are evaluated for earthquake-induced forces and deformations while secondary components only for earthquake-induced deformations. Component actions (forcing and deformation response) are additionally categorized as deformation-controlled or force-controlled. Capacity calculations and acceptance criteria measures differ based on the component-action classification. Figure 2.2 provides a flowchart of the entire ASCE 41 methodology. The Tier 3 procedure is shown on the right side of the flow chart.

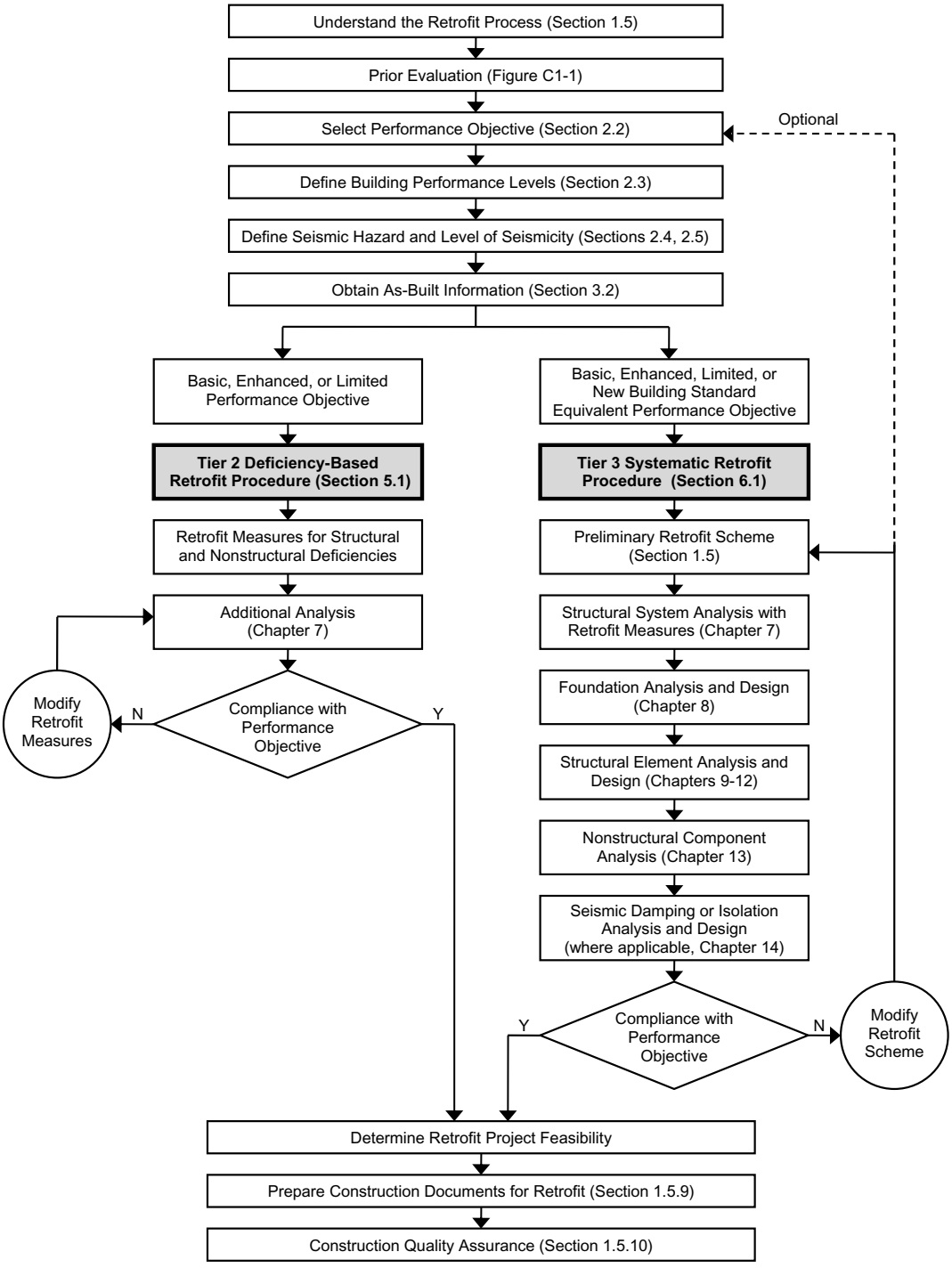

Figure 2.2: Flowchart of ASCE 41 Methodology, with Tier 3 Assessment on Right Side [ASCE-41, 2014]

Outcomes of a Tier 3 Systematic Evaluation are the component-level identification of the demand-to-capacity ratios (DCRs) relative to the desired performance level. Component actions that fail to meet the acceptance criteria are deemed unacceptable with respect to the desired performance state and necessitate the design of a retrofit measure and iterative analysis. Retrofit options may pertain to the increased strength of certain vulnerable components or an improvement to the deformation capacity of the primary lateral force-resisting system. In the case that the selected analysis method (e.g. linear static procedure) results in unacceptable building or component performance, the engineer may re-analyze the structure, without retrofit, using a dynamic time-history analysis or invest time into a non-linear model. Once the analysis results fall within acceptable limits, the as-built or retrofit structure is acceptable per the ASCE 41 standard.

2.2 ATC 78-7

The analysis methodology underpinning the *Seismic Evaluation of Older Concrete Buildings for Collapse Potential* [ATC-78, 2018] was developed specifically for the City of Los Angeles. The objective was aimed to "(1) identify the most seismically hazardous non-ductile concrete buildings; and (2) [be] easier and less expensive..." [ATC-78, 2018] than the existing procedures set in ASCE 41 (Tiers 2 and 3). This procedure seeks to characterize structural response through the use of more sophisticated estimates of component strength and deformation capacity. A building performance level of collapse prevention (CP) is assumed per the emphasis on collapse vulnerability, where 'collapse vulnerability' is defined as the loss of vertical load-carrying capacity. Building analysis is detailed in separate chapters of the report based on the lateral force-resisting system (*Frame*, *Frame-Wall*, *Bearing Wall*, *Infill Wall*). Global system response are calculated based on the formation of the most likely plastic mechanism. Local component response is defined by resulting deformation demands. The methodology makes use of component DCR values to output an estimate an approximation of the probability of collapse. This measure of risk, termed as the Building Rating (BR), is an "indication of the relative potential for collapse across an inventory of buildings" [ATC-78,

2018]. Similar to the ASCE 41 Tier 1 assessment, the intent of this methodology is provided a means for broad, but efficient, screening across a collection of buildings. Tabulations of BR with respect to a large number of buildings would permit the prioritization of more rigorous analysis and retrofit efforts.

2.3 Modeling Assumptions beyond ASCE 41 Guidelines

ASCE 41 provides guidelines for evaluation of existing structures. These guidelines address model development, analysis, and the processing of results, though it is important to acknowledge that the standard is meant for broad application and thus cannot be all-inclusive. Use of outside resource material thus permitted by the standard, so long as it does not contradict explicitly defined methods. For this study, several aspects of the nonlinear modeling fell outside the scope of ASCE 41-17. In these cases, the results of research conducted by others and published in peer-reviewed journal articles were used to support model development. All nonlinear modeling was conducted in the Open System for Earthquake Engineering Simulation (OpenSees), a finite-element analysis framework with specific application towards seismic analysis [McKenna et al., 2004]. All reference to materials and elements within this software framework was sourced from the OpenSees Wiki [Pacific Earthquake Engineering Research Center, 2012]. The following sections present modeling assumptions adopted for this study as well as provide a brief discussion of available research as sourced from the literature: Section 2.3.1 discusses a method for modeling masonry infill using dual, compression-only diagonal struts; Section 2.3.2 discusses the nonlinear element formulation selected for use for all column elements; and Section 2.3.3 discusses a means by which brittle shear failure was coupled with the flexural column elements.

2.3.1 Modeling Masonry Infill with Diagonal Struts

ASCE-41 [2017] provides explicit guidance on modeling the in-plane strength and stiffness of RC frames infilled with full-height masonry panels: *Section 11.4.2.1* defines frame stiffness by representing each bay as a composite cantilever column, and *Section 11.4.2.2* provides

an adjustment for the case of a single opening within the infill panel, with the opening size limited to less than 40% of the panel area. Beyond specific guidelines and calculations, ASCE 41-17 also includes a passage in *Section 11.4.2* that "the use of simplified numerical models with diagonal struts to simulate the effect of the infill shall be permitted to model infilled frames" [ASCE-41, 2017]. All three methods are presented with respect to full-height infill, and little emphasis exists to define modeling approaches for partial-height infill (which is prevalent throughout the buildings considered in this study). ASCE 41-17 comments that "frames with partial-height masonry infill. . . shall include the reduced effective length of the columns above the infilled portion of the bay" [ASCE-41, 2017]. No additional guidance was found to substantiate a more sophisticated means to modeling the presence of such infill. As such, this study sought to extend use of the diagonal strut methodology cited in ASCE 41-17.

Partial-height masonry infill was modeled using coupled, single-direction diagonal struts. The struts were assigned as compression-only truss elements for which the strength and cyclic force-deformation response was characterized as 'weak concrete' and simulated using the OpenSees *Concrete01* material model. A linear-elastic constitutive model (assigned in SAP2000) was substituted in place of *Concrete01* for the linear analysis. Strut geometry was defined by an effective width considering surrounding component geometry and elastic modulii and depth equal to infill thickness. Effective width calculation was based on *Section 7.5.2.1* of FEMA 356 *Prestandard and Commentary for the Seismic Rehabilitation of Buildings* [FEMA-356, 2000]. With respect to the nonlinear behavior of the struts, reference was made to research performed by [Mohammad Noh et al., 2017], [Tarque et al., 2015], and [Burton and Deierlein, 2014]:

- Mohammad Noh et al. [2017] investigated modeling RC frames with masonry infill. This study used experimental data from two tests of single-story, single-bay fully-infilled frames to evaluate nonlinear cyclic backbone curves and strength calculations with respect to modeling masonry with equivalent, compression-only struts. Both the

curves and equations were sourced from available literature. The best-fit backbone curve and strength model were combined and used to define input parameters parameters for three OpenSees constitutive models to instead define the cyclic response. Outcomes from this study include that a dual, single-strut approach "is a good match to the experimental results... [and] is a worth tool to be used in design practice," that OpenSees *Pinching4* hysteretic model was "the most suitable to reproduce the cyclic response of infills," and that OpenSees *Concrete01*, with respect to cyclic response, offers "a good compromise between simplicity and accuracy... [and] can be used for envelope analysis" [Mohammad Noh et al., 2017].

- Tarque et al. [2015] reviewed multiple methods, as proposed in the literature, for the numerical modeling of RC frames with full-height masonry infill. The authors posit that "the stiffness and strength of the infills should be accounted for in the seismic analysis of new buildings... and, more importantly, in the seismic vulnerability assessment of existing buildings" [Tarque et al., 2015]. Accordingly, the study addresses three levels of modeling sophistication by which to represent infill masonry within an RC frame: micro-modeling (detailed and simplified element representations for individual bricks and mortar joints), meso-modeling (smeared infill as a homogeneous continuum), and macro-modeling (equivalent strut representation), for which macro-modeling is more common in engineering practice. Within the classification of macro-modeling, the authors discuss model variations that involve various strut orientations, quantity, connectivity, and constitutive models. Outcomes from this study include that multiple (off-diagonal) eccentric struts best predict column responsive (and include shear vulnerability), though single strut models should be sufficient to reproduce the influence of the infill.

- A study by Burton and Deierlein [2014] sought to advance modeling of full-height masonry infill to provide accurate assessment of the pollapse risk posed by RC infill frames. This study built on previous research to describe shear failure potential resulting from

column-infill interaction, which many strut models fail to consider. The result of the result was a model comprising (2) coupled, single-direction diagonal struts. For each direction, one strut was aligned diagonal within the framing and the other was added off-diagonal, connecting above the bottom column node and below the opposite column top node. Full in-plane stiffness was divided between the two struts in a single direction at a ratio of 75% to 25%, respectivly. The nonlinear behavior was defined with an OpenSees *Ibarra-Medina-Krawinkler* hysteretic model adapted for axial deformations. The OpenSees platform was used for model numerical analysis, and the model was calibrated using experimental data from the literature. The model was then tested in a collapse assessment study of a prototype building.

2.3.2 Nonlinear Column Response

ASCE 41-17 defines the rotation capacity of plastic hinges that develop in RC columns, but provides no additional guidance on the modeling specifics. In practice, engineers typically make use of elastic beam-column elements bounded by zero-length plastic hinges at either end. These hinges represent the nonlinear **moment-rotation** response of the columns as expected for a constant axial load based on predefined backbone curves. All frame deformations are thus an outcome of the moment-rotation definition. One limitation to this method, however, is that it does not capture the impact of axial load fluctuation on the moment-curvature response. This is of particular importance with axial load amplification resulting from overturning effects during cyclic loading.

This study employed the OpenSees *BeamWithHinges* beam-column element with fiber-type section models to simulate 1) nonlinear moment-rotation response and 2) axial-moment interaction. The *BeamWithHinges* element is a force-based element formulation (linear moment distribution and constant axial force as assumed along the length of the element) defined by a plastic hinge region at either end of the member separated by an elastic interior region. End-point integration was selected to define behavior based on the maximum moment demand experienced by the element. Four integration points were assigned to the

element, with one was located at the end-point of each hinge region and two were located within the elastic interior. A discretized fiber-type cross-section was assigned to the integration points in the hinge regions to define the the bi-directional moment-curvature response including moment-axial interaction. Column rotation is calculated as the fiber-section curvature multiplied by the length of the plastic hinge. In the selection and development of this element formulation, reference was made to research performed by Scott and L. Fenves [2006] and Mohammad Noh et al. [2017].

- Scott and L. Fenves [2006] developed a new plastic hinge integration method for implementation within the OpenSees *BeamWithHinges* beam-column element. The method is derived from the Gauss-Radau quadrature rule to integrate element deformations over user-specified plastic hinge regions. Additionally, the user is able to define the specific integration scheme (Midpoint, Endpoint, Gauss-Radau, or Modified) to further define the distribution of deformations. The *BeamWithHinges* element employs a force-based formulation and confines nonlinear behavior within specified hinge regions at the ends of the element. Fiber-type section models can be assigned to the element hinge regions to define the nonlinear moment-curvature response at the ends of the element. Use of the *BeamWithHinges* offers advantages beyond concentrated plasticity and distributed plasticity models is that it 1) enables coupling of axial-moment response via the fiber-type section model (which is a limitation of moment-rotation models), 2) enables accurate simulation of response using a single element along the length of the frame member (a modeling simplification over displacement-based elements), and 3) prevents the localization of deformations in cases of strain softening (resulting in loss of objectivity in force-based elements). The EndPoint method enables use of a fiber section model at the element ends (where moment demand is greatest for columns) and specification of a hinge length such that member deformation and rotation demands are calculated via multiplication of fiber-section curvature against hinge length. The authors recommend the *BeamWithHinges* element (with improved integration method)

"for the nonlinear analysis of frame structures when softening and degradation of the members is expected" [Scott and L. Fenves, 2006].

- Mohammad Noh et al. [2017] employed two modeling approaches for RC frames with full-height infill masonry. One model variation comprised elastic elements bounded by zero-length concentrated plasticity hinges and the other incorporated distributed plasticity elements. The concentrated hinges employed a predetermined moment-rotation backbone for deformation response. The distributed plasticity elements were modeled with OpenSees *NonlinearBeamColumn* force-based elements and discretized fiber-type cross-sections assigned to each integration point. Both approaches were able to replicate the experimental results; however, the authors recommend use of the distributed plasticity elements, as this modeling approach provided better representation of the deterioration of strength and stiffness of framing elements.

2.3.3 Nonlinear Shear Failure Model

One limitation to the standard nonlinear beam-column elements available in OpenSees (including *BeamWithHinges*) is that they cannot simulate nonlinear shear response or flexure-shear interaction. In this study, zero-length shear springs were included at the tops of all columns to define the nonlinear response. The force-deformation characteristics were defined by a trilinear backbone. Linear-elastic stiffness defined the initial slope up to the column nominal shear capacity. An assumed degrading slope (negative stiffness) then reduced the available shear strength down to a residual capacity of 20% of nominal strength. This was implemented through use of the OpenSees *Hysteretic* material model. Pinching was included in the model but not cyclic deterioration. This simple modeling approach was deemed to be acceptable as the objective was to identify the onset of strength loss (at the instance that shear demand exceeded capacity). Initial efforts were made to implement a more sophisticated model linking flexure to shear demand-to-capacity via the OpenSees *LimitStateMaterial* material model; however, it was not pursued due to a change in the project scope.

In defining the shear response model, reference was made to research performed by Elwood [2004] and Burton and Deierlein [2014]:

- Elwood [2004] presents an OpenSees material model (*LimitStateMaterial*) that can be used to "detect and initiate strength degradation" in column elements [Elwood, 2004]. This material has definition for both shear and axial failure. To implement, the material model is assigned in series with a flexural beam-column element to "trace the response... and change the backbone [of the *LimitStateMaterial*] to include strength degradation once the [force and/or deformation] demands of the beam-column element exceed a predefined limit state" [Elwood, 2004]. The model is based on the OpenSees *Hysteretic* material and follows a similar, trilinear backbone curve. The limit state surface, assigned using an OpenSees *LimitCurve*, is defined by the user and is linked to the *LimitStateMaterial*. For RC columns, shear capacity is defined to deteriorate with column drift demand. Once column shear and drift demands are such that shear demand exceeds capacity, the deteriorating backbone of the limit state material model engages, and the column begins to lose shear capacity. Once the column shear deteriorates to a residual shear capacity defined in the material model, the axial limit state material is activated and the axial strength loss initiates. If column shear and drift demands are sufficiently small that shear demand does not exceed capacity, no limit state effects are triggered. Elwood [2004] discusses the development of the shear and axial limit state models and compares the implementation of analytical models within RC frames against shake table results from a previous study.

- Burton and Deierlein [2014] incorporated shear degradation into an RC frame model through use of zero-length shear springs to define a hysteretic, rigid-softening force-deformation response. These springs were aggregated,[1] in series, with the moment-

[1] 'Aggregate' is an OpenSees command that combines multiple uniaxial material models (e.g. [1] moment-rotation model coupled with [2] orthogonal shear models) into a single section comprising different individual material responses in their respective, assigned direction

rotation hinges at the ends of column elements. A 'rigid,' initial stiffness was calculated from elastic properties and extended up to a calculated nominal shear capacity. Shear strength degradation (negative stiffness) defined the post-peak response. Deformation parameters necessary for defining the slope values were sourced from Elwood [2004]. Loss of axial load-carrying capacity was assumed at complete loss of shear strength; the authors correlated this with collapse. The authors conclude that "incorporating the shear failure of columns, caused by large forces developed in the infill, is critical to the accurate collapse assessment of infill frames" [Burton and Deierlein, 2014].

Chapter 3
SUMMARY OF BUILDING DAMAGE

3.1 Background

On February 5th, 2016 an earthquake struck the southwestern portion of Taiwan. Damage was localized to the areas surrounding Tainan City and the community of Meinong. In response to the hazard, the National Science Foundation (NFS) Rapid Response Research (RAPID) program funded national and international teams to secure reconnaissance data in the aftermath of the earthquake. The information was collected in the form of photographs of the on-site structural damage, sketches of structural layout, and relevant construction documents. Acquisition of these resources was critical for post-event analysis and in the estimation/prediction of probable modes of damage and/or collapse.

These structures ranged in construction date from early 1960s to later 2000s and varied in height between two and fourteen stories. The primary structural layout was that of reinforced-concrete buildings, of various occupancy types, composed of moment frame lateral force resisting systems coupled with slab-beam-column gravity framing. Many structures featured architectural masonry infill framing between the columns. Damage was characterized by diagonal cracking along many of the columns and walls (both infill and structural), with the majority to all damage concentrated within the first story.

3.2 Seismicity

Ground acceleration records were collected from local recording sites tracked by the Taiwan Central Weather Bureau (CWB). Access to this information was provided in collaboration with the ATC 134 research team for use in the dynamic analyses. This allowed for evaluation using earthquake-specific motions. One caveat is that the location of recording sites did not

necessarily correspond to the location of the damaged buildings. Since seismic amplification is sensitive to local geology, these recordings are not site-specific and thereby simply a means to approximate the motion experienced. The value for use of these motions is that they still provide context towards amplitude, frequency content, and duration that was endured by the structures. Supplemental to the recorded information, Figure 3.1 gives two visualizations of the intensity of the event as produced by the US Geological Survey (USGS).

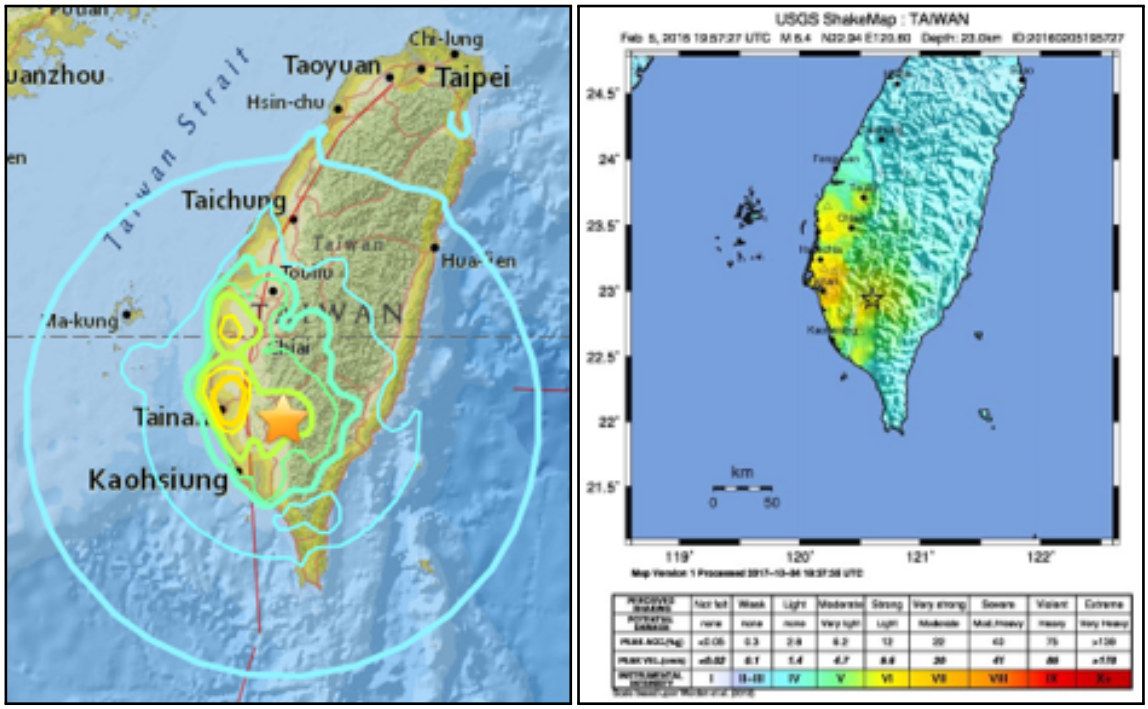

(a) Intensity Propogation (b) USGS ShakeMap

Figure 3.1: Visualization of Earthquake Intensity U.S. Geological Survey [2018]

Figure 3.2 gives the location of sixteen damaged structures with respect to the fault epicenter. Each marker reflects the location of a separate structure. The selection basis considered similar lateral force-resisting system (moment framing) as well as available of the structural plans. Condensed from the sixteen identified, Table 3.1 highlights typical component damage for low- to mid-rise buildings of various occupancy classifications but

featuring moment framing lateral-force resisting systems.

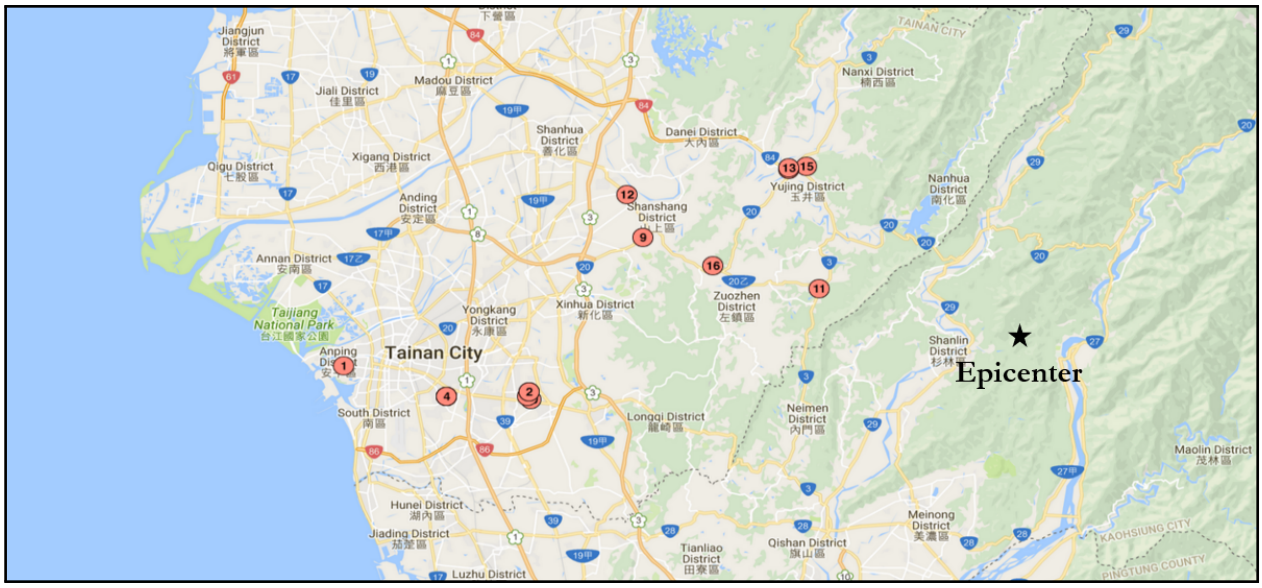

Figure 3.2: Damaged Structures Relative to Fault Epicenter

Two structures were selected from the suite of damaged buildings for the purpose of further investigation: Nanhau District Office (#11) and Xingfu Building (#10). These structures differ in height, occupancy, framing, and damage. Nanhau meets near all classifications of an ASCE 41 baseline structure with respect to simple and consistent geometry and design. Xingfu has a complicated geometric layout and obvious torsional irregularities. It was also one of the few buildings that collapsed as a result of the earthquake. Figure 3.3 gives visual reference, per structure, as to the building site (shown with a purple arrow), the fault epicenter (shown with black, concentric circles), and various ground motion recording stations identified within close proximity of the buildings (shown with a pink, seismic wave icon). Labeling of recording stations is given in Table 3.2 with the respective distance between stations and the building site.

Table 3.1: Summary of Observed Building Damage

Observed Damage	Xingfu Bldg.	Guiren District Apt.	Nanhau District Office	Shanshang District Office	Zhouzheng District Office	Yujing Elementary, NW Wing	Yujing Elementary, W Wing	Yujing Jr. High, Special Classroom	Guiren Jr. high, Guanghua Bldg.
Column									
Diagonal Cracks			✓	✓	✓	✓	✓	✓	✓
Vertical Cracks				✓	✓				
Horizontal Cracks			✓		✓				
Spalling		✓							
Wall									
Cracked RC		✓				✓		✓	
Cracked Infill	✓	✓	✓	✓	✓				

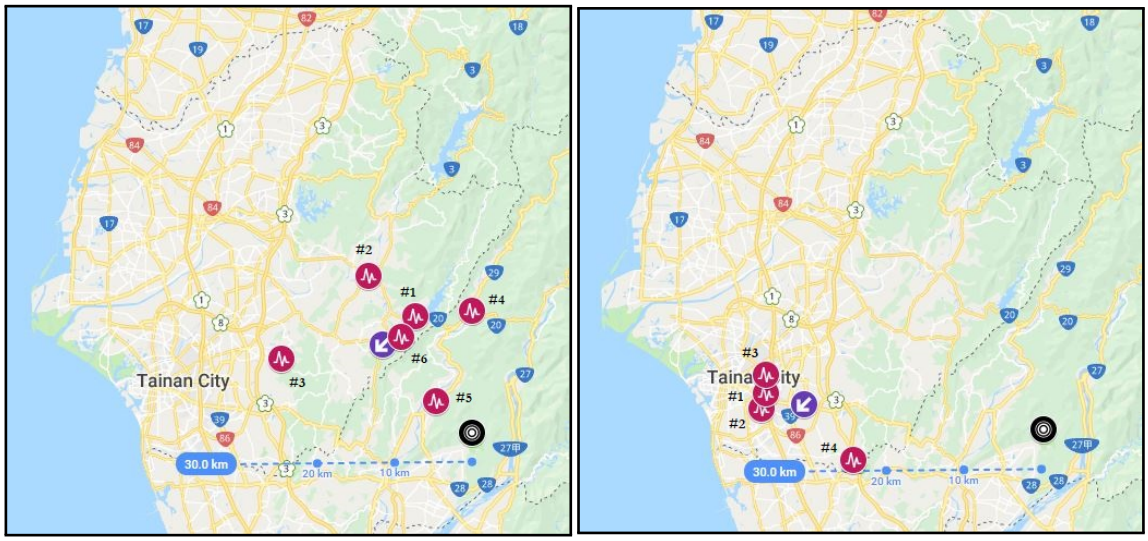

(a) Nanhau District Office (b) Xingfu Building

Figure 3.3: Free-field Ground Motion Recording Stations within Close Proximity to Model Buildings and Seismic Epicenter

Table 3.2: Identified Recording Stations with Marked Distance from Site

Nanhau District Office			Xingfu Building		
#1	CHY061	3.45mi	#1	CHY096	3.24mi
#2	CHY062	5.64mi	#2	CHY070	3.41mi
#3	CHY063	8.24mi	#3	CHY064	3.86mi
#4	KAU047	7.64mi	#4	CHY065	5.96mi
#5	KAU068	6.24mi			
#6	A730	1.55mi			

Original selection of ground motion for use in analysis was based on closest proximity: Station CHY061 for Nanhau and Station CHY096 for Xingfu. Geotechnical engineer and independent consultant, John Egan, performed an investigation into the local soil conditions

at the Nanhau site. No inquiry was made for Xingfu. He estimated that the building was located over site class C soil with a shear wave velocity, V_s, of approximately $570^{m}/_{s}$. He noted that seismic faulting ruptured towards the structures with west-northwest directionality. This corresponds with the observed damage at Nanhau. Per use of recording station data for this study, Egan recommended use of CHY061 and CHY062 based on similar soil characteristics to findings at Nanhau. Stations CHY063 and KAU047 overlay too soft of soil to prove representative. Station KAU068 is too close to fault initiation to accurately describe dynamic response at Nanhau. Egan also suggested use of an additional ground motion record, Station A730. This new record was posited to provide the most similar representation based on a close proximity to Nanhau ($1.55mi$) and similar soil V_s characteristics.

Figure 3.4 gives plots of the tri-directional acceleration records as received for the best-fit motion attributed to Nanhau (A730) and the closest proximity recording station to Xingfu (CHY096). The absolute value of maximum amplitude is provided for each recorded direction. A Newmark, constant-acceleration, time integration was performed to develop individual response spectra. An average spectrum was determined as the square-root-sum-of-squares (SRSS) combination of the two directions: east-west (EW) and north-south (NS); this lines shows an an approximation of the bi-directional nature of the ground shaking as applied to the frequency content. The ASCE 41-17 design response spectrum for the City of Seattle was provided for comparison. Figure 3.5 shows the result for two structures in this study: Nanhau District Office and Xingfu Building. Arbitrary values of fundamental period, T_1, are marked with dotted lines at locations of 0.25, 0.50, and 1.0 seconds. Note of the substantial differences in frequency content, amplitude, and duration between the motions originating from the same source.

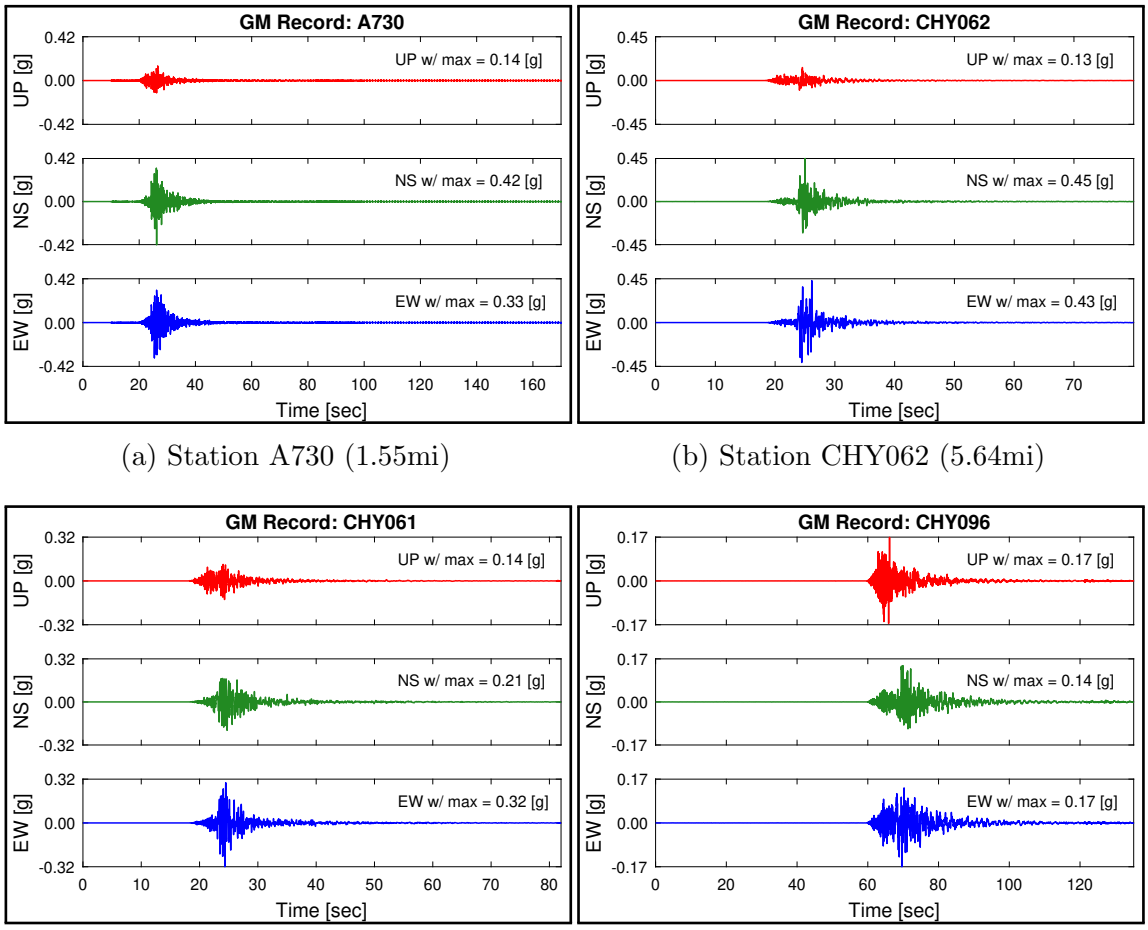

(a) Station A730 (1.55mi)

(b) Station CHY062 (5.64mi)

(c) Station CHY061 (3.45mi)

(d) Station CHY096 (3.24mi)

Figure 3.4: Ground Motion Acceleration for Stations near Nanhau and Xingfu

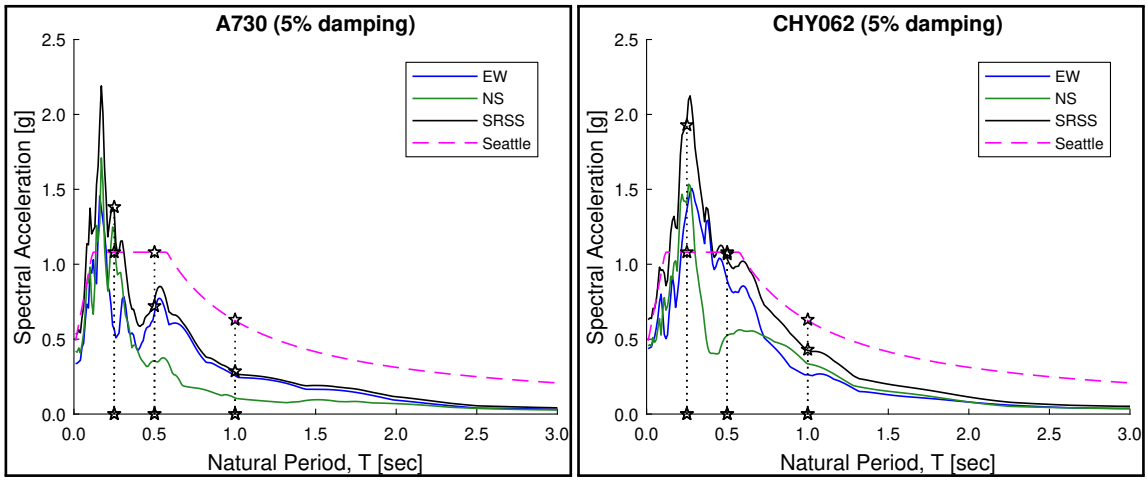

(a) Station A730 (1.55mi)

(b) Station CHY062 (5.64mi)

(c) Station CHY061 (3.45mi)

(d) Station CHY096 (3.24mi)

Figure 3.5: Response Spectra for Ground Motion Records given in Figure 3.4

3.3 Selected Structures for Evaluation

3.3.1 Nanhau District Office

The Nanhau District Office was a three-story reinforced concrete office building located outside of Tainan City, Taiwan ($23°2'32.7''N$, $120°28'39.8''E$) as shown in Figure 3.3a. It was constructed in 1967. Plan dimensions were approximately $33m$ in the EW direction and $18m$ in the NS direction (referred to as the X and Y building directions, respectively, in this thesis). Gross area per floor totaled approximately $531m^2$. The building contained three stories above grade with typical story heights of $3.6m$ ($4.2m$ first story) for a total height approximately $11.6m$. Figure 3.6 shows several perspective views of the structure.

The framing system consisted of two-way slab-beam-column moment framing to resist both vertical and lateral loads. The slab was $12cm$ thick with beam cross-sections of $24\times60cm$ and $36\times85cm$ (integral with the slab) and column cross-section of $24\times40cm$ and $36\times50cm$ oriented such that the strong-axis was in the plan Y direction. Full-height masonry infill was located primarily on the plan northwest and north portions of the building; partial-height infill ran along the outer perimeter at each level. An exterior stair was noted on the northeast side of the building, but was not included in the analysis.

Damage was concentrated to the first story and predominately in the X direction, which is consistent with the direction of seismic wave propagation. The primary damage mode observed was that of diagonal cracking of the columns indicative of a shear or flexure/shear limit state. Cracking appeared to to be constrained to the clear span as defined above the height of the infill and below the column-beam joint. This loading direction happened to be in line with the weak-axis response of all columns. On-site photographs of the observed damage are given in Figures 3.7 and 3.8.

Given the poor quality of the original structural drawings, the building layout was redrawn in Revit. Figures 3.9 and 3.10 show the location of framing components with respect to an imposed grid system. The framing is consistent up the height of the structure. Figures 3.11 and 3.12 show elevation views for both the X and Y directions. In reference to

analysis results documented in later chapters, columns and beams were assigned numeric ID numbers as shown on plan. For use in later analysis, Figures 3.13 to 3.16 provide a sample of key structural parameters shown on elevation views for different grid lines for both columns and beams.

Any information not available from the construction documents had to be estimated using ASCE 41 approximations, general time and location assumptions, or standards of practice. One such example is that, given slight photographic evidence as revealed in Figure 3.6d, it was assumed that the material make-up of the masonry infill was that of hollow clay tile (HCT). A secondary limitation to the structural plans as received is that to do not include reference to an addition to the original structure constructed at a later date. This portion was excluded from analysis due to a lack of information on the structural framing, component sizing, material strengths, and connection to the main portion. It would otherwise be located in the open area at the northwest of the structure, as denoted on Figure 3.9.

(a) South Face of Structure

(b) East Face of Structure

(c) Stair and North Side Bump-out of Structure

(d) Diagonal Wall Cracks Revealing assumed Hollow Clay Masonry.

Figure 3.6: Photos of Nanhau District Office

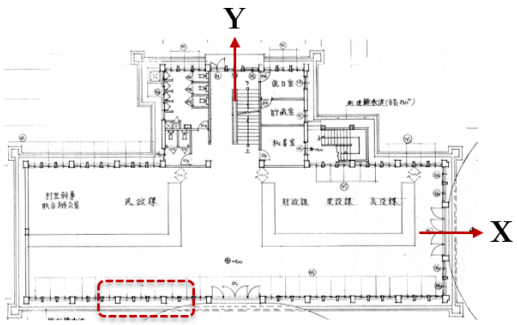

(a) Plan View

(b) Columns A3 and A4

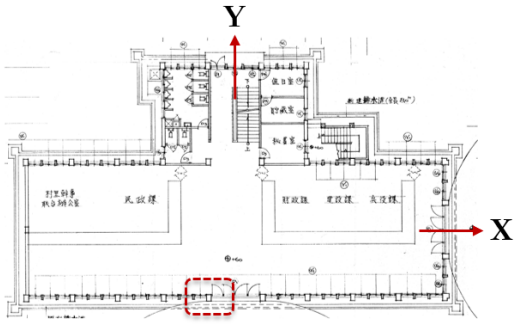

(c) Plan View

(d) Column A5

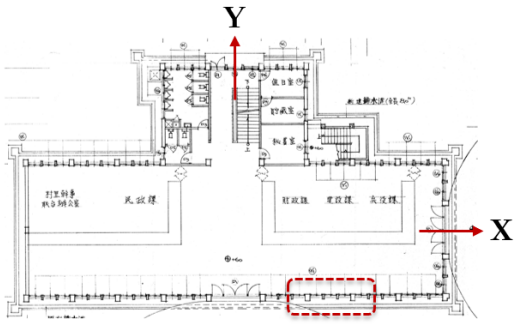

(e) Plan View

(f) Columns A7 and A8

Figure 3.7: Post-Earthquake Damage

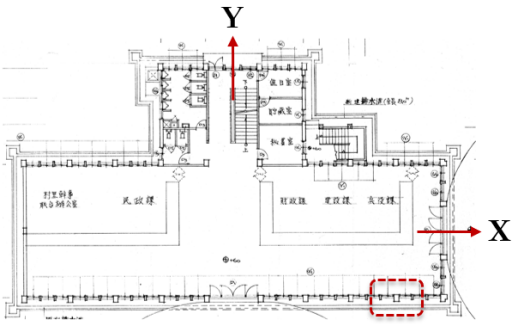

(a) Plan View

(b) Column A9

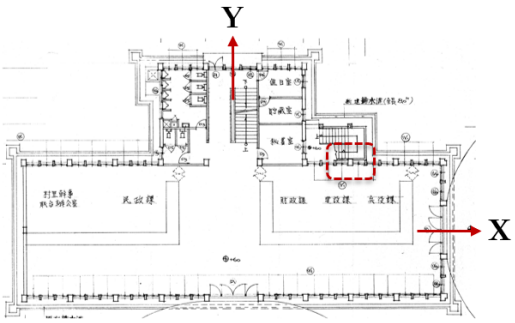

(c) Plan View

(d) Column C8

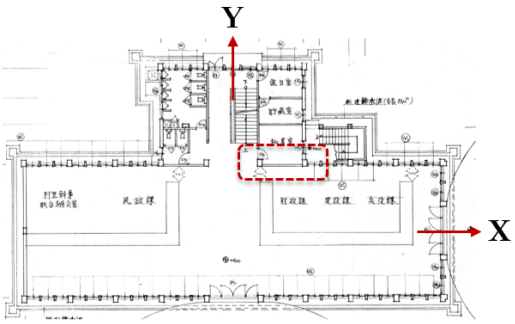

(e) Plan View

(f) Cracked Interior Wall

Figure 3.8: Post-Earthquake Damage

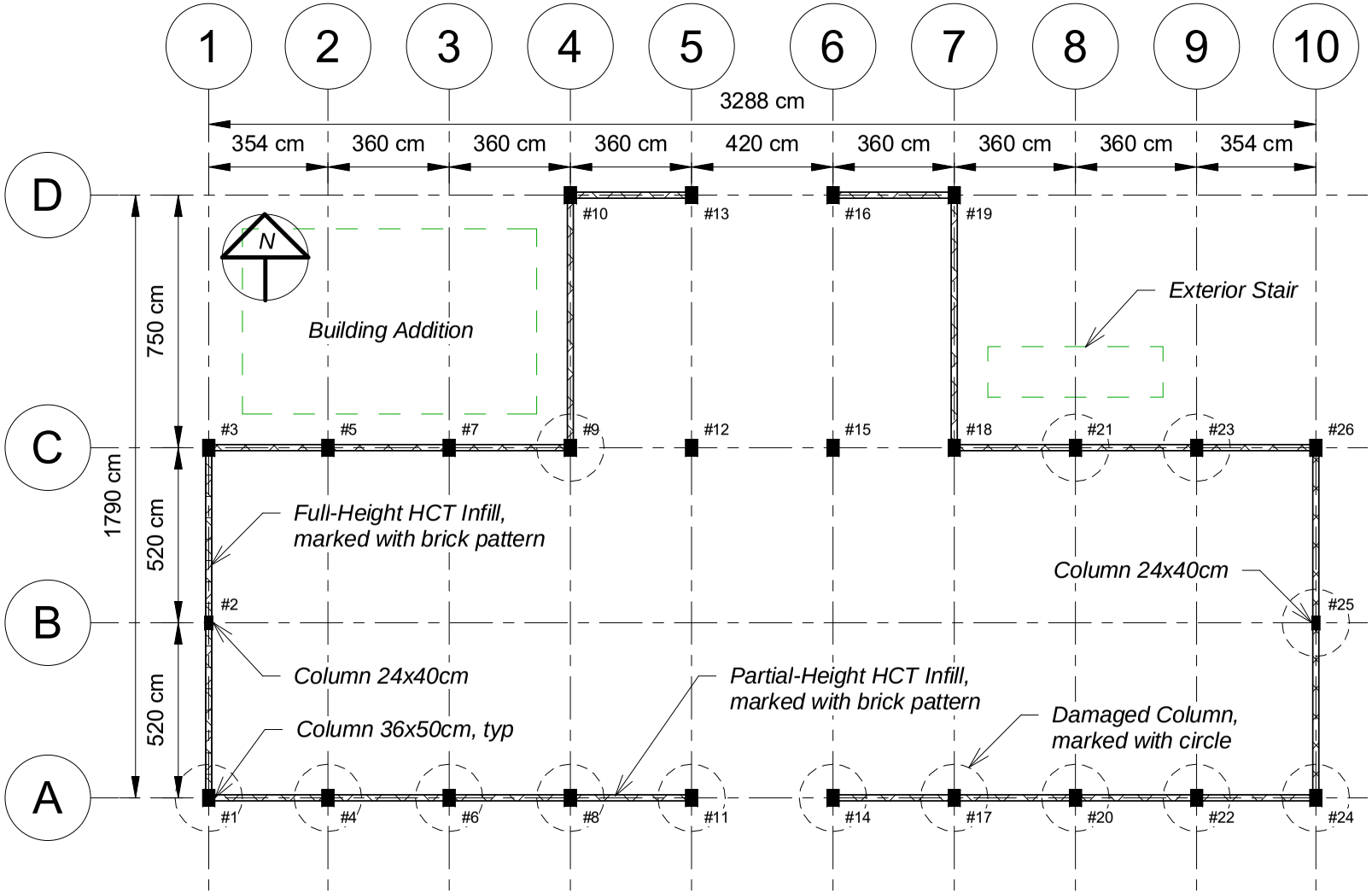

Figure 3.9: Column Layout Reproduced from Original Construction Documents

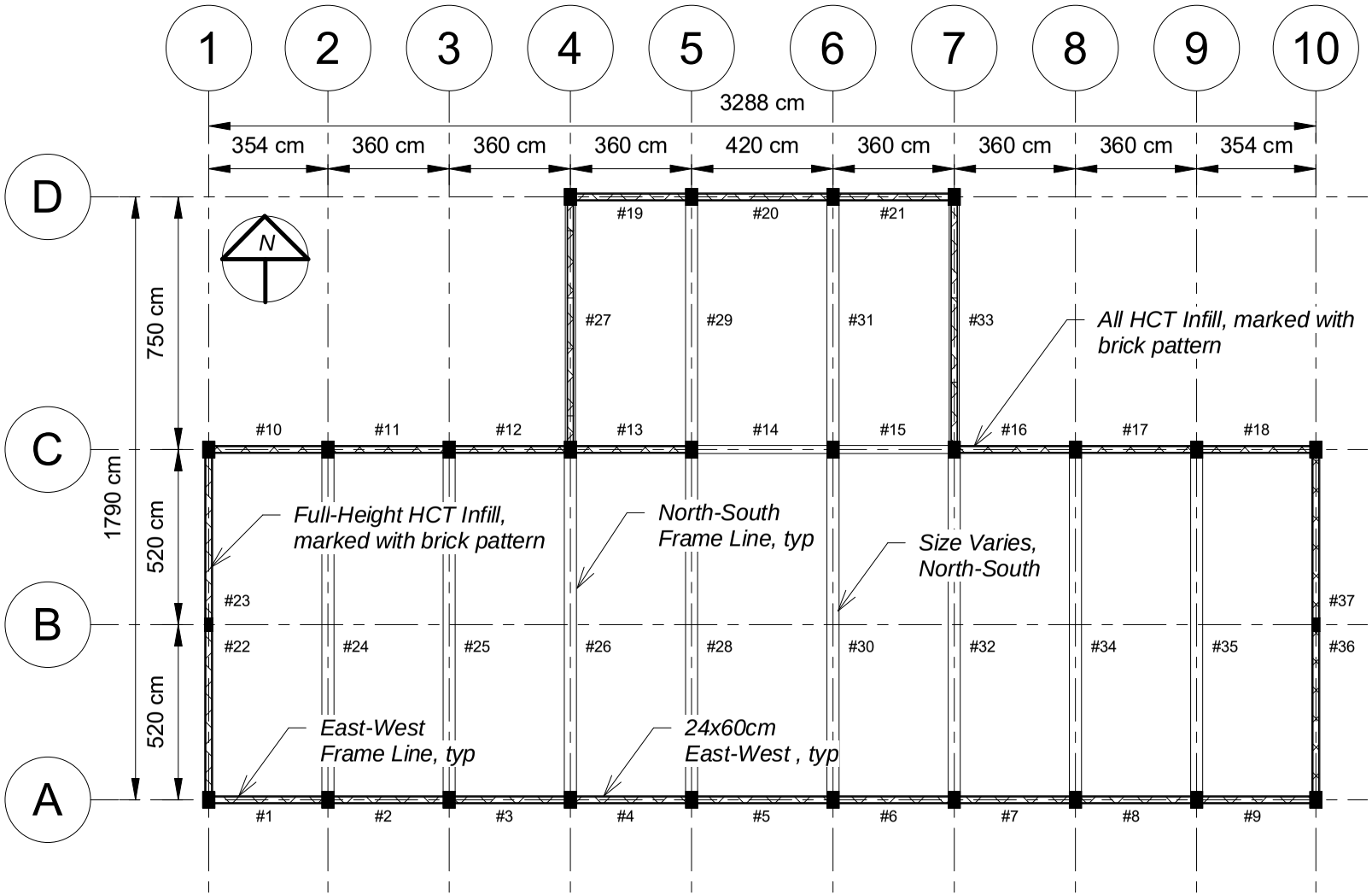

Figure 3.10: Beam Layout Reproduced from Original Construction Documents

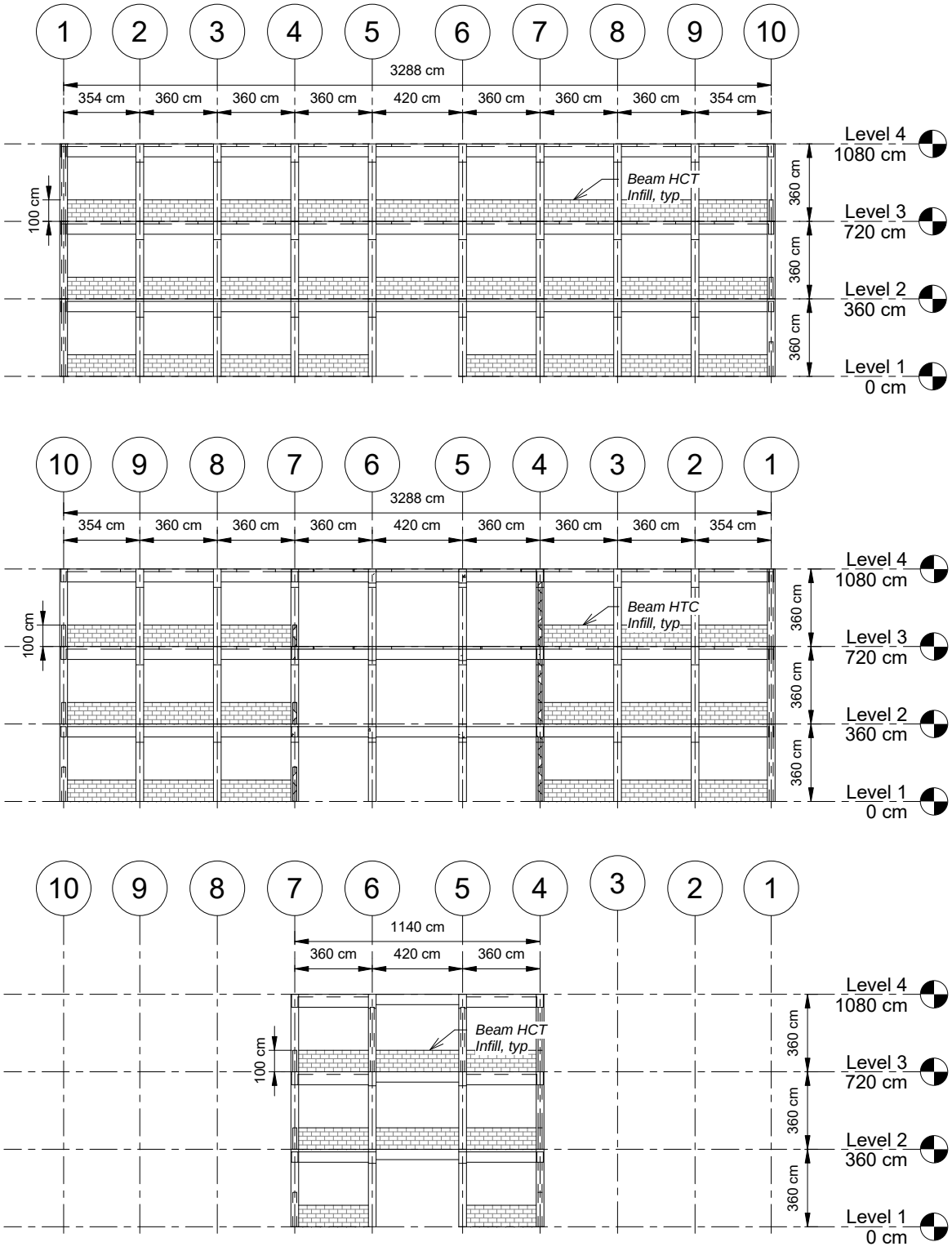

Figure 3.11: Elevation Views of Grids A, C, and D, Respectively

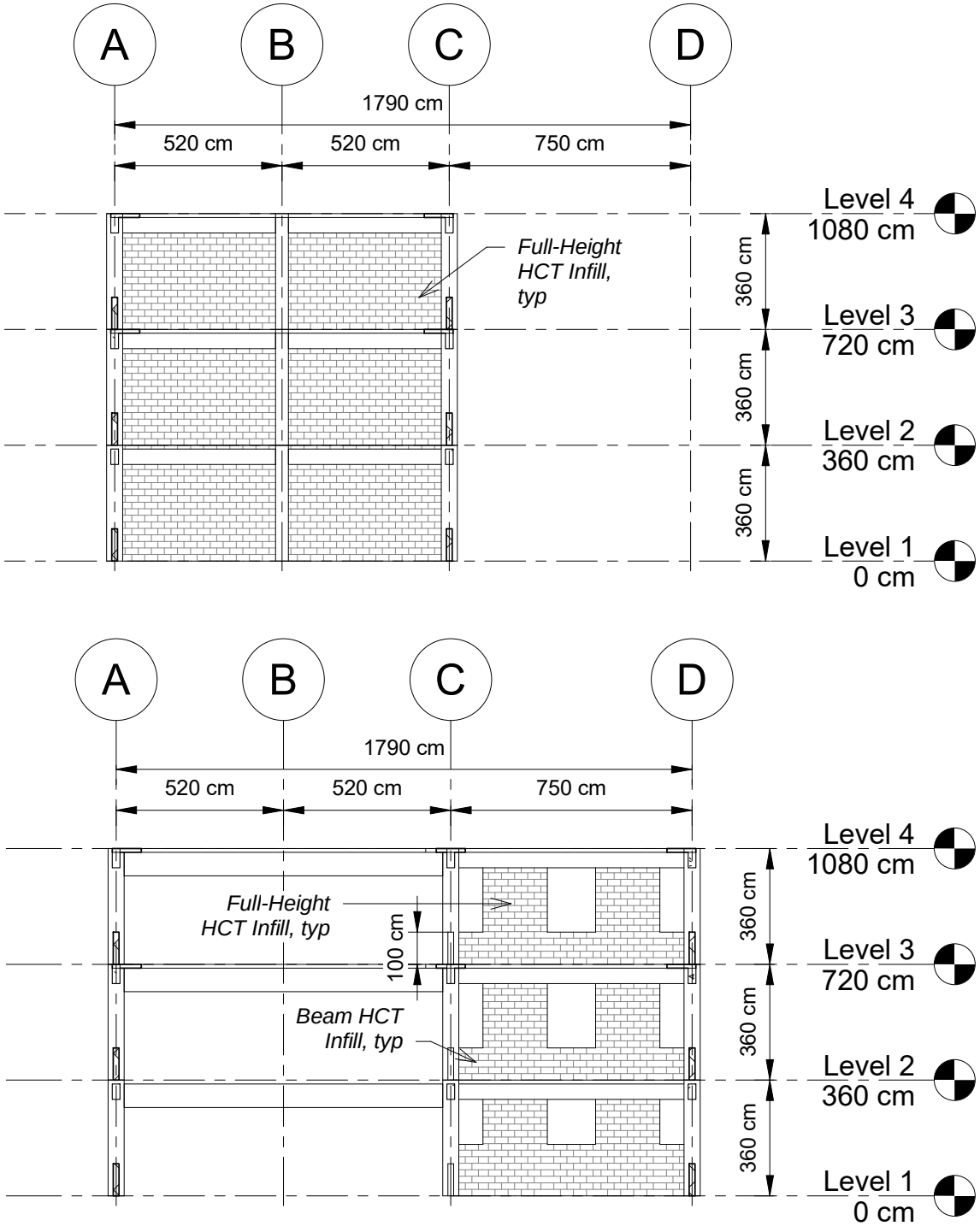

Figure 3.12: Elevation Views of Grids 1 and 4, Respectively

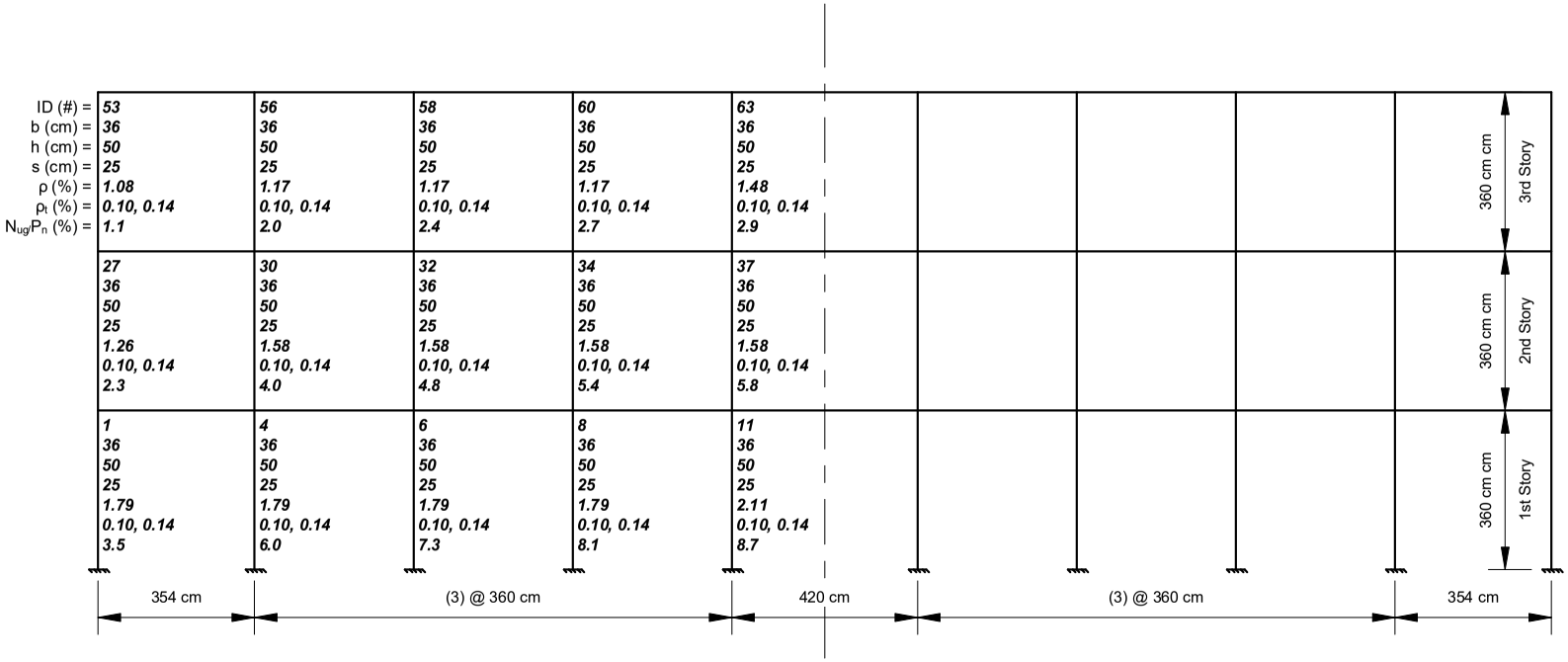

Figure 3.13: Grid A, EW, Structural Parameters for (1st Story) Columns

Figure 3.14: Grid A, EW, Structural Parameters for (1st Story) Beams

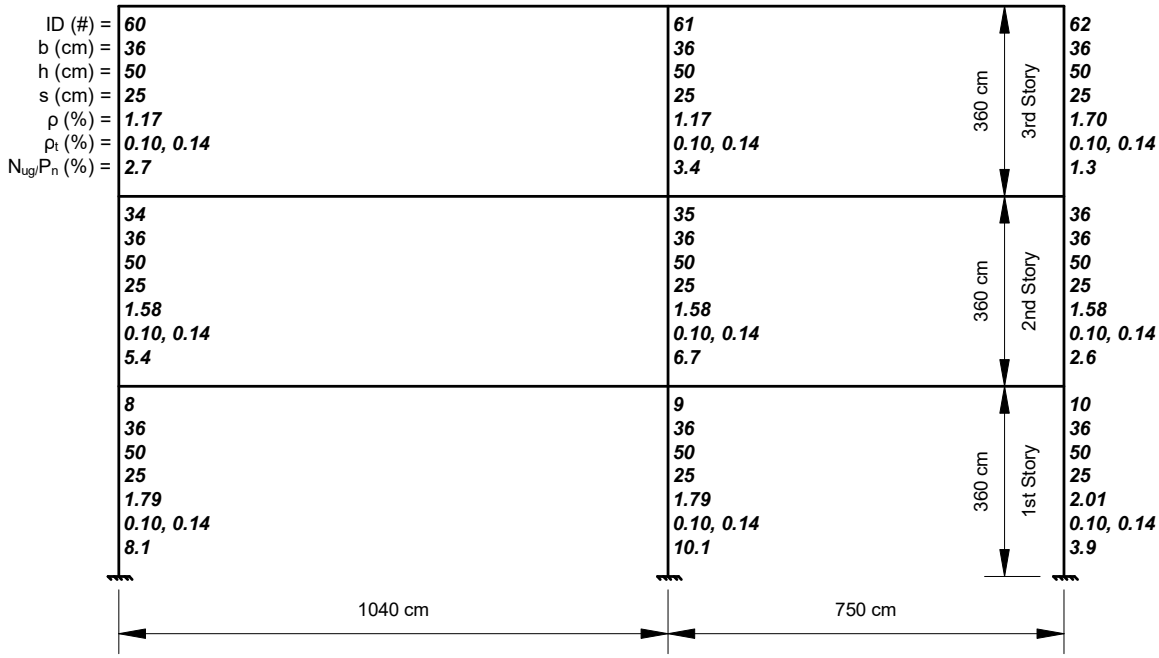

Figure 3.15: Grid 4, NS, Column Structural Parameters

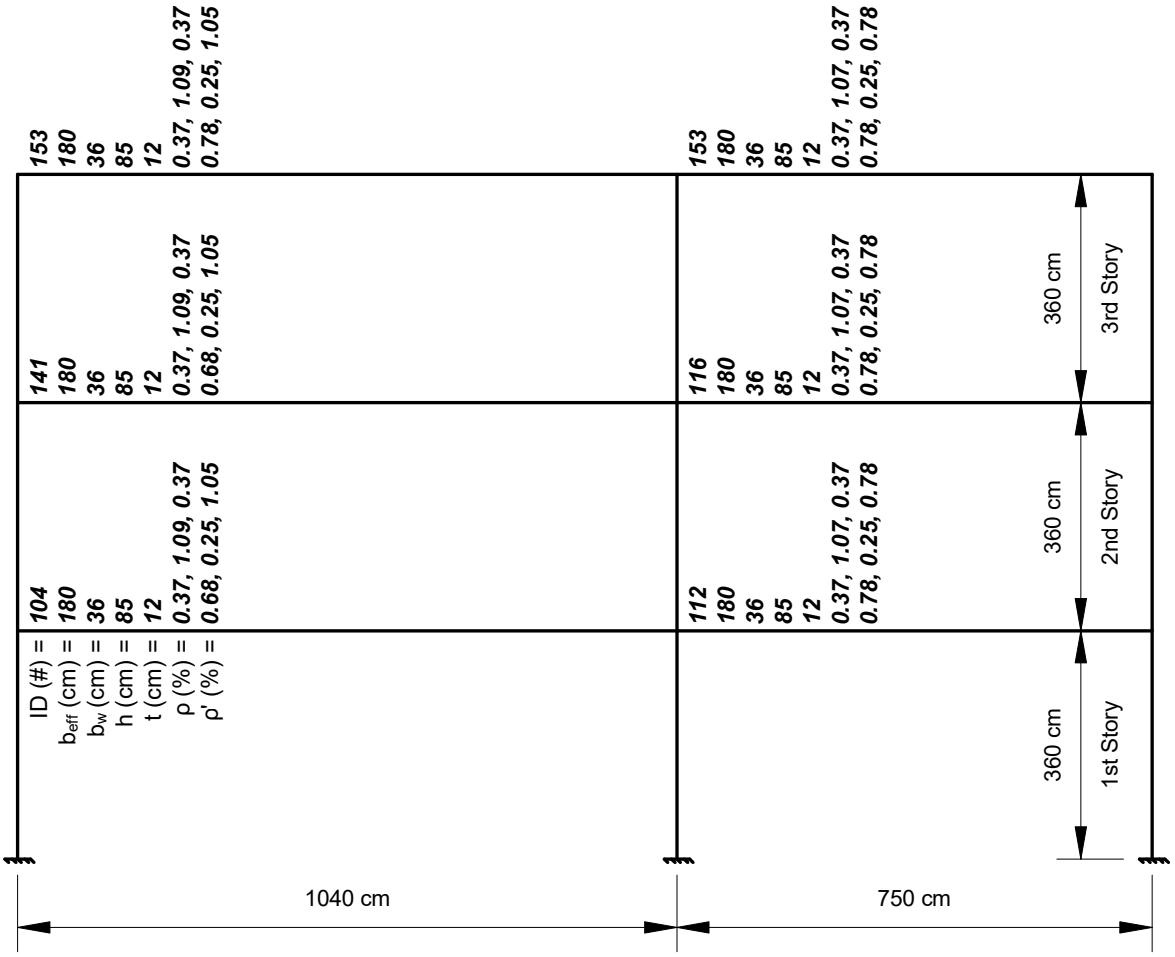

Figure 3.16: Grid 4, NS, Beam Structural Parameters

3.3.2 Xingfu Building

The Xingfu Building was a seven-story reinforced concrete building located outside of Tainan City, Taiwan ($22°58'8.4''N$, $120°17'22.2''E$) as shown in Figure 3.3b. The structure was multi-use consisting of below-grade parking, first-level commercial, and residential apartments. It was constructed in 2000. Plan dimensions were approximately $20m$ in the EW direction and $21m$ in the NS direction (referred to as the X and Y building directions, respectively, in this thesis). Gross area per floor ranged between $358m^2$ at basement level, $175m^2$ at ground level, and $264m^2$ for levels 2 to roof. The building contained one level below grade and seven levels above grade with typical story heights of $2.8m$ ($3.8m$ first story) for a total height approximately $22.4m$. Figure 3.17 shows several perspective views of the structure.

The framing system consisted of two-way slab-beam-column moment framing to resist both vertical and lateral loads. The slab was $12cm$ thick with beam cross-sections of $24\times60cm$ (integral with the slab and analyzed as T-beams and column cross-section of $50 \times 65cm$ and $55 \times 80cm$. Two grid systems (one corresponding to the primary orthogonal directions and a second with respect to a coordinate shift) describe the column positioning. It was approximated, based on physical measurements of the columns, that the coordinate rotation was 40° off vertical; thus, columns in the southern region were oriented such that the strong-axis was in the plan Y direction, while columns in the northern region do not align with either X or Y directions but rather are consistent with the rotated framing. Full-height RC walls were located along the southern face and surrounding the elevator and stair cores. Partial-height infill ran along the outer perimeter at each level.

This structure collapsed as a result of the earthquake. Global system failure largely obscured local component damage, though photographs indicate possible vulnerabilities associated with the joint regions at the first story for columns towards plan north. Figure 3.18 gives a stunning before-and-after perspective of the building as well as some of the local damage sustained by individual components.

Given the poor quality of the original structural drawings, and the more complicated

geometry of this building, effort was made to visually match the analytical model to construction documents. Full model replication was not conducted in Revit, though Figure 3.19 marks the column numbering for the first level to which subsequent analysis refers. This was, in part, due to time constraints. Figure 3.20 gives several perspective views of the SAP model relative to the construction documents. The irregular and non-orthogonal geometry prevented the identification of distinct frame lines. Without a good means to visualize, key structural information for first-story columns is given in Table 3.3.

(a) East Face of Structure

(b) RC Wall at South Face with View of Stair Core to the Far Right with Visible Beams

Figure 3.17: Photos of Xingfu Building

(a) North and West Faces of Structure

(b) Collapse, Crushing Stories 1 and 2

(c) Visible Tilt of the Structure (West to East) During Demolition

(d) Exposed and Buckled Rebar on Collapsed Side.

Figure 3.18: Post-Earthquake Damage

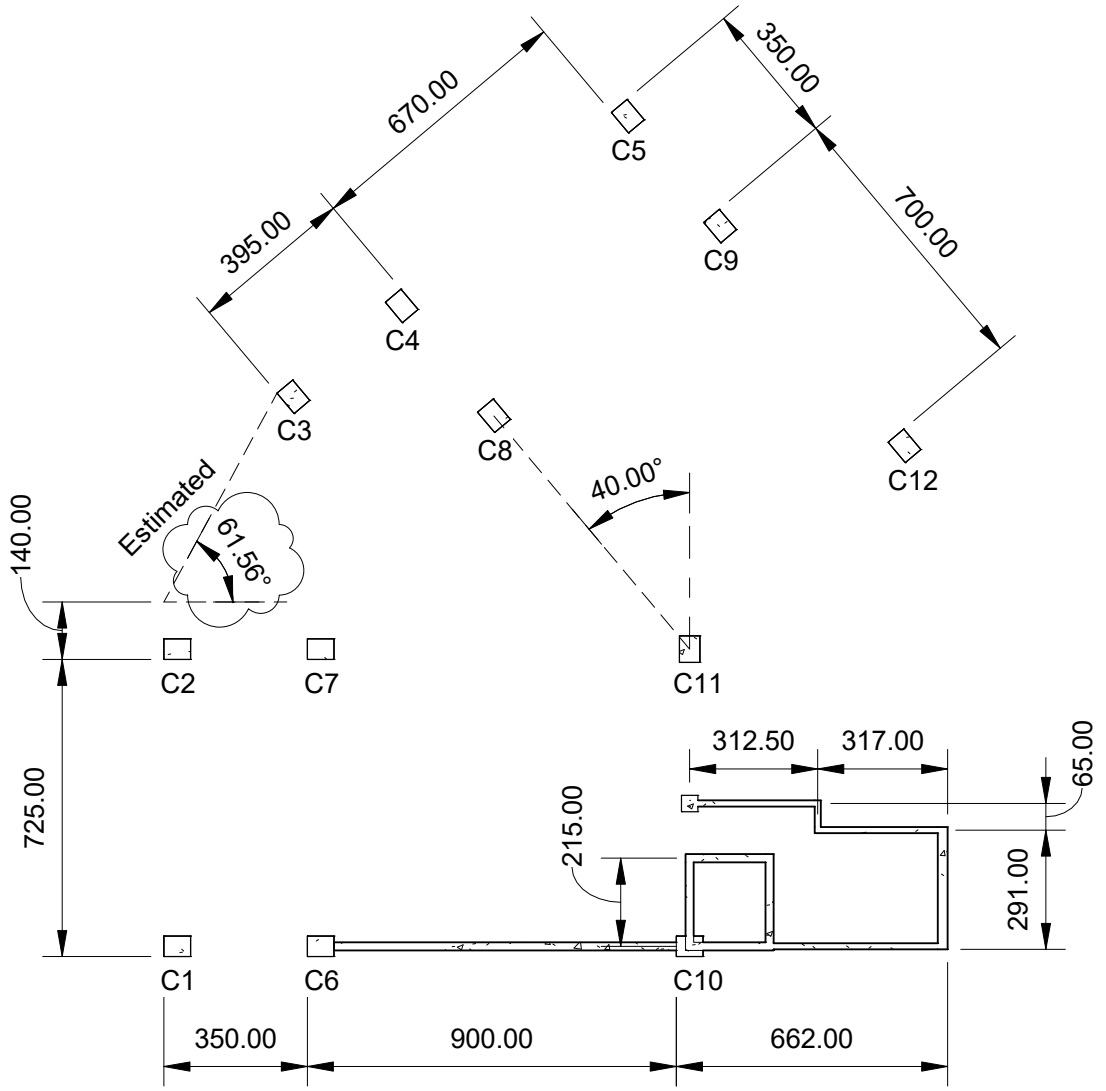

Figure 3.19: Column Layout Reproduced from Original Construction Documents [cm]

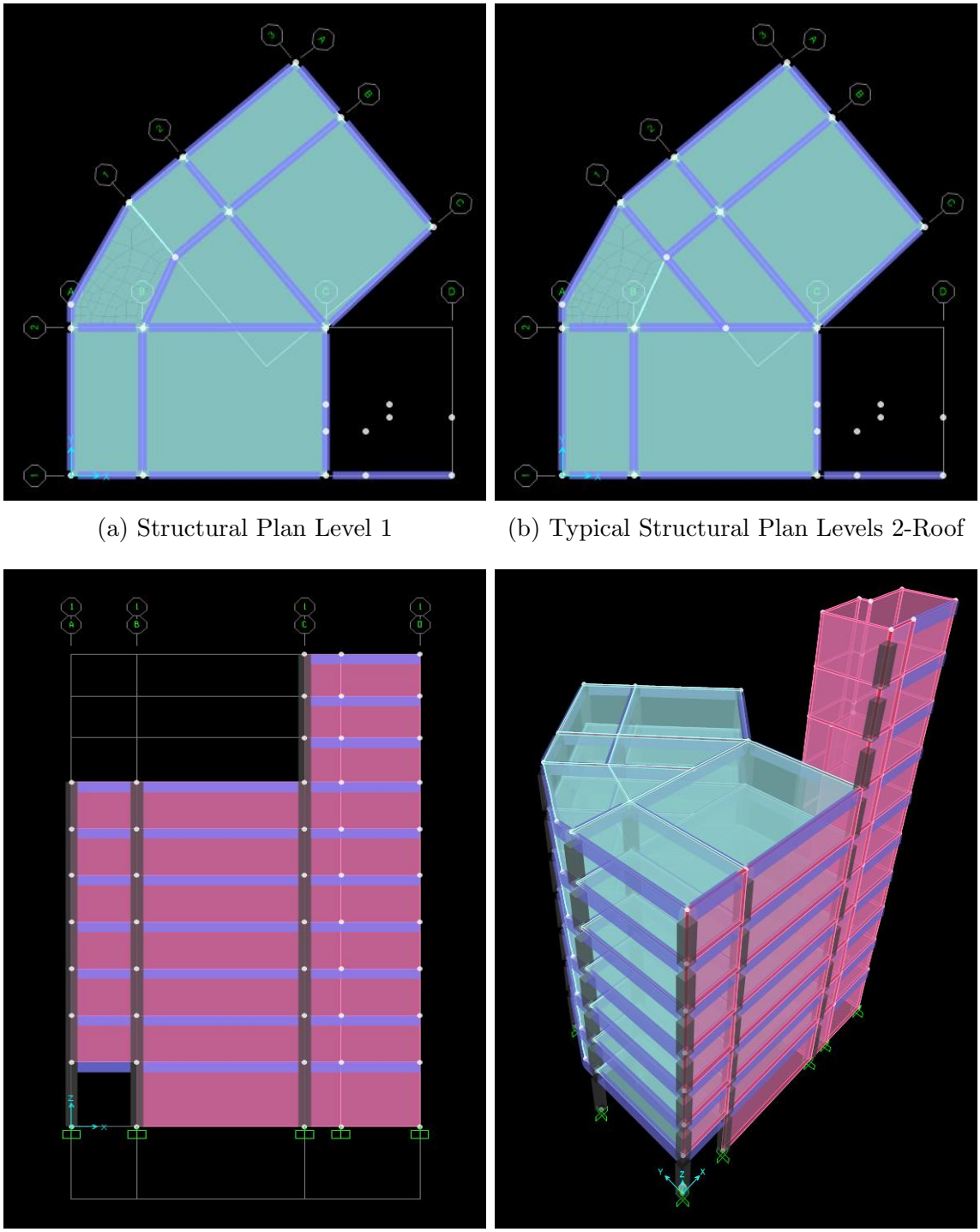

(a) Structural Plan Level 1

(b) Typical Structural Plan Levels 2-Roof

(c) RC Wall on South Face

(d) 3D Perspective

Figure 3.20: SAP Modeling of Xingfu Building

Table 3.3: First-Story Column Key Structural Parameters

Column	C1	C2	C3	C4	C5	C6	C7	C8	C9	C10	C11	C12	Units
b	50	50	50	50	50	50	50	50	50	50	55	50	cm
h	65	65	65	65	65	65	65	65	65	65	80	65	cm
s	12	12	12	12	12	12	12	12	12	12	12	12	cm
ρ	2.5	2.2	2.8	2.2	2.2	3.5	3.8	2.4	2.2	2.5	2.8	2.2	%
$\rho_{t,SA}$	0.47	0.47	0.47	0.35	0.47	0.47	0.47	0.47	0.47	0.47	0.43	0.47	%
$\rho_{t,WA}$	0.36	0.36	0.36	0.27	0.36	0.45	0.45	0.36	0.36	0.36	0.37	0.36	%
N_{ug}/P_n	6.9	8.2	5.9	7.3	5.4	16.1	23.2	18.1	12.5	11.2	25.1	9.4	%

3.4 Material Properties

Material properties for use in calculating component strengths and deformation capacities were largely unavailable in the documentation collected during the reconnaissance. Initial efforts assumed a concrete compressive strength, f'_c, of 4000psi [27.6MPa] and reinforcing steel of yield strength, f_y, of 60ksi [413.7MPa]. Both values are acknowledged by ASCE 41-17 Chapter 10 as having been available during the construction of the two buildings, though it was later identified that lower quality materials were more prevalent and probably used in the construction of the buildings. As such, this analysis considered lower bound material strengths of $f'_c = 3000$psi [20.7MPa] and $f_y = 40$ksi [275.8MPa] for use in calculating nominal component strengths. Elastic moduli for concrete, E_c, and steel, E_s, were calculated based on typical procedures.

Given the age of the structures and the deformability of lower grade steel, ASCE-41 [2017] *Table 10-1* specifies an increase beyond lower-bounded strength of $\times 1.50$ for concrete ($f'_{ce} = 4500$psi [31.0MPa]) and $\times 1.25$ for steel ($f_{ye} = 50$ksi [344.7MPa]) for use in calculating expected component strengths. All self-weight calculations assumed a unit weight of

150pcf for concrete and 60pcf for masonry infill (assumed hollow clay tile). For modeling of the masonry infill, ASCE 41-17 gives reference to the compressive capacity of unreinforced masonry. Acknowledging that the strength is a function of material, mortar, construction, etc., an intermediary value of f'_m = 1200psi [8.27MPa] was selected. This corresponds to a modulus of elasticity, E_m, equal to 700 times the compressive strength, per *Section 1.8.2.2.1* of *The Masonry Society (TMS)* TMS-402 [2011]. Similar to concrete and steel, this nominal capacity was multiplied $\times$1.30 (f'_{me} = 1560psi [10.8MPa]) for expected strength as denoted in ASCE 41-17.

Chapter 4

EVALUATION OF ASCE 41 TIER 1

4.1 Research Overview

From the set of buildings identified in the NFS RAPID reconnaissance project (introduced in Chapter 3), low- to mid-rise buildings of various occupancy categories were used to conduct an ASCE 41 Tier 1 evaluation. All featuring moment framing lateral force-resisting systems, and all had sustained moderate to severe damage due to the strong ground shaking. Buildings selected from the reconnaissance collective formed an analysis suite. Criteria for selection included availability of the construction documents and comprehensive documentation of the damage state (including on-site photography). Following selection, first steps to evaluate the relevant information required correlating the inventory of information, i.e. matching of damage photos with locations on the structural plans, as well as reconciling component details with the as-built condition. This study was largely conducted by a prior student, Francesca Galeotti, and was funded by the NSF.

The objective sought to capitalize on this repository of damaged structure, to which substantial information was known both preceding and following the Meinong earthquake, to conduct an evaluation of the ASCE Tier 1 Screening. The objective was to evaluate the accuracy and reliability of the Tier 1 methodology using the recorded ground motions and the known damage state. This would be compared to the outcome predictions from the procedure based on the structural plans and component detailing. Standard calculations and compliance checklists, upon which the Tier 1 methodology is based, were assessed to determine predicted vulnerability for each of the buildings studied.

4.2 Tier 1 Screening

Section 2.1.1 gives a brief introduction to the Tier 1 Screening. The standard is written to act as a quick and simple methodology by which to highlight potential component vulnerabilities based on calculations and visible irregularities. This process is distinct for each lateral force-resisting system, e.g. moment framing, and is itemized such that individual components are to be marked *compliant* (C), *noncompliant* (NC), or *not applicable* (N/A) based on the relevant criteria. An additional option of *not checked* (NC) was included to acknowledge areas outside the scope of this study. The checklists are also respective to the desired post-event performance state, e.g. collapse prevention, and to the level of seismicity for the region. Supplemental checks are required if the desired performance is high or the site in located in an area of high seismicity. For all structures in this collection, the building type was classified as *Concrete Moment Frames (C1)* per ASCE-41 [2014] *Table 3.1.* An example of such checklist is given in Figure 4.1. Take note that this figure is from the ASCE 31-03 standard, as it was format selected by the previous student while conducting the evaluation. For items that reference structural calculations, material strengths are noted in Section 3.4.

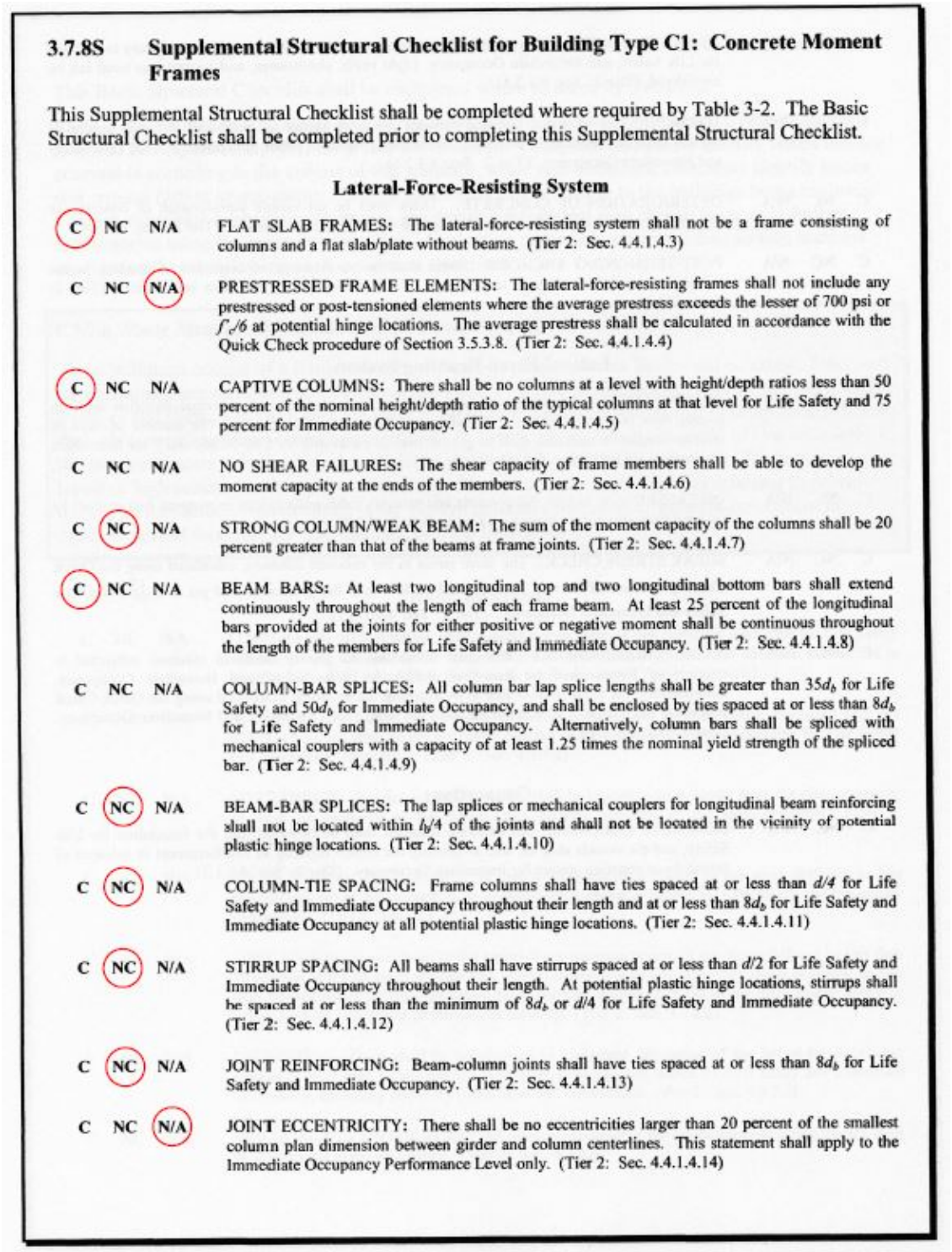

3.7.8S Supplemental Structural Checklist for Building Type C1: Concrete Moment Frames

This Supplemental Structural Checklist shall be completed where required by Table 3-2. The Basic Structural Checklist shall be completed prior to completing this Supplemental Structural Checklist.

Lateral-Force-Resisting System

(C)	NC	N/A	FLAT SLAB FRAMES: The lateral-force-resisting system shall not be a frame consisting of columns and a flat slab/plate without beams. (Tier 2: Sec. 4.4.1.4.3)
C	NC	(N/A)	PRESTRESSED FRAME ELEMENTS: The lateral-force-resisting frames shall not include any prestressed or post-tensioned elements where the average prestress exceeds the lesser of 700 psi or $f'_c/6$ at potential hinge locations. The average prestress shall be calculated in accordance with the Quick Check procedure of Section 3.5.3.8. (Tier 2: Sec. 4.4.1.4.4)
(C)	NC	N/A	CAPTIVE COLUMNS: There shall be no columns at a level with height/depth ratios less than 50 percent of the nominal height/depth ratio of the typical columns at that level for Life Safety and 75 percent for Immediate Occupancy. (Tier 2: Sec. 4.4.1.4.5)
C	NC	N/A	NO SHEAR FAILURES: The shear capacity of frame members shall be able to develop the moment capacity at the ends of the members. (Tier 2: Sec. 4.4.1.4.6)
C	(NC)	N/A	STRONG COLUMN/WEAK BEAM: The sum of the moment capacity of the columns shall be 20 percent greater than that of the beams at frame joints. (Tier 2: Sec. 4.4.1.4.7)
(C)	NC	N/A	BEAM BARS: At least two longitudinal top and two longitudinal bottom bars shall extend continuously throughout the length of each frame beam. At least 25 percent of the longitudinal bars provided at the joints for either positive or negative moment shall be continuous throughout the length of the members for Life Safety and Immediate Occupancy. (Tier 2: Sec. 4.4.1.4.8)
C	NC	N/A	COLUMN-BAR SPLICES: All column bar lap splice lengths shall be greater than $35d_b$ for Life Safety and $50d_b$ for Immediate Occupancy, and shall be enclosed by ties spaced at or less than $8d_b$ for Life Safety and Immediate Occupancy. Alternatively, column bars shall be spliced with mechanical couplers with a capacity of at least 1.25 times the nominal yield strength of the spliced bar. (Tier 2: Sec. 4.4.1.4.9)
C	(NC)	N/A	BEAM-BAR SPLICES: The lap splices or mechanical couplers for longitudinal beam reinforcing shall not be located within $l_b/4$ of the joints and shall not be located in the vicinity of potential plastic hinge locations. (Tier 2: Sec. 4.4.1.4.10)
C	(NC)	N/A	COLUMN-TIE SPACING: Frame columns shall have ties spaced at or less than $d/4$ for Life Safety and Immediate Occupancy throughout their length and at or less than $8d_b$ for Life Safety and Immediate Occupancy at all potential plastic hinge locations. (Tier 2: Sec. 4.4.1.4.11)
C	(NC)	N/A	STIRRUP SPACING: All beams shall have stirrups spaced at or less than $d/2$ for Life Safety and Immediate Occupancy throughout their length. At potential plastic hinge locations, stirrups shall be spaced at or less than the minimum of $8d_b$ or $d/4$ for Life Safety and Immediate Occupancy. (Tier 2: Sec. 4.4.1.4.12)
C	(NC)	N/A	JOINT REINFORCING: Beam-column joints shall have ties spaced at or less than $8d_b$ for Life Safety and Immediate Occupancy. (Tier 2: Sec. 4.4.1.4.13)
C	NC	(N/A)	JOINT ECCENTRICITY: There shall be no eccentricities larger than 20 percent of the smallest column plan dimension between girder and column centerlines. This statement shall apply to the Immediate Occupancy Performance Level only. (Tier 2: Sec. 4.4.1.4.14)

Figure 4.1: Tier 1 Checklist for Concrete Moment Frame (C1) per ASCE 31-03 Standard Format [ASCE-31, 2004]

Table 4.1 shows a compilation of results for the more critical checks across the inventory of buildings. Summary descriptions for the individual criteria as shown in the the table are provided below. These definitions are sourced from ASCE-41 [2014], as the current edition of this Standard at time of study, and pertain specifically to *Checklist 16.1.2LS* for *Life Safety Basic Configuration* and *Checklist 16.9LS* for *Life Safety for Building Type C1.*

- Load Path: The structure shall contain a complete, well defined load path, including structural elements and connections, that serves to transfer the inertial forces associated with the mass of all elements of the building to the foundation.
- Vertical Irregularities: All vertical elements in the seismic-force-resisting system are continuous to the foundation.
- Geometry: There are no changes in the net horizontal dimension of the seismic-force-resisting system of more than 30% in a story relative to adjacent stories, excluding one-story penthouses and mezzanines.
- Mass: There is no change in effective mass more than 50% from one story to the next. Light roofs, penthouses, and mezzanines need not be considered.
- Torsion: The estimated distance between the story center of mass and the story center of rigidity is less than 20% of the building width in either plan dimension.
- Redundancy: The number of lines of moment frames in each principal direction is greater than or equal to 2. The number of bays of moment frames in each line is greater than or equal to 2.
- Column Axial Stress: The axial stress caused by unfactored gravity loads in columns subjected to overturning forces because of seismic demands is less than $0.20f'_c$.
- Column Shear Stress: The shear stress in the concrete columns, calculated using the Quick Check procedure of *Section 4.5.3.2*, is less than the greater of $100psi$ or $2\sqrt{f'_c}$.

- Flat Slab Frames: The seismic-force-resisting system is not a frame consisting of columns and a flat slab or plate without beams.
- Captive Columns: There are no columns at a level with height/depth ratios less than 50% of the nominal height/depth ratio of the typical columns at that level.
- No Shear Failures: The shear capacity of frame members is able to develop the moment capacity at the ends of the members.
- Strong Column–Weak Beam (SCWB): The sum of the moment capacity of the columns is 20% greater than that of the beams at frame joints.
- Column-Tie Spacing: Frame columns have ties spaced at or less than $d/4$ throughout their length and at or less than $8d_b$ at all potential plastic hinge locations. Variable d is the column effective depth to longitudinal reinforcement, and d_b is the longitudinal reinforcement bar diameter.
- Stirrup Spacing: All beams have stirrups spaced at or less than $d/2$ throughout their length. At potential plastic hinge locations, stirrups are spaced at or less than the minimum of $8d_b$ or $d/4$. Variables are as defined for Column-Tie Spacing.
- Joint Reinforcing: Beam–column joints have ties spaced at or less than $8d_b$.
- Diaphragm Discontinuity: The diaphragms are not composed of split-level floors and do not have expansion joints.

Table 4.1: Summary of Key Tier-1 *Quick-Checks* for Selected Buildings

Tier 1 Checklist Legend	
✓	Compliant
✗	Noncompliant
NA	Not Applicable
NC	Not Checked
MF	Moment Frame

	Xingfu Bldg.	**Guiren District Apt.**	**Nanhau District Office**	**Shanshang District Office**	**Zhouzheng District Office**	**Yujing Elementary, NW Wing**	**Yujing Elementary, W Wing**	**Yujing Jr. High, Special Classroom**	**Guiren Jr. high, Guanghua Bldg.**
Lateral System	MF	MF	MF	MF	MF	MF	MF	MF	MF
Number of Stories	7	4	3	3	3	2	3	3	3
Load Path	✓	✓	✓	✓	✓	✗	✓	✓	✓
Vertical Discontinuities	✓	✓	✓	✓	✓	✓	✓	✓	✓
Geometry	✓	✓	✓	✓	✓	✓	✓	✓	✓
Mass	✓	✓	✓	✓	✓	✓	✓	✓	✓
Torsion	✗	✓	✗	✗	✗	✓	✓	✓	✓
Redundancy	✓	✓	✓	✓	✓	✓	✓	✓	✓
Column Axial Stress	✓	✓	✓	✓	✓	✓	✓	✓	✓
Column Shear Stress	✗	✗	✓	✗	✗	✗	✗	✗	✗
Flat Slab Frames	✓	✓	✓	✓	✓	✓	✓	✓	✓
Captive Columns	✓	✓	✓	✓	✓	✓	✓	✓	✓
No Shear Failures	✓	✓	✓	✓	✓	✓	✓	✓	✓
SCWB	✓	✓	✗	✗	✗	✗	✓	✗	✓
Column-Tie Spacing	✓	✗	✗	✗	✗	✗	✗	✗	✗
Stirrup Spacing	✓	✗	✗	✓	✓	✓	✓	✓	✓
Joint Reinforcing	✗	✓	✓	✗	✗	✗	✗	✗	✓
Diaphragm Continuity	✓	✓	✓	✓	✓	✓	✓	✓	✓

4.3 Tier 1 Evaluation

In synopsis of the summary results for the building inventory, the Tier 1 Screening resulted in identification of the following deficiencies among the standard checklist items:

1. Column Shear Stress: consistently high calculated shear stresses.
2. Strong Column-Weak Beam: moment ratios in excess of the permissible ratio of 1.2 in cases of observed soft-story damage mechanisms.
3. Column-Tie Spacing: column details reveal locations along the column height where the transverse reinforcement was spaced wider than $^{d}/_{4}$.

All three of these deficiencies were investigated further. Their consistency in violation across all buildings in the inventory highlights a distinct concern for this type of structure.

4.3.1 Shear Demand-to-Capacity Ratio

The first item required an investigation into the ASCE 41 Tier 1 approach to assess the likelihood of shear failure in a column. As stands, the calculation is rudimentary and simplified, and is based on an average shear stress v_j^{avg} as shown in the following equation:

$$v_j^{avg} = \left(\frac{1}{M_s}\right)\left(\frac{n_c}{n_c - n_f}\right)\left(\frac{V_j}{A_c}\right) \tag{4.1}$$

where n_c is the total number of columns, n_f is the total number of frames in the direction of loading, V_j is the story shear based on a pseudo-static analysis similar to ASCE 7-10, A_c is the total summation of all column cross-sections, M_s is a system modification factor, and all other variables are as defined earlier in this document. This equation assumes that all columns in the frame(s) have similar stiffness and that the end columns carry half the load as compared to the interior columns. It also assumes a uniform distribution of the shear demand across the structure. On the capacity side of the ratio, the criterion permits use of a lower-bound estimate that does not take into consideration the axial load ratio.

It is likely that all buildings, including new buildings, would likely fail this limit state. Since it is well known that shear vulnerability results from the plastic shear demand exceeding the shear capacity, different approaches to determine a new shear capacity to compare against a calculated plastic shear demand. Equations 4.2 to 4.4 present four different expressions for the nominal shear capacity, V_n, as defined by different codes and provisions:

- ACI 318-14, Concrete Material Standard

$$V_n = \left(\frac{A_v f_{yt} d}{s}\right) + 2\lambda\sqrt{f'_c} b_w d \times \left(1 + \frac{N_u}{2000 A_g}\right) \tag{4.2}$$

- ASCE 41-13, Chapter 10 for Concrete Materials

$$V_n = k\left[\left(\frac{A_v f_y d}{s}\right) + \lambda\left(\frac{6\sqrt{f'_c}}{M/(V*d)} \times \sqrt{1 + \frac{N_u}{6\sqrt{f'_{ce}} A_g}}\right) 0.8 A_g\right] \tag{4.3}$$

- ASCE 41-17, Chapter 10 for Concrete Materials

$$V_n = k_{nl}\left[\alpha_{Col}\left(\frac{A_v f_{ytE} d}{s}\right) + \lambda\left(\frac{6\sqrt{f'_{cE}}}{M_{UD}/(V_{UD}*d)} \times \sqrt{1 + \frac{N_{UG}}{6\sqrt{f'_{cE}} A_g}}\right) 0.8 A_g\right] \tag{4.4}$$

- ATC 78(-7), Screening Provision for Collapse Potential of RC Structures

$$V_n = V_n \text{ from Equation 4.4, but with } k_{nl} \text{ assumed equal to 1.0} \tag{4.5}$$

where V_n is the nominal shear capacity defined by different codes and provisions, A_g is the gross cross-sectional area of the column; A_v is the area of shear reinforcement; b_w is the column width; d is the effective column depth; s is the spacing of shear reinforcement; f_{yt} is the yield strength of transverse reinforcing steel using expected, e or E, material strength; N_u and N_{UG} are representations for the axial compressive force due to gravity; $M/(V*d)$ and $M_{UD}/(V_{UD}*d)$ represent the largest ratio of moment to shear under design loading condition, but not less than 2 or greater than 4; k and k_{nl} represent a shear strength degradation factor based on displacement ductility demand (value assumed at the lower bound as 0.70); α_{col} is a reduction factor attributed to the steel contribution that depends on s/d; λ is a factor to adjust for lightweight concrete; and all other variables are as defined earlier in this document.

As for the demand calculation, the plastic shear demand, V_p, is based on flexural hinging at the top and bottom of the column resulting in a constant shear demand:

$$V_p = \frac{2M_n}{l_{inf}} \tag{4.6}$$

where M_n is the nominal moment capacity using expected material strength, l_{inf} is taken as half of the column unbraced length, l_u, and all other variables are as defined earlier in this document.

Figure 4.2 gives a comparative summary of the equations as the ratio of plastic shear demand, V_p, to calculated shear capacity, V_n. Supplemental to the standard equations for nominal shear capacity, an additional consideration was made to implement a limit state model developed at the University of Washington (UW) [Hua et al., 2018]. Column bars reflect the average ratio across all columns with observed damage. Maximum and minimum values are plotted with square symbols. Error bars reflect a single standard deviation. Only the primary orientation of damage (plan East-West) is shown. A horizontal line indicates the failure DCR of 1.0.

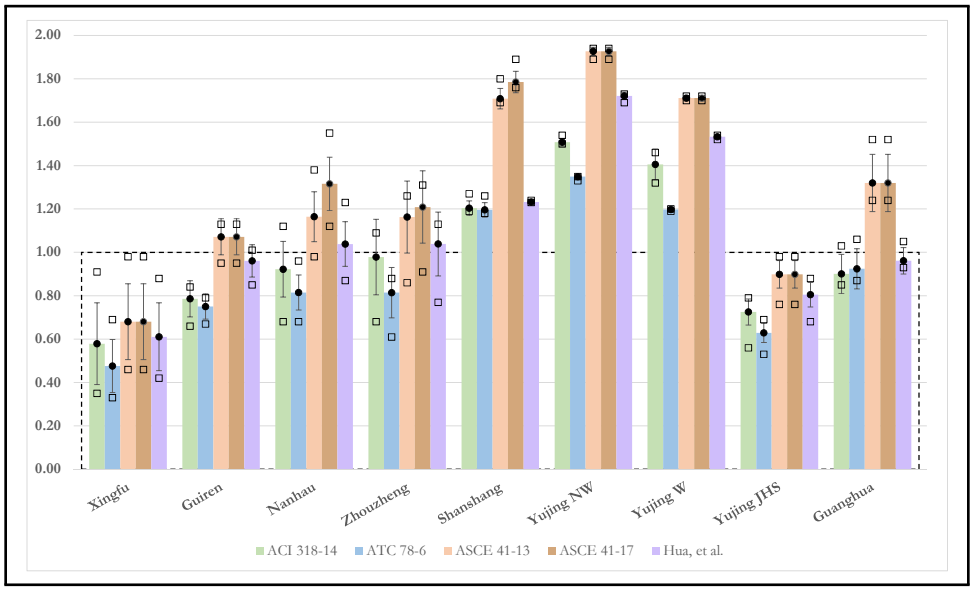

Figure 4.2: Comparison of Shear DCR Expressions, as $^{V_P}/_{V_n}$

4.3.2 Column-to-Beam Moment Ratio

The second item pertains to an out-of-date limit for the SCWB criterion. It has been well-established that a column-to-beam moment ratio (CBMR) of 1.2 is not sufficient to develop a full-frame plastic mechanism. For buildings investigated as part of this project, soft-story failure was was the primary damage mode. This is true even for structures to which the CBMR was calculated above 1.20. Figure 4.3 gives the average calculation as the ratio of column moment capacity, M_{nc}, to beam moment capacity, M_{nb}, where the capacity was calculated using expected material strength. Values are respective for only columns with observed damage. Maximum and minimum values are plotted with square symbols. Error bars reflect a single standard deviation. The direction of bending (necessary for identifying component local axes) corresponds with the direction of damage to the structure (denoted as plan EW). A horizontal line indicates the failure criterion of 1.2.

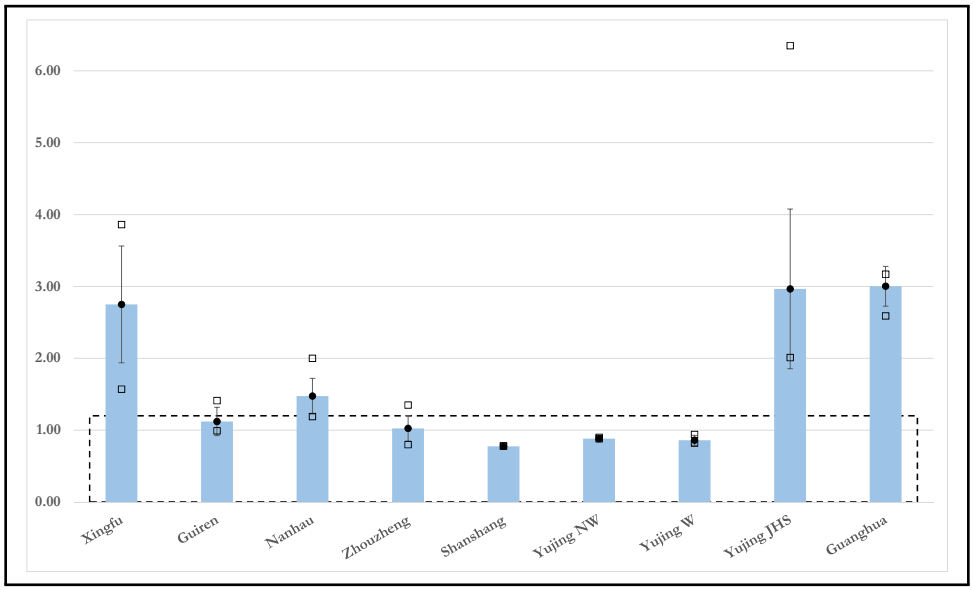

Figure 4.3: Calculated Average First-Story CBMR, as $^{\Sigma M_{nc}}/_{\Sigma M_{nb}}$

4.3.3 Column-Tie Spacing

The third item makes reference to the design standards in practice at the time of construction of the buildings. Most of the structures, with the exception of Xingfu, were built between the 1960s and 1980s. It can be assumed by the detail drawings, pertinent to column-tie spacing, that seismic engineering and ductile detailing were not considered. As such, it is expected that this criterion would fail when held against older design practices without specific seismic requirements. Given that widely spaced column ties greatly reduce the deformation capability of a column, this item is a good check on seismic vulnerability.

4.4 Observations and Recommendations for Improvement

Based on the analysis and investigation above, the following observations and recommendations are an outcome of this evaluation:

- The Tier 1 evaluation identified columns as potentially vulnerable components, which was consistent with the observed damage. Commonly identified vulnerabilities include:

column shear stress, strong-column-weak-beam, column-tie spacing, and joint reinforcing. Many of which are associated with non-ductile seismic performance, which is consistent with post-earthquake damage.

- For all of the damaged buildings, the outcome of this evaluation indicates that the observed structural damage would be likely. This outcome motivates the need for further, more rigorous, investigation or the design of a retrofit measure.

- Results indicate the evaluation procedure under-estimates column shear demand and over-estimates column shear strength for the case of shear failure or shear-controlled response. This was commonly identified for columns that exhibited post-earthquake diagonal cracking. The calculation of column shear stress assumes that the base shear distributes up the height of the structure. This criteria, as written, would likely deem insufficient many new structures for which are designed considering different limit states. Based on this conclusion, a different approach was evaluated, using the plastic shear demand, based on the flexural capacity, and different shear strength expressions.

- Five different expressions for column shear capacity, V_n, were evaluated against the observed column damage: ACI 318-14, ATC 78-7, ASCE 41-13, ASCE 41-17 and a new expression by Hua et al. [2018]. Results were shown for only the columns with observed diagonal cracking. It is recommended that V_n be estimated using the existing expression in ASCE 41, but with parameter $k_{nl} = 0.70$. This results in the least suggested change and a sufficient identification of shear vulnerable columns, if not rather conservation.

- It is well established that a CBMR of 1.2 does not guarantee a full frame, beam-yielding plastic mechanism. This limit should be reconsidered if the intent is to identify building susceptible to a soft-story mechanism. Evaluation of the set of damaged buildings here suggests that the limit should be 1.5. This is supported by numerous studies available in the literature.

- Partial-height masonry infill restrains deformation in the columns and may also add deformation restraint to the underlying beams. Many of the damaged buildings contained partial-height infill and also resulted in soft-story damage modes. It is recommended that the presence of partial-height infill be identified and considered in the screening process.

Chapter 5
EVALUATION OF ATC 78-7

5.1 Introduction

The ASCE 41 Tier 1 evaluation presented in Chapter 4 provides a very high-level investigation into the seismic vulnerability of a structure, supported by visual identification and limited calculations. Employing the ASCE 41 Standard, a Tier 1 evaluation may be supplemented with either a Tier 2 or Tier 3 evaluation. Both procedures attempt to provide an enhanced understanding of the system response to strong ground motion and permit quantification of seismic vulnerability based on linear or nonlinear analyses performed on the building system. For a building owner, these secondary evaluations represents a significant financial investment based on the scope of investigation and the desired performance state. The FEMA-funded ATC 78 project was initiated with the objective of providing a cost-effective evaluation procedure to quantify collapse potential based on limited calculation and without explicit modeling. This chapter presents the ATC-78 [2018] evaluation procedure as documented in: *Seismic Evaluation of Older Concrete Buildings for Collapse Potential*. Application of this procedure was performed considering two model buildings: Nanhau District Office and Xingfu Building. Collaboration and review was supported by practicing engineers: Insung Kim (Degenkolb) and Peter Somers (Magnusson Klemencic Associates).

5.2 Procedure Implementation

The procedure is intended for use with non-ductile reinforced concrete structures consisting of either frame (moment framing), frame-wall (coupled moment frame with shear walls), bearing-wall lateral, or infill-wall lateral force resisting systems. Requisites and requirements

of each system type are defined in ATC-78 [2018] *Chapter 5*. The objective of this document aims to provide a more targeted building screening, as compared to the ASCE 41 Tier 1 methodology, while also remaining quick and simple enough for broad implementation. Figure 5.1 gives a drafted flow chart as a condensed summary of the procedure. The flow chart offers a view of the order and organization of report as well as highlights key considerations and substantive calculations. ATC 78 is founded heavily in plastic analysis and on concepts and content within the ASCE 41 standard, though demand and capacity quantities derive empirically from probabilistic assessments of archetypical structures. The report also permits use of alternative methods (e.g. ASCE 41 Standard) for calculating structural parameters to then use within the ATC 78 methodology. Primary focus is placed on *Frame* and *Frame-Wall* structures, as those were the systems investigated per this study.

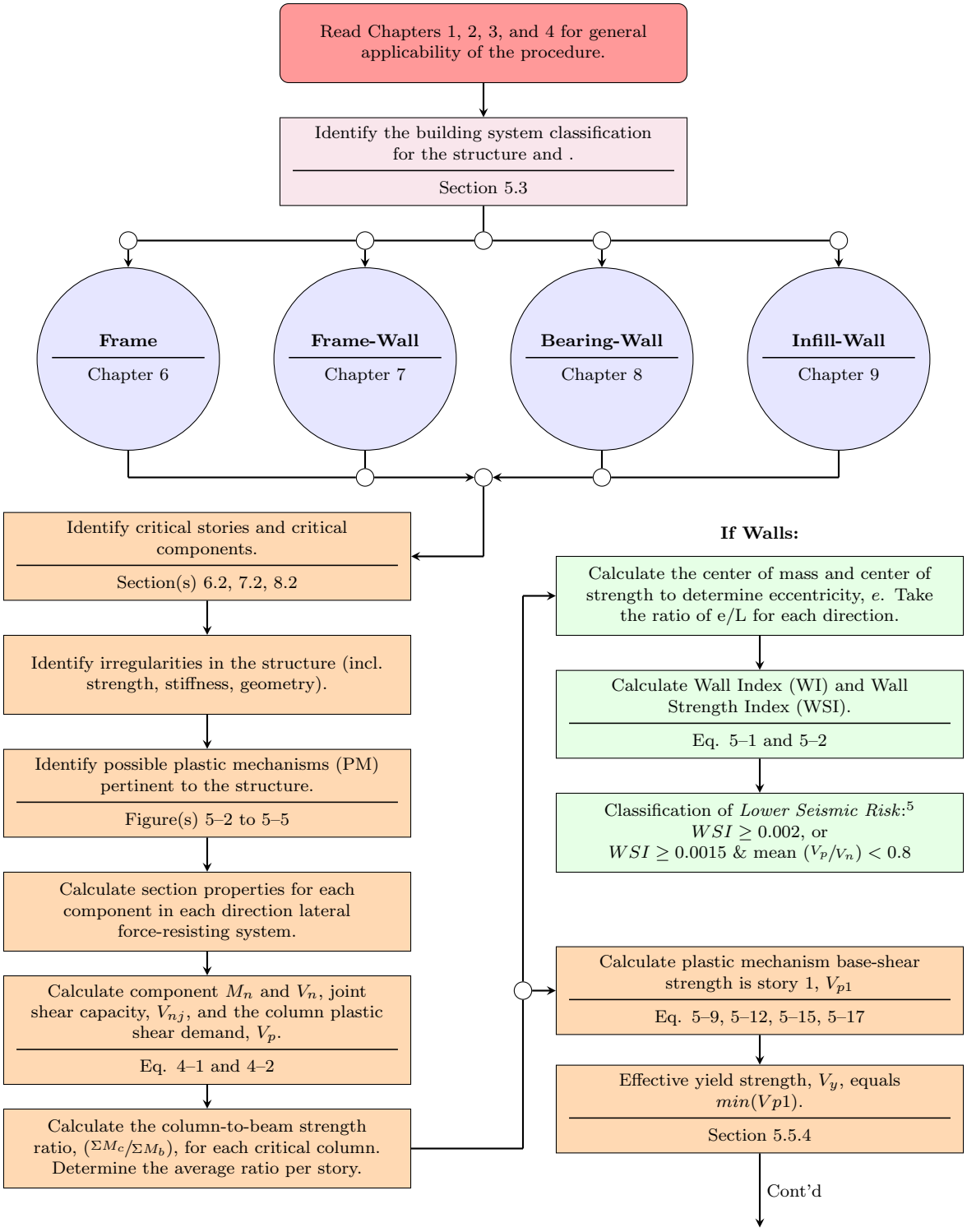
Read Chapters 1, 2, 3, and 4 for general applicability of the procedure.
Identify the building system classification for the structure and .
Section 5.3
Frame
Chapter 6
Frame-Wall
Chapter 7
Bearing-Wall
Chapter 8
Infill-Wall
Chapter 9
Identify critical stories and critical components.
Section(s) 6.2, 7.2, 8.2
Identify irregularities in the structure (incl. strength, stiffness, geometry).
Identify possible plastic mechanisms (PM) pertinent to the structure.
Figure(s) 5–2 to 5–5
Calculate section properties for each component in each direction lateral force-resisting system.
Calculate component M_n and V_n, joint shear capacity, V_{nj}, and the column plastic shear demand, V_p.
Eq. 4–1 and 4–2
Calculate the column-to-beam strength ratio, $(\Sigma M_c/\Sigma M_b)$, for each critical column. Determine the average ratio per story.
If Walls:
Calculate the center of mass and center of strength to determine eccentricity, e. Take the ratio of e/L for each direction.
Calculate Wall Index (WI) and Wall Strength Index (WSI).
Eq. 5–1 and 5–2
Classification of *Lower Seismic Risk*:[5]
$WSI \geq 0.002$, or
$WSI \geq 0.0015$ & mean $(V_p/V_n) < 0.8$
Calculate plastic mechanism base-shear strength is story 1, V_{p1}
Eq. 5–9, 5–12, 5–15, 5–17
Effective yield strength, V_y, equals $min(Vp1)$.
Section 5.5.4
Cont'd

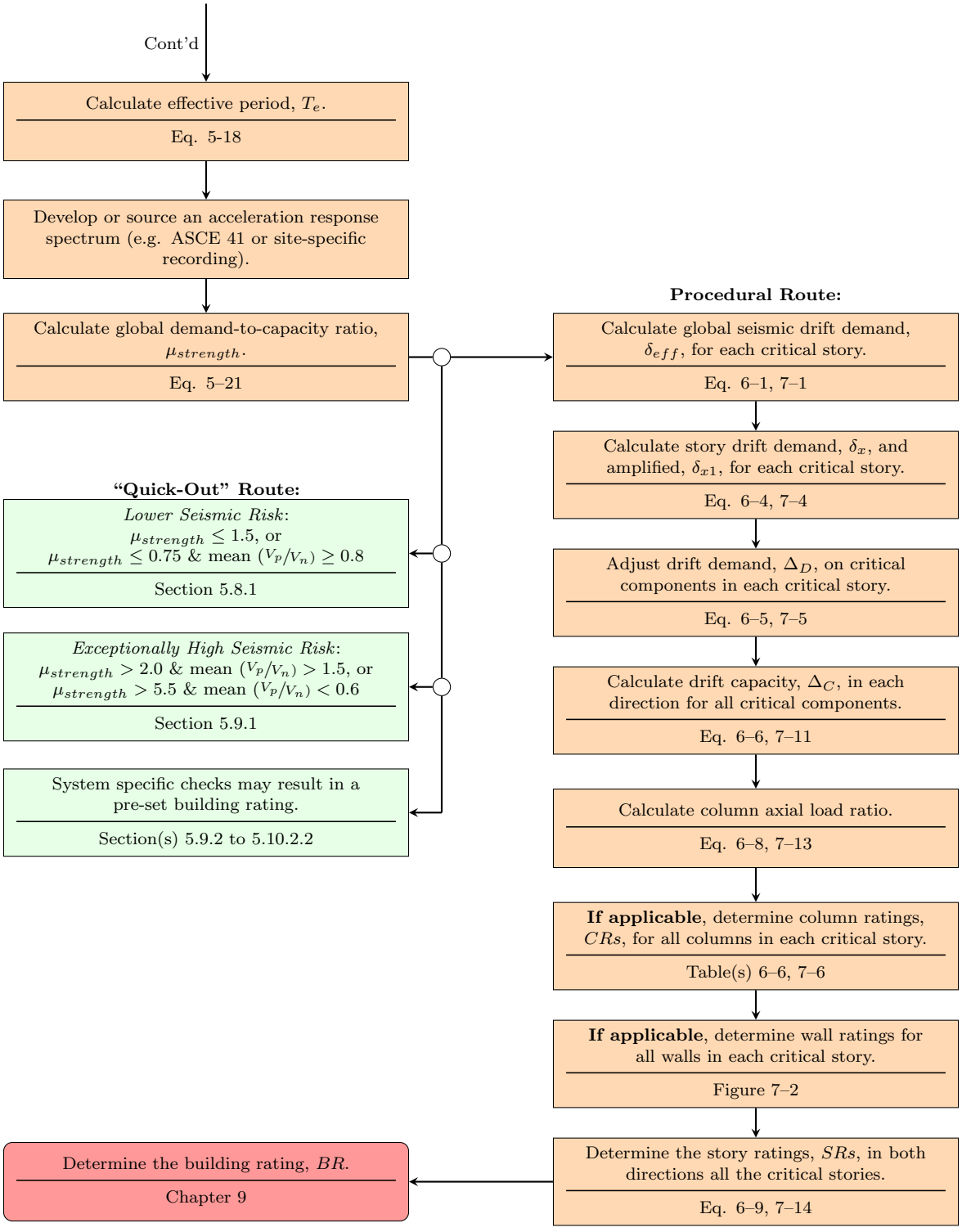

Figure 5.1: Simplified Flow Chart for ATC-78 [2018] *Frame* and *Frame-Wall* Systems

5.2.1 Plastic Mechanism (PM)

With the building system selected, the first step of the procedure involves the identification of all possible plastic mechanisms to which the structure maybe be reasonable susceptible. This requires specific information on individual components of the structure as well as forehand identification of areas of concern and apparent irregularities. The procedure provides a series of calculations to take into account soft-story and distributed beam hinging failure modes as well as two cases of weak or soft stories above the first level. The formation of each mechanism pertains to limit state analysis at which the structure loses axial load carrying capacity. Examples of the first two modes are given in Figure 5.2.

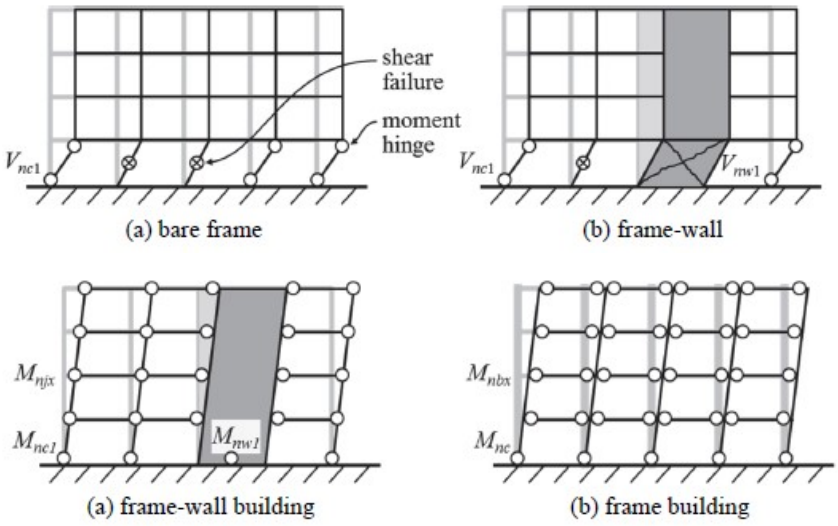

Figure 5.2: Examples of Typical Plastic Mechanisms, #1 (Top) and #2 (Bottom) [ATC-78, 2018]

Explicit calculations assess the strength associated with each PM. The mechanism with the lowest calculated strength is thus predicted most likely collapse mode, as it will trigger at the lowest base shear demand (i.e. manifests the lowest base shear strength). Determination of this value is a function of component strength, structural design, and building configuration. It is permitted that the engineer forego consideration of unlikely

failure modes and focus on the few more relevant to the structure under consideration. The plastic mechanism base-shear strength in story 1, V_{p1}, for PM #1 (soft-story) is as follows:

$$V_{p1} = \Sigma V_{nc1} + \Sigma V_{nw1} \tag{5.1}$$

$$V_{nc1} = min(V_{nc}, \Sigma^{M_{nc}}/_{l_u}) \tag{5.2}$$

$$V_{nw1} = \text{Shear strength of walls per ATC-78 [2018] } \textit{Section 4.3.6} \tag{5.3}$$

where V_{nc1} is the lateral strength of a column in story 1, V_{nc} is the shear strength calculated in accordance with Equation 4.5, ΣM_{nc} is sum of column flexural strength top and bottom, l_u is the column clear height, and all other variables are as defined earlier in this document. The plastic mechanism base-shear strength in story 1, V_{p1}, for PM #2 (distributed beam yielding) is as follows:

$$V_{p1} = \frac{\Sigma M_{nc1} + \Sigma M_{njx} + \Sigma M_{nw1}}{h_{eff}} \tag{5.4}$$

$$M_{njx} = min(\Sigma M_{nc}, \Sigma M_{nb}) \tag{5.5}$$

where M_{njx} is the smallest moment that can be developed at the joint, h_{eff} is the effective height of the lateral force-resisting system (assumed 70% of the total height), and all other variables are as defined earlier in this document. Calculations for mechanism #3 and #4 are not shown but can be referenced in ATC-78 [2018].

The controlling, minimum, value of V_{p1} is to be considered the effective yield strength, V_y, for the building. With acknowledgement that dynamic loading effects the formation of plastic mechanisms, a provision is included for frame-based systems (classifications frame and frame-wall) that a soft-story mechanism (PM #1) controlled unless the strength predicted for distributed beam yielding (PM #2) is less than 75% of PM #1.

For frame and frame-wall structures, the building effective fundamental period, T_e (Equation 5.6), is determined from the effective yield strength as a ratio against the building

seismic weight, W. This equation mirrors the ASCE 41 standard for the Nonlinear Static Procedure. T_e attempts to characterized the effective stiffness (following inelastic deformations). It is at this period that the magnitude of spectral acceleration, S_a, is to be sourced from a design response spectrum. For this study, however, the response spectrum for ground motion recording A730 (Figure 3.5) was employed in place of a design spectrum. The global demand-to-capacity ratio, $\mu_{strength}$ (Equation 5.8), then ties capacity estimates and system parameters into a preliminary prediction of global demand. $\mu_{strength}$ mirrors the calculation of the same quantity in the ASCE 41 standard.

$$T_e = 0.07(h_n)^{0.5}(V_y/W)^{-0.5} \tag{5.6}$$

$$S_a = f(T_e) \tag{5.7}$$

$$\mu_{strength} = \frac{S_a}{V_y/W} C_m \tag{5.8}$$

where h_n is the total height of the building, C_m is an effective mass factor, and all other variables are as defined earlier in this document.

5.2.2 "Quick-Outs"

Several instances in the procedure flag exit conditions based on system properties or calculated values. These instances, termed "Quick-Outs," acknowledge that the procedure is intended as a screening tool applicable to a large variety of RC structures. Given the inherent breathe of possible use, but simplified objectives, it is necessary for certain conditions to trigger a pre-determined assignment of risk. This is similar to use restrictions in ASCE 41 linear analysis methods in cases of extreme irregularities, that the system characteristics simply fall outside the scope and the provisions within cannot be employed for a reliable estimate of performance. One example of a "Quick-out" pertains to the calculated value of $\mu_{strength}$ relative to the column plastic shear DCR, though several exist in the procedure. When the value of $\mu_{strength}$ is sufficiently low, the structure is assumed exceptionally strong (*lower seismic*

risk) and thus no reason for further evaluation. However, high values of $\mu_{strength}$ outright indicate severe seismic deficiencies (*exceptionally high seismic risk*) for which continuation of the evaluation is unnecessary. In either case, the exit condition is permissible based on built-in probabilistic data and exists to save time during the evaluation process at extreme ends of structural performance.

5.2.3 Deformation Demand

Global seismic drift demand, δ_{eff} (Equation 5.9), is calculated by idealizing the structure as a single-degree-of-freedom (SDOF) system, translated into projected story drift demands, δ_x (Equation 5.10), and modified based on flexural demands and torsional amplification for a per-component adjusted drift demand, Δ_D (Equation 5.14). To account for P-Delta effects, δ_x is increased to an amplified story drift demand, δ_{x1} (Equation 5.13). These calculations pertain only to critical components in critical stories for which Δ_D is associated with individual columns.

$$\delta_{eff} = C_1 C_2 S_a \frac{T_e^2}{4\pi^2} g \tag{5.9}$$

$$\delta_x = \alpha_x h_{sx} \left(\frac{\delta_{eff}}{h_{eff}}\right) \tag{5.10}$$

$$C_1 = 1 + \frac{\mu_{strength} - 1}{a T_e^2} \tag{5.11}$$

$$C_2 = 1 + \frac{1}{800}\left(\frac{\mu_{strength} - 1}{T_e}\right)^2 \tag{5.12}$$

$$\delta_{x1} = \delta_x \left[\frac{1}{1 - (W_x \delta_x)/(V_{px} h_x)}\right] \tag{5.13}$$

$$\Delta_D = A_T \gamma \delta_{x1} \tag{5.14}$$

where C_1 is a modification factor to relate expected maximum inelastic displacement to displacement calculated for linear elastic response, C_2 is a modification factor to represent the effect of pinched hysteresis shape, cyclic stiffness degradation, and strength deterioration on maximum displacement response, g is the acceleration of gravity, a is a site class factor

equal to 60 for Site Class D, E, and F, h_x and h_{sx} are the height of story x, W_x is the seismic weight above story x, V_{px} is the plastic mechanism shear strength at story x, A_T is a torsional amplification factor, γ is a drift factor representing fraction of story drift affecting the component, α_x is a coefficient to modify story drifts considering number of stories in a building, the yield mechanism, and whether the story is a critical story and all other variables are as defined earlier in this document.

5.2.4 Deformation Capacity

For columns, plastic rotation capacity, θ_c, is determined primarily on the basis of response mode: *flexure-controlled* (FC), *flexure-shear* (FS), and *shear-critical* (SC) and also on the basis of axial load ratio. A column is classified as FC if the plastic shear demand ratio is low ($V_p/V_n \leq 0.6$), the reinforcement detailing is modest ($\rho_t > 0.2\%$), and the ratio of transverse reinforcement spacing to column effective depth ($s/d < 0.5$). Columns not classified as FC are designated as FS or SC without distinction made between the two response modes. This deviates from ASCE-41 [2014] *Table 10-11*, in that the classification of FS pertains to columns with ($1.0 \geq V_p/V_n > 0.6$) and SC for all cases where ($1.0 > V_p/V_n$). Table 5.1 presents equations that calculate θ_c per deformation mode classification:

Table 5.1: Column Plastic Rotation Capacity, θ_c, per Response Mode, for Tied Columns

FC $\implies \langle V_p/V_n \leq 0.60$ and $\rho_t > 0.002$ and $s/d < 0.50 \rangle$,		
$\theta_c = 11.4\rho_t + 0.034 - \left(\frac{P}{A_g f'_{ce}}\right)(14\rho_t + 0.036) \geq 0.0$	if	$\left(\frac{P}{A_g f'_{ce}}\right) \geq 0.10$
$\theta_c = 1.15\left[10\rho_t + 0.03\right] \geq 0.0$	if	$\left(\frac{P}{A_g f'_{ce}}\right) < 0.10$
FS or SC $\implies$ otherwise,		
$\theta_c = \frac{0.65}{5 + \left(\frac{P}{0.8 A_g f'_{ce}}\right)(1/\rho_t)(f'_{ce}/f_{ye})} \geq \theta_{c,min}$		

where ρ_t is the transverse steel reinforcement ratio, P is the component axial load considering both gravity and overturning forces, and all other variables are as defined earlier in this document. For classifications of FS and SC, the calculated value of θ_c must be reduced linearly from it's value at axial load ratio ($\frac{P}{A_g f'_{ce}} = 0.5$) to zero at ($\frac{P}{A_g f'_{ce}} = 0.7$). Column drift capacity, Δ_C (Equation 5.16), is the calculated from θ_c with respect to a minimum value of plastic rotation capacity, $\theta_{c,min}$ (Equation 5.15).

$$\theta_{c,min} = 0.42 - 0.23(\frac{P}{A_g f'_{ce}}) + 0.63\rho_t - 0.023(V_p/V_n) \geq 0.0 \tag{5.15}$$

$$\Delta_C = l_u[\theta_c + 0.01] \tag{5.16}$$

where all variables are as defined earlier in this document. Separate conditions are specified for the capacity of corner connections and for walls and wall segments. Appendix A in ATC 78-7 makes reference to ASCE 41-13 tables and mechanics-based-equations in the development of expressions for plastic rotation quantities as a statistically median estimate. Reference is made to experimental tests on concrete columns and models developed by [Elwood and P. Moehle, 2005] and [Ghannoum and Matamoros, 2014].

5.2.5 Column Ratings

Table 5.2 defines column ratings, CRs, which range from 0.0 to 0.93, based on the deformation DCR (Δ_D/Δ_C). The magnitude of CR represents "the relative likelihood that an individual column... will lose its ability to support vertical loads under the assumed earthquake loading" [ATC-78, 2018].

Table 5.2: Column Rating Assignment

Magnitude of $\left(\Delta_D/\Delta_C\right)$	CR
$\left(\Delta_D/\Delta_C\right) \geq 0.25$	0.0
$0.25 \geq \left(\Delta_D/\Delta_C\right) > 0.25$	0.1
$0.4 \geq \left(\Delta_D/\Delta_C\right) > 0.4$	0.2
$0.5 \geq \left(\Delta_D/\Delta_C\right) > 0.5$	0.3
$0.7 \geq \left(\Delta_D/\Delta_C\right) > 0.7$	0.4
$0.9 \geq \left(\Delta_D/\Delta_C\right) > 0.9$	0.5
$1.1 \geq \left(\Delta_D/\Delta_C\right) > 1.1$	0.6
$1.4 \geq \left(\Delta_D/\Delta_C\right) > 1.4$	0.7
$1.8 \geq \left(\Delta_D/\Delta_C\right) > 1.8$	0.8
$2.5 \geq \left(\Delta_D/\Delta_C\right) > 2.5$	0.9
$\left(\Delta_D/\Delta_C\right) > 3.0$	0.93

5.2.6 Story Ratings

Story Ratings, SRs, are computed as the weighted and adjusted average of the column ratings (or critical component ratios for buildings with walls). Equations 5.17 to 5.19 present the process used for calculating values of SR per critical story.

$$SR = 1.5R_{adj} - 0.1 \tag{5.17}$$

$$R_{adj} = R_{avg} + 0.625R_{avg}(COV - 0.4) \tag{5.18}$$

$$R_{avg} = \sum_{i=1}^{n_{col}} f_{col,i} \times CR_i \tag{5.19}$$

where COV is the standard deviation of all the column ratings at a story divided by the weighted average column rating, R_{avg}, at that story, R_{adj} is the adjusted average column rating in the story, i is an identifier of the current column iteration, n_{col} is the total number of columns in a story, $f_{col,i}$ is the fraction of gravity loads supported by column i with total sum value of 1.0, and all other variables are as defined earlier in this document.

5.2.7 Building Rating

Global collapse vulnerability is quantified by the resultant building rating, BR, ranges from 0 to 1.0 and is calculated as the maximum SR of any critical story considering both principal orthogonal directions. Seismic risk is assigned per the magnitude of BR: *lower seismic risk* for ($0 \leq BR < 0.3$), *high seismic risk* for ($0.3 \leq BR < 0.7$), and *exceptionally high seismic risk* for ($BR \geq 0.70$). Whereas this number does not hold independent significant meaning, the purpose behind condensing a building system down to a single, numerical representation of collapse potential allows for comparative ranking of multiple structures.

5.3 Evaluation of Nanhau

This section summarizes the application of the ATC-78 [2018] evaluation procedure as applied to the Nanhau District Office. Implementation of this procedure was based funding provided

by ATC.

The Nanhau District Office comprised RC moment frames in both orthogonal directions. Full-height masonry infill located at the west end of the building, and partial-height masonry infill was present in most exterior frame bays. This structure was classified as a *Frame* building per ATC-78 [2018] terminology; *Infill-Wall* classification was not applicable given the significant percentage of partial-height infill violating the limitations of allowable open area. Component details were sourced from data collected during the post-earthquake reconnaissance (as described in Chapter 3). Collapse risk analysis was performed per ATC-78 [2018] *Chapters 5* and *6*. Figure 3.9 shows the first story column layout for the building, redrawn from construction documents. Given the symmetry of the structural layout, all calculations considered only the left half of the structure.

Table 5.3 gives the calculated plastic mechanism base-shear strength of story 1, V_{p1}, for both soft-story hinging (PM #1) and distributed beam yielding (PM #2). The other two mechanisms were not considered due to the regular geometry and component layout up the height of the building.

Table 5.3: Plastic Mechanism Base-Shear Strength, V_{p1}

Direction		PM #1	PM #2	Units
X	=	1066	588	kip
Y	=	1319	994	kip

Based on minimum calculated value, PM #2 would be predicted to control for both building directions. However, because the value of PM #2 in the Y-direction is not less than 75% of PM #1, PM #1 controls. Effective yield strength, V_y, for the X and Y building-directions is thus calculated at $588kip$ and $1319kip$, respectively. This outcome predicts a higher collapse vulnerability in the X-direction based on lower calculated strength. This is consistent with the observed damage having manifested primarily in the long, X, building-

direction. However, the observed damage disagrees with the predicted failure mode in that the majority of damage was concentrated within the first story. Much of the damage resulted in diagonal cracking at the tops and bottoms of columns with limited to no indication of damage into the beams or stories above the first level.

In spite of the inconsistency between predicted collapse mode and post-event observations, the intent of this evaluation was to proceed with the analysis of the structure. Table 5.4 presents key structural parameters for each primary orthogonal direction. Section 5.2.1 gives a more detailed explanation towards the calculation of the following quantities.

Table 5.4: Nanhau System Properties

Direction		V_y [kip]	V_y/W	T_e [sec]	S_a [g]	$\mu_{strength}$
X	=	588	0.24	0.88	0.35	1.3
Y	=	1319	0.54	0.58	0.73	1.2

The bulk of the analysis targeted the component-level response (demand and capacity) for the columns of the first story. No modifications were made to account for torsion, as it is neglected for *Frame* buildings. Column response is calculated for each orthogonal direction. Deformation demand and capacity follow the description and equations detailed in Sections 5.2.3 and 5.2.4. DCR values establish the basis for collapse vulnerability assessment. Column ratings, CRs, and story ratings, SRs, then follow the procedure as described in Sections 5.2.5 and 5.2.6. The total building rating, BR, is taken as the maximum story rating in either direction. Table 5.5 gives a summary tabulation of the key results for each step.

Table 5.5: Nanhau Column Response

X-direction

Line	Frame A					Frame C					Frame D		
Column	A1	A2	A3	A4	A5	C1	C2	C3	C4	C5	D4	D5	Units
(P_g/P_n)	3.1%	8.7%	8.8%	8.8%	9.5%	3.1%	8.7%	8.8%	12.0%	14.3%	4.2%	4.4%	kip
(M_{nc}/M_{nb})	1.87	1.44	1.44	1.44	1.16	1.87	1.44	1.44	1.55	1.20	1.58	0.76	
Δ_D	1.01	1.28	1.28	1.28	1.46	1.01	1.28	1.28	1.22	1.44	1.19	1.77	in
Δ_C	4.03	3.26	3.25	3.11	2.92	4.03	3.26	3.25	3.11	4.18	3.82	3.84	in
(Δ_D/Δ_C)	0.25	0.39	0.40	0.41	0.50	0.25	0.39	0.40	0.39	0.34	0.31	0.46	
CR	0.1	0.1	0.1	0.2	0.3	0.1	0.1	0.1	0.1	0.1	0.1	0.2	
$R_{avg,i}$	0	0.01	0.01	0.02	0.03	0	0.01	0.01	0.01	0.02	0	0.01	
R_{avg}	0.13												
SR	0.11												

Y-direction

Line	Frame 1			Frame 2		Frame 3		Frame 4			Frame 5			
Column	A1	B1	C1	A2	C2	A3	C3	A4	C4	D4	A5	C5	D5	Units
(P_g/P_n)	3.1%	9.0%	3.1%	8.7%	8.7%	8.8%	8.8%	8.8%	12.0%	4.2%	9.5%	14.3%	4.4%	
(M_{nc}/M_{nb})	1.78	0.72	1.78	0.89	0.89	0.89	0.89	0.67	0.61	2.15	0.67	0.58	0.92	
Δ_D	1.21	2.04	1.21	1.88	1.88	1.88	1.88	2.09	2.14	0.94	2.09	2.16	1.86	in
Δ_C	3.39	3.46	3.39	3.98	3.98	3.96	3.96	3.78	2.52	3.18	3.52	3.34	4.81	in
(Δ_D/Δ_C)	0.36	0.59	0.36	0.47	0.47	0.47	0.47	0.55	0.85	0.30	0.59	0.65	0.39	
CR	0.1	0.3	0.1	0.2	0.2	0.2	0.2	0.3	0.4	0.1	0.3	0.3	0.1	
$R_{avg,i}$	0.00	0.01	0.00	0.02	0.02	0.02	0.02	0.03	0.05	0.00	0.03	0.04	0.00	
R_{avg}	0.25													
SR	0.27													

The evaluation of the building resulted in a BR of 0.27 and the collapse risk classification of *lower seismic risk*. This outcome pertains to a soft-story mechanism controlling in the short, Y, building-direction. Whereas the mechanism predicted is consistent with the observed damage, the directionality is not. Photos of the damage give no indication that the beams yielded at the first story, but rather that the columns 'hinged' (or exhibited shear failure) above the infill before beam yielding. On the matter of risk classification, *lower seismic risk* is likely not appropriate given the observed damage. ATC 78 states that buildings of this classification "should be given lowest priority for further evaluation" [ATC-78, 2018]. This fails to acknowledge that the damage observed was inordinately large relative to the earthquake magnitude. This designation reads as diminutive and inaccurate to the aftermath condition.

5.4 Evaluation of Xingfu

This section summarizes the application of the ATC-78 [2018] evaluation procedure as applied to the Xingfu Building. Implementation of this procedure was based funding provided by ATC.

The Xingfu Building contained RC moment frames, a concrete shear-wall, a concrete stair core, and partial-height masonry infill present in most exterior frame bays. This structure was classified as a *Frame-Wall* building per ATC-78 [2018] terminology; *Infill-Wall* classification was not applicable given the significant percentage of partial-height infill violating the limitations of allowable open area. Component details were sourced from data collected during the post-earthquake reconnaissance (as described in Chapter 3). Collapse risk analysis was performed per ATC-78 [2018] *Chapters 5* and *7*. Figure 3.19 shows the first story column and wall layout, redrawn from construction documents.

Due to the irregular geometry and the non-orthogonal framing of the members, there was no clear distinction of individual frame lines; rather, capacity calculations considered the combined contributions of all columns individually. In order to account for the rotated columns (which would engage in biaxial response), individual calculations were made for

both strong and weak axis demands and capacities. These values were then transformed into north/south quantities (conforming to ground motion directions) by conducting a linear slope interaction between the two local, principal axis and the known 40° positioning off the global horizontal. While a crude approximation in itself, this calculation allowed for some amount of acknowledgement of biaxial bending experienced by the columns.

On the matter of geometric irregularities (indicative of a large torsional vulnerability), this structure may not meet applicability requirements for use of the procedure and would be prematurely designated as *exceptionally high seismic risk*. This study opted to neglect this disqualification and proceed with use of the ATC 78 procedure. Table 5.6 gives the calculated plastic mechanism base-shear strength of story 1, V_{p1}, and also the contribution to V_{p1} due to the walls aligned in that direction. These values are respective only to PM #1. It was elected on the part of this study to only consider the case of soft-story mechanism in reference damage observed from the building collapse state. Photo evidence indicated a probable vulnerability present at the first level, and PM #1 accounts only for the strength contribution at the first level. Section 5.2.1 gives a more detailed explanation towards the calculation of the following quantities.

Table 5.6: Plastic Mechanism (PM) Base Shear Strength, V_{p1}

Direction		V_{w1} [kip]	V_{p1} [kip]	Ratio
X	=	813	2334	35%
Y	=	61	1480	4%

Table 5.7 presents key structural parameters for each global coordinate directions, X and Y, as there was no consistent orthogonality to the structure.

Table 5.7: Xingfu System Properties

Direction		V_y [kip]	V_y/W	T_e [sec]	S_a [g]	$\mu_{strength}$
X	=	2334	0.61	0.77	0.30	0.44
Y	=	1480	0.39	0.96	0.30	0.69

The bulk of the analysis targeted the component-level response (demand and capacity) for the columns of the first story. Additional considerations were required to adjust deformation demands to account for torsional amplification. Column deformation demand was increased based on column location relative to the calculated center of strength. Coordinates of the center of strength were determined in a similar process to the geometric centroid, but with capacity values at corresponding column locations. The result was a linear distribution of amplification factors, A_T, (values equal to or greater than 1.0) that multiplied against the calculated displacement demand. Torsional amplification was computed separately for the global X- and Y-directions.

Column response is calculated for each orthogonal direction. Deformation demand and capacity follow the description and equations detailed in Sections 5.2.3 and 5.2.4. DCR values establish the basis for collapse vulnerability assessment. Column ratings, CRs, and story ratings, SRs, then follow the procedure as described in Sections 5.2.5 and 5.2.6. Calculated wall ratings, WR, are based on the interaction between values of axial load ratio and story drift demand given in ATC-78 [2018] *Figure 7-2*. The total building rating, BR, is taken as the maximum story rating in either direction. Values of calculated WRs are given in Table 5.8. Table 5.9 gives a summary tabulation of the key results for each step, where the WRs are treated as a CRs for additional summation in the weighted average column rating process in determining the SRs.

Table 5.8: Xingfu Wall Rating Averaging

Wall	B	C	E	G	I	D	F	H
X-direction								
(P_g/P_n)	1.7%	1.6%	1.6%	1.6%	14.2%			
WR	0.0	0.0	0.0	0.0	0.0			
$f_{wall,i}$	0.04	0.01	0.01	0.01	0.01			
$R_{avg,i}$	0.0	0.0	0.0	0.0	0.0			
Y-direction								
(P_g/P_n)						1.6%	1.6%	1.6%
WR						0.00	0.00	0.00
$f_{wall,i}$						0.01	0.01	0.02
$R_{avg,i}$						0.00	0.00	0.00

Table 5.9: Xingfu Column Response

X-direction													
Column	C1	C2	C3	C4	C5	C6	C7	C8	C9	C10	C11	C12	Units
(P_g/P_n)	6.9%	8.2%	5.9%	7.3%	5.4%	16.1%	23.2%	18.1%	12.5%	11.2%	25.1%	9.4%	
(M_{nc}/M_{nb})	2.64	2.97	5.93	2.79	3.01	1.75	2.50	1.99	2.02	2.60	3.40	4.00	
A_T	1.31	1.50	2.10	2.35	2.86	1.31	1.50	2.05	2.56	1.31	1.50	1.97	
Δ_D	0.65	0.74	2.35	2.63	3.20	1.05	0.74	3.18	3.89	0.65	1.72	2.20	in
Δ_C	5.99	7.32	9.76	7.03	6.44	3.84	5.32	6.02	6.85	5.09	3.09	5.57	in
(Δ_D/Δ_C)	0.11	0.10	0.24	0.37	0.50	0.27	0.14	0.53	0.57	0.13	0.56	0.40	
CR	0.0	0.0	0.0	0.1	0.2	0.1	0.0	0.3	0.3	0.0	0.3	0.1	
$R_{avg,i}$	0.00	0.00	0.00	0.00	0.01	0.01	0.00	0.03	0.02	0.00	0.06	0.01	
R_{avg}	0.16												
SR	0.14												

Y-direction													
Column	C1	C2	C3	C4	C5	C6	C7	C8	C9	C10	C11	C12	Units
(P_g/P_n)	6.9%	8.2%	5.9%	7.3%	5.4%	16.1%	23.2%	18.1%	12.5%	11.2%	25.1%	9.4%	
(M_{nc}/M_{nb})	3.23	1.83	1.44	1.33	3.23	3.55	2.67	2.16	2.80	3.04	3.33	2.66	
A_T	1.31	1.31	1.07	1.20	1.77	1.05	1.05	1.43	2.01	1.99	1.99	2.47	
Δ_D	1.51	2.32	2.46	2.91	2.13	1.21	1.21	2.12	2.41	2.29	0.98	2.97	in
Δ_C	6.82	8.41	9.31	4.99	7.35	8.28	6.69	6.75	7.84	5.75	3.33	6.31	in
(Δ_D/Δ_C)	0.22	0.28	0.26	0.58	0.29	0.15	0.18	0.31	0.31	0.40	0.30	0.47	
CR	0	0.1	0.1	0.3	0.1	0	0	0.1	0.1	0.1	0.1	0.2	
$R_{avg,i}$	0.00	0.00	0.00	0.01	0.00	0.00	0.00	0.01	0.01	0.01	0.02	0.01	
R_{avg}	0.07												
SR	0.10												

The evaluation of the building resulted in a BR of 0.14 and the collapse risk classification of *lower seismic risk*. This outcome pertains to a soft-story mechanism controlling in the global X-direction. The result, however, is inconsistent with the observed response: full system collapse. An explanation to this discrepancy is that acting mechanism was not a soft-story failure, and thus calculations with this mechanism assumed estimate far too large a capacity. This is exemplified in the building rating. Further investigation into the structural drawings indicate that the columns appear to have been detailed with closely spaced transverse reinforcing. This would have aided in a more ductile behavior, in resistance to soft-story developments. The damage photos identified substantial damage to the joints (a condition not checked with an assumed PM #1) on the collapsed side of the structure. With this in mind, it can be said that the procedure did identify little risk associated with soft-story failure, even if the correct failure mode was not addressed and the risk assessment does not match the damage state.

5.5 Observations and Recommendations for Improvement

Given the differing results of this procedure from the observed damage recorded at the sites of the buildings, the following observations and recommendations are outcomes of this evaluation:

- The ATC 78-7 procedure represents an advancement beyond the ASCE 41 Tier 1 screening as it considers plastic behavior and damage modes to improve assessment of collapse risk. While more rigorous than the ASCE 41 Tier 1 procedure, the process remains relatively quick.

- The use of a building rating system enables prioritization of retrofit across a suite of evaluated structures. This is viewed as a significant strength in comparison with the ASCE standard.

- The calculation of the effective building period, T_e, assumes that the lateral force-resisting system is sufficiently ductile to undergo stable softening (cracking, yielding,

rotation, etc.) without strength loss out to the point of collapse initiation. This is not an appropriate assumption for systems vulnerable to brittle failure modes. Following the earthquake, many columns in Nanhau exhibited diagonal cracking concentrated within the first story.

- The calculation of too long of an effective building period, T_e, when applied to a typical design response spectrum, results in a correspondingly small spectral acceleration. Under-estimating the input demand leads to artificially lower calculated deflections and an unconservative estimate of deformation demand-capacity and building performance. The presence of infill in the system will stiffen the structure an amplify the seismic demand. Partial-height infill is not addressed is the *Infill-Wall* chapter of ATC-78 [2018] and treated only as a reduction of the column effective height.

- For Nanhau, the method fails to predict a soft-story mechanism, resulting from column shear failure, and instead predicts a 'distributed beam yielding' mechanism. This issue could be addressed by reducing the calculated column shear strength, V_n (Equation 4.5), using the ASCE 41 equation and $k_{nl} = 0.70$. This is the same recommendation given for the Tier 1 evaluation. This parameter refers to displacement ductility, though the procedure specifies a constant value of 1.0 as compared to the linear scale (between 1.0 and 0.70) for the same variable in ASCE 41 provisions. Overestimating the shear capacity of columns may be resulting in an overestimate of V_{p1} and thus shifting analysis focus away from the mechanism (soft-story) more representative of building collapse mode.

Chapter 6

EVALUATION OF ASCE 41 TIER 3 LINEAR DYNAMIC PROCEDURE

Further study followed the Tier 1 and ATC 78-7 evaluations through implementation of the ASCE 41 Tier 3 systematic evaluation. More rigorous analysis was segmented into two phases, where the first phase of the Tier 3 evaluation employed a linear time-history analysis through use of SAP2000. Preliminary modeling considered both model buildings, the Nanhau district Office and the Xingfu Building, though analysis was performed exclusively for Nanhau. This chapter discusses the modeling and analysis of four model variations developed from a consistent baseline: 1) without modeled masonry infill, 2) with masonry infill represented by rigid offsets at the base of columns, 3) with masonry infill represented by shell elements, and 4) with masonry infill modeled as diagonal, compression-only struts. Results were evaluated on the basis of absolute value forcing demands (flexure and shear) output by column elements. Demand-to-capacity ratios were calculated according to ASCE 41 acceptance criteria for individual actions. Result evaluation was limited to only the first-story columns based on observed structural damage.

6.1 Research Overview

Because the Tier 3 evaluation consists of both linear analysis and nonlinear analysis, the research was conducted in two phases: an initial linear analysis (Phase 1) and a complimentary nonlinear analysis (Phase 2). To the extent possible, the analyses were conducted following the standard as written to best-represent the selected methodology. Whenever possible, ASCE-41 [2017] was the primary reference. *Chapter 7* outlined how to conduct the specific analyses, *Chapter 6* referenced for descriptions of the Tier 3 procedure, and *Chapters*

10 and *11* referenced for concrete and masonry materials, respectively. In cases that the modeling approach required guidance outside of ASCE-41 [2017], reference was sourced from external literature, as detailed in Chapter 2.

6.2 Overview of ASCE 41 Linear Analysis

Phase 1 of the Tier 3 evaluation employed a linear time history analysis to calculate forcing demands experienced as a result of selected ground motion records. ASCE 41-17 terminology refers to this method as the Linear Dynamic Procedure (LDP). Precursory steps required the development of a full system model in which all elements that contribute to the strength or stiffness of the structure are identified and characterized. This is a more rigorous extension beyond the Tier 1 and ATC 78-7 evaluations. ASCE 41 provides guidance on the use of material assignments, capacity calculations, and load applications.

Performance acceptability was based on DCRs attributed to both forcing and deformation. ASCE 41 separates component response between force-controlled and deformation-controlled actions, and each maintains distinct acceptance criteria. Flexure was considered to be deformation-controlled (sufficiently ductile) and shear to be force-controlled (brittle). Force-controlled actions compare forcing demands against lower-bound strength (calculated using specified material strength); strengths corresponding to deformation-controlled actions were determined using expected material strengths. Column flexure was assumed to be a deformation-controlled action based on ASCE-41 [2017] *Section 10.3.2.1* and *Table 10-10a*. Column shear was assumed to be a force-controlled based on passages *10.3.2.1* and *7.5.1.2* in which the standard states "where linear and nonlinear acceptance criteria are not specified... actions shall be taken as force-controlled" [ASCE-41, 2017]. The use of different material strengths for different actions corresponding to the same component conforms with *Sections 7.5.1* and *10.3.2*. Specified material strengths and the corresponding expected strength modifiers are outlined in Section 3.4. An overview of the steps for this evaluation are as follows:

1. Determine necessary structural components to be modeled and draw them in the mod-

eling software.

2. Define response behavior of elements (beam-column, truss, shear spring) based on structural drawings and linear-elastic material assignments.

3. Assign distribution of force and mass into the model to be representative of the original structure.

4. Perform linear time-history analysis and extract results at the end of analysis as the peak minimum and maximum values per component.

5. Process output results and compare to ASCE 41-17 acceptance criteria.

6.3 Modeling

All linear analysis was performed using proprietary software SAP2000 developed by Computers and Structures, Inc. (CSI). This software package was selected based on resource availability (as compared to similar product ETABS) as well its frequency of use in engineering practice, being self-advertised as "the most integrated, productive and practical general purpose structural program on the market today" [Computers and Structures, Inc., 2018].

6.3.1 Baseline Model

A single, baseline model was developed from general modelling assumptions to govern the appearance and structural response of the system. Subsequent models utilized this baseline as the framework upon which to building in specific variations considered in this study. This is most pertinent in inclusion of partial-height masonry infill. Table 6.1 serves to summarize key aspects of the general modeling assumptions as applied to different model variations. Basis model characteristics are as follows:

- Nodes defining centerline column and beam connectivity match measurements from the construction documents. These nodes mapped the skeletal structure of the building and outline the moment framing system.

- Mass was assigned to all story nodes in the translational degrees of freedom. Mass allocation was based on tributary floor area and includes consideration of masonry infill. The self-weight of framing elements was also lumped at the nodes (and material self-weight was set to zero in SAP2000). This simplification was selected to reduce the file size and run-time of the model by eliminating distributed mass and thus the size of the mass matrix. Total seismic weight equaled $2493kip$.

- All base nodes were fully restrained against translation and rotation. This assumes no foundation or soil flexibility. Construction documents show well-reinforced spread footings at column based, but available soil information was inadequate to enable modeling of foundation flexibility. This was consistent with the linear analysis.

- Columns were modeled as 2D line elements, termed 'frame elements' in SAP2000, and assigned full gross dimensions as rectangular cross-sections corresponding to the structural drawings. Additional features of this element are as follows:

  - Steel reinforcing was not included.
  - Self-weight was turned off.
  - Effective section flexural, axial, and shear stiffness were defined as $0.3EI_{gross}$, EA_{gross}, and $0.4GA_{gross}$, respectively. The flexural stiffness modifier is with respect to ASCE-41 [2017] *Table 10-5*.
  - No modification of the axial stiffness.
  - Automatic frame meshing was employed to discretize the single-height elements into five integration lengths that also to split at each intersection with a frame or shell element.

- Beams were modeled as 2D line elements, termed 'frame elements' in SAP2000, and assigned full gross dimensions as rectangular cross-sections corresponding to the structural drawings. Additional features of this element are as follows:

  - Steel reinforcing was not included.
  - Self-weight was turned off.
  - Effective section flexural, axial, and shear stiffness were defined as $0.3EI_{gross}$, EA_{gross}, and $0.4GA_{gross}$, respectively. The flexural stiffness modifier is with respect to ASCE-41 [2017] *Table 10-5*.
  - No modification of the axial stiffness.
  - The insertion point (point of connection with other elements) was assigned at the cross-section center-top. This was to align the top of the beams flush with the top of the slab. Stiffness was set to transform to account for the shift from centroid positioning.
  - Automatic frame meshing was employed to discretize single-span elements into five integration lengths that also split at each intersection with a frame or shell element.

- Floor slabs were modeled with shell area elements bounded between bays. Elements were assigned with a thin-plate formulation and gross thickness for membrane and bending action. Automatic area meshing was assigned to discretize into sub-elements with rectangular dimensions no greater than $200cm$. Out-of-plane effective stiffness was modified to match that of beam elements in flexure: $0.3EI_{gross}$. No modification was made to the in-plane or shear stiffness.

- Joint offsets were assigned at the tops of columns and at both ends of the beams. The rigidity of the offsets referenced ASCE-41 [2017] *Figure 10-2*.

Table 6.1: Summary of Baseline Model

Elements				
Type	Geometry	Assignment	Comments	
Column	Rectangular	Frame	Gross section geometry	
Beam	Rectangular	Frame	Gross section geometry	
Slab	Area	Shell	Gross section thickness	
Effective Stiffness Modifiers				
Type	Flexure	Shear	Axial	Comments
Column	0.30	0.40	1.0	ASCE-41 [2017] *Table 10-5*
Beam	0.30	0.40	1.0	ASCE-41 [2017] *Table 10-5*
Slab	0.30	1.0	1.0	Equivalent to Beam
Diaphragm: No diaphragm constraints. Slab modeled directly with use of shell (thin-plate formulation) elements.				

6.3.2 Model Variations

Separate model variations were developed as a means to gauge the impact of individual modeling approaches towards the treatment of partial-height infill. ASCE-41 [2017] provides guidelines for the treatment of full-height infill, e.g. in composite action with the adjacent frame or through use of "simplified numerical models with diagonal struts;" though, though few references in the standard pertain to partial-height infill. *Section 10.6.2* states that "frames with partial-height masonry infill. . . shall include the reduced effective length of the columns above the infilled portion of the bay" [ASCE-41, 2017]. The methodology to perform this provision is not detailed further in the ASCE standard. As such, this study endeavoured to assess various techniques for modeling of the partial-height infill. Each approach was considered as a model variation off the baseline model. Descriptions of the model variations are as follows:

1. Neglect all presence of masonry infill, (denoted as [BF] for 'bare-frame'). It was assumed that the infill is either already cracked from previous loading conditions no longer acts as a singular component, is poorly connected to the framing elements and thus cannot transfer forces or resist deformations, or otherwise does not engage with the lateral force-resisting system. The column is full story height and no short-column effects are considered. Beam-column joint flexibility was modeled according to ASCE-41 [2017] *Section 10.4.2.2* with calculation of the strong-column-weak-beam (SCWB) moment ratio: $^{\Sigma M_c}/_{\Sigma M_b}$, where ΣM_c is the summation of column nominal moment capacities above and below the joint in question and ΣM_b is the summation of column nominal moment capacities to each side of the joint in question. Expected material strength was considered in this calculation. A visual representation of this model is given in Figure 6.1.

2. Assign rigid end-zones extending up from the bottom of the column equal to the height of the masonry infill (denoted as [CM] for 'ASCE 41 Compliant'). Full-height infill was not explicitly considered. Rigid offsets offer a simple means by which to induce a

short-column effect by eliminating deformability over the offset region. However, it is important to acknowledge that rigid offsets augment the flexural stiffness both in-plane and out-of-plane directions; in a real structure, masonry infill does not confine the out-of-plane direction. Beam-column joint flexibility was modeled explicitly with full rigidity assigned to both column and beam offsets. A visual representation of this model is identical to that given in Figure 6.1, because end-zone offsets do not involve the assignment of new elements.

3. Use shell elements to model the masonry infill (denoted as [SH] for 'Shell Elements'). This approach was used for both full- and partial-height infill. Shell elements were assigned with a thin-plate formulation and thickness equal to that of the infill for membrane and bending action. Single elements were bounded between adjacent columns with automatic area meshing assigned to discretize into sub-elements with rectangular dimensions no greater than $200cm$. Values of compressive strength, f'_m, and elastic modulus, E_m, are noted in Section 3.4. As ASCE 41-17 does not provide guidance for effective stiffness modifiers for masonry, reference was made to National Institute of Standards and Technology (NIST) report Heintz [2017]: *Recommended Modeling Parameters and Acceptance Criteria for Nonlinear Analysis in Support of Seismic Evaluation, Retrofit, and Design.* Effective section flexural, axial, and shear stiffness were defined as $0.15EI_{gross}$, EA_{gross}, and $0.29GA_{gross}$, respectively. Beam-column joint flexibility was modeled explicitly, with rigid column offsets and flexible beam offsets. A visual representation of this model is given in Figure 6.2.

4. Represent infill through use of compression-only diagonal struts, modeled as truss elements, connected to nodes on adjacent columns (denoted as [DS] for 'Diagonal Struts'). This approach was used for both full- and partial-height infill. Element thickness equaled that of the masonry infill ($24cm$) and effective width, a, was calculated given surrounding component geometry and elastic modulus sourced from FEMA-356 [2000] *Section 7.5.2.1*:

$$\lambda_1 = \left[\frac{E_{me} t_{inf} \sin(2\theta)}{4 E_{fe} I_{col} h_{inf}}\right]^{1/4} \tag{6.1}$$

$$a = 0.175(\lambda_1 h_{col})^{-0.4} \times r_{inf} \tag{6.2}$$

where λ_1 is a coefficient used to determine equivalent width of infill strut, h_{col} is the column height between centerlines of beams, h_{inf} is the height of infill panel, t_{inf} is the thickness of infill panel and equivalent strut, r_{inf} is the diagonal length of infill panel, E_{me} is the expected modulus of elasticity of infill material, E_{fe} is the expected modulus of elasticity of frame material, I_{col} is the moment of inertia of adjacent columns, θ is an angle whose tangent is the infill height-to-length aspect ratio, and all other variables are as defined earlier in this document. Beam-column joint flexibility was modeled explicitly, with rigid column offsets and flexible beam offsets. In order to produce a compression-only response, the truss elements were assigned a zero tension limit. This modification, however, required a shift from linear to nonlinear analysis, per limitations within SAP2000, so as to permit shifts in stiffness between positive in compression and zero. A visual representation of this model is given in Figure 6.3.

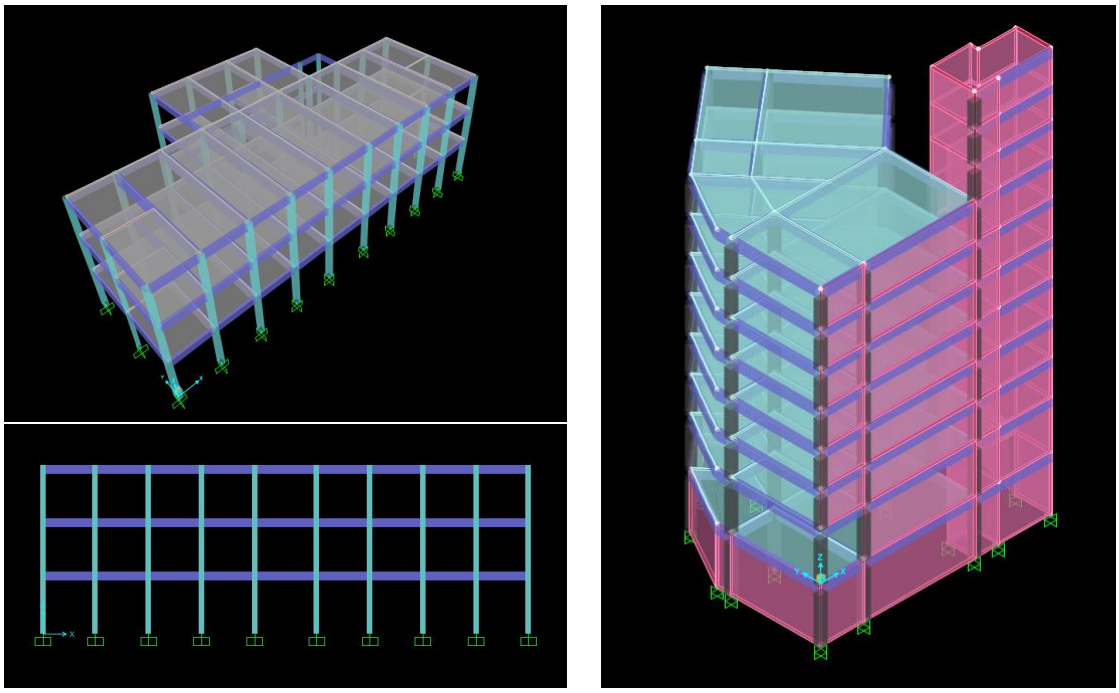

(a) Nanhau (b) Xingfu

Figure 6.1: Linear Model(s) #2 and #3

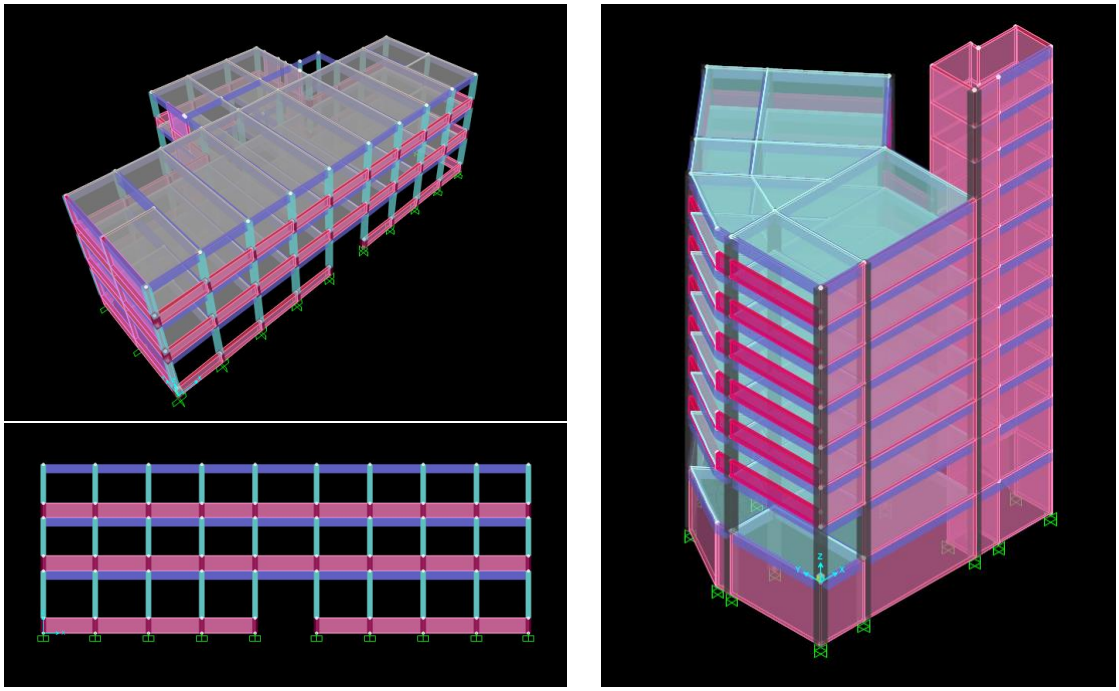

(a) Nanhau (b) Xingfu

Figure 6.2: Linear Model(s) #5

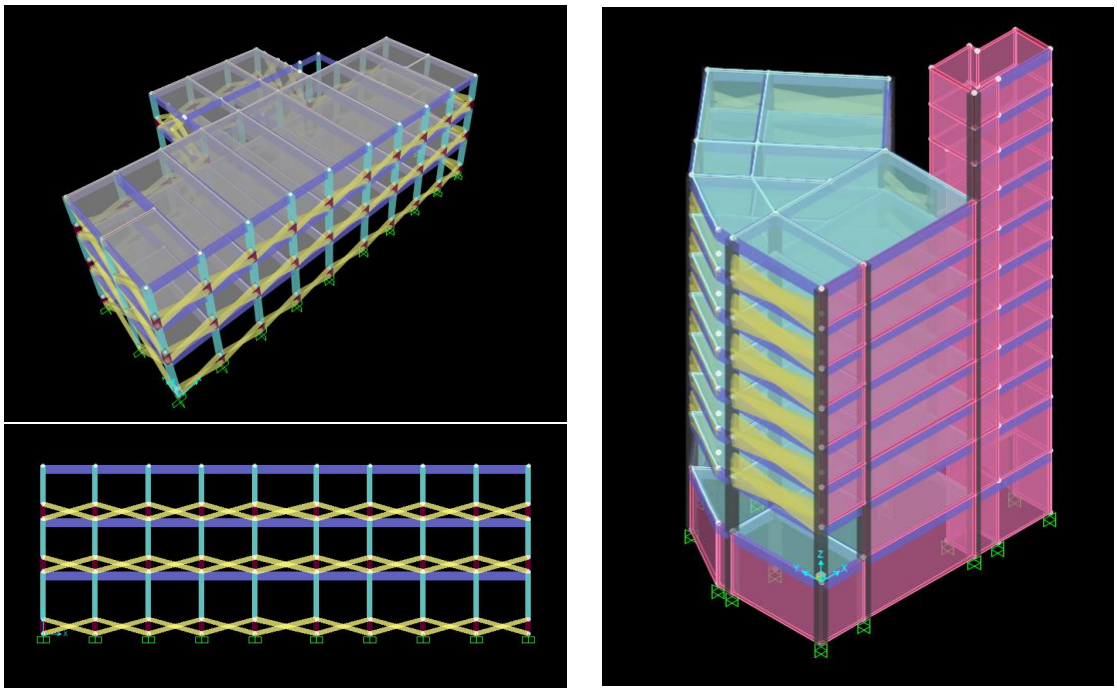

(a) Nanhau (b) Xingfu

Figure 6.3: Linear Model(s) #6

By presence alone, masonry infill stiffens the underlying and adjacent components and has a substantial influence on the system response. With respect to seismic analysis, the amount of force input from the ground motion is a function of the building stiffness; ground motion frequency content tends to have higher spectral accelerations at higher frequency (or lower periods). However, the material type, connections to the structural system, and properties of the masonry are uncertain. Recommendations from the previous evaluations, Tier 1 (in Chapter 4) and ATC 78-7 (in Chapter 5), highlight that removal of infill from the system is not accurate, in particular if the stiffness provided by the masonry impacts or induces a torsional demand. For this reason, Model BF features the case without masonry infill to provide a comparison of forcing demands.

6.4 Analysis

Linear analysis was performed by three distinct operations. Linear-elastic properties of the materials and elements permit superposition of the results rather than sequential loading. Eigenvalue analysis considered the original, undamaged condition of the structure to assess the elastic building periods. Gravity loading comprised several dead load (DL) and live load (LL) combinations to which the minimum and maximum forcing results for each element were tabulated and stored. Lateral loading was defined using coupled, single-direction acceleration histories. Time history analysis returned output of the minimum and maximum forcing demands for each element across all time steps. Calculated component demand was assessed per action on the basis of the absolute value maximum product from the load combinations considered.

6.4.1 Eigenvalue Analysis

An eigenvalue analysis was conducted independent of gravity or lateral loading to determine the natural periods corresponding to natural frequency response of the structure. SAP2000 terms this a 'modal' analysis. Table 6.2 gives the output for the first three mode shapes and corresponding mass participation factors for the two primary translational (UX and UY) and

one torsional (RZ) degrees of freedom. This is provided for all four model variations. For all models, mass participation exceeded 95% cumulative by the sixth mode. As an estimate of forcing demand from the above ground motions, Table 6.3 gives the corresponding values of spectral acceleration, per T_1, for each ground motion response spectrum. The values in the table reflect the SRSS combination of the EW and NS individual directions. The ground motion recommended most applicable, Station A730, is shown in bold.

Table 6.2: Natural Periods, T, from Modal Analysis

Model	Mode	T [sec]	UX	UY	RZ
BF	1	0.92	0.92	0.00	0.01
	2	0.73	0.01	0.29	0.63
	3	0.70	0.00	0.63	0.92
CM	1	0.59	0.94	0.00	0.00
	2	0.49	0.00	0.40	0.53
	3	0.47	0.00	0.52	0.92
SH	1	0.65	0.97	0.00	0.00
	2	0.47	0.00	0.62	0.34
	3	0.23	0.00	0.34	0.95
DS	1	0.70	0.96	0.00	0.00
	2	0.42	0.00	0.50	0.45
	3	0.31	0.00	0.44	0.93

Table 6.3: Spectral Acceleration, S_a, at T_1

Model	T_1 [sec]	**A730** [g]	CHY062 [g]	CHY061 [g]
BF	0.92	**0.33**	0.52	0.22
CM	0.59	**0.73**	1.01	0.41
SH	0.67	**0.63**	0.92	0.46
DS	0.70	**0.57**	0.81	0.43

6.4.2 Gravity Loading

Table 6.4 gives a summation of the values considered for the gravity loading. The gross floor area was $4262 ft^2$. Unit weights of concrete and masonry were considered as $150 pcf$ and $60 pcf$, respectively. Area loads were applied to the model as surface pressures acting down on the slab elements. Slab and beam self-weights were calculated using gross section properties and averaged across the floor. Column self-weight was calculated per element at applied as a concentrated point load at the top of each column. Masonry infill self-weight was distributed as a line load along the length of supporting beams. Per ASCE-41 [2017], the following gravity load combinations were considered:

$$Q_{G1} = 1.1(DL + 0.25LL) \tag{6.3}$$

$$Q_{G2} = 0.9DL \tag{6.4}$$

where Q_{G1} is a load combination where the combination of gravity and lateral loading on a component yields net addition of forcing, Q_{G2} is a load combination where gravity loading impedes overturning forces and would otherwise act as subtractive to the net forcing demand, and all other variables are as defined earlier in this document.

Table 6.4: Dead and Live Area Loads

Variable	Value	Units	Comments
DL	25	psf	office space per ASCE-7 [2013]
LL	40	psf	office space per ASCE-7 [2013]
Partition DL	10	psf	partition load per ASCE-7 [2013]
Slab DL	59.1	psf	self-weight (area-converted)
Beam DL	52.3	psf	self-weight (area-converted)
Column DL	varied	lb	self-weight (concentrated-point)
Infill DL	varied	plf	self-weight (linear-distributed)

6.4.3 Linear Time-History Analysis

Linear time-history analysis was performed using pairs of acceleration records acquired from ground motion recording stations, as presented in Section 3.2. The records were not scaled. A Newmark (constant acceleration) time integration scheme was used, where the number of steps and the time step matched those of the acceleration records. Mass- and stiffness-proportional damping of 5% (per ASCE-41 [2017] *Section 7.2.3.6*) was included via Rayleigh damping bounded by the first and third modes. Maximum forcing was calculated across the time history data as the absolute maximum value per action per component.

6.5 Acceptance Criteria

ASCE-41 [2017] outlines separate measures by which to evaluate force-controlled, Q_{UF}, and deformation-controlled, Q_{UD}, actions. Per-action forces are calculated from analysis output as follows:

$$Q_{UD} = Q_G \pm Q_E \tag{6.5}$$

$$Q_{UF} = Q_G \pm \frac{\chi Q_E}{C_1 C_2 J} \tag{6.6}$$

where Q_G are the demands caused by gravity loads (either Q_{G1} or Q_{G2}) that maximizes the combination with Q_E which are the demands resulting from time-history lateral forcing, χ is a factor for adjusting per performance level and assumed equal to 1.0, C_1 and C_2 are modification factors assumed equal to 1.0, J is a force-delivery reduction factor calculated from the moment DCR ${}^{M_{UD}}/_{M_{nCE}} \geq 1.0$, and all other variables are as defined earlier in this document. Variable J is a "force-delivery reduction factor" [ASCE-41, 2017] to reduce the magnitude of force-controlled actions for cases where deformation-controlled actions indicate yielding (and thus limiting the increase in forcing demand permitted by linear-elastic response).

Component acceptability was held relative to DCRs respective to the action designation, whether deformation-controlled (i.e column flexure) or force-controlled (i.e. column shear). Q_{UD} forcing is compared against expected component strength, Q_{CE}, multiplied by an m-factor, and Q_{UF} forcing with lower-bound component strength, Q_{CL}. The two ratios for acceptance evaluation are as follows:

$$Flexure \rightarrow mKQ_{CE} \geq Q_{UD} \tag{6.7}$$

$$Shear \rightarrow KQ_{CL} \geq Q_{UF} \tag{6.8}$$

where m is a capacity modification factor to account for allowable, expected deformation ductility, K is a knowledge factor assumed equal to 1.0 based on the availability of structural drawings, and all other variables are as defined earlier in this document. ASCE-41 [2017] provides a tabulation for the calculation of m-factors in *Table 10-10a*. Input parameters include the axial load ratio, $\frac{N_{UD}}{A_g f'_{cE}}$, transverse steel ratio, ρ_t, and ratio of plastic shear demand to shear capacity, ${}^{V_{yE}}/_{V_{Col0E}}$, calculated using expected material strengths. Component

estimated deformation ductility, which would be compared to the *Table 10-10a* allowable, was calculated from the ratio of maximum moment demand to moment capacity, $^{M_{UD}}/_{KM_{CE}}$, calculated using expected material strengths. Flexure and shear acceptance was thus based on the following demand-to-capacity ratios:

$$Flexure \rightarrow \frac{^{M_{UD}}/_{KM_{CE}}}{m} \leq 1.0 \tag{6.9}$$

$$Shear \rightarrow {}^{V_{UF}}/_{KV_{CL}} \leq 1.0 \tag{6.10}$$

where M_{CE} represents the nominal moment capacity, M_n, calculated using expected material strengths, V_{CL} represents the lower bound shear capacity, V_n, calculated using specified material strengths, and all other variables are as defined earlier in this document. M_n was calculated based on a axial load and moment (PM) interaction developed from fiber-type sections for each column. M_n corresponds to the maximum compressive axial load, P_{UD}, from load combination Q_{UD}. V_n was calculated using Equation 4.4 with variable $k_{nl} = 1.0$.

6.6 Results

The objective of the linear analysis was to draw similarities between the calculated acceptance criteria, as outlined in ASCE-41 [2017], (namely, the analytical prediction) versus the observed damage of the Nanhau District Office. Figures 6.4, 6.5, and 6.6 give plots of the DCR values calculated using the ASCE 41-17 acceptance criteria per the description in Section 6.5. Results are provided only for columns located at the first level of the structure, as this was consistent with the observed damage mechanism. Similarly, joint shear was not considered due to a primary damage pattern within the column and not extending to the beams or connections. To interpret the results, $DCR \geq 1.0$ was regarded as 'failure' and is marked with a black, dashed line. This would be an analytical prediction of damage (in that the demand exceeds capacity) given the constraints of the analysis method and would be a prediction of damage. The following figures include all four model variations and are

provided for each considered ground motion. Note how the values differ with respect to the modeling of the infill, which is a engineer assumption, and also to the input motion, which is attributed to the uncertainty of the 'correct' acceleration record. Column numbering is in reference to Figure 3.9, and filled markers identify the columns where damage was observed in the real structure.

Although the figures above provide analytical results for three considered ground motions, record A730 was identified as the most-representative of the Meinong earthquake. Table 6.5 provides a tabulation of the values as show in Figure 6.4, and Table 6.6 presents key parameters that were used in the calculation of the acceptance criteria. Figure 6.7 contextualizes the DCR values for this ground motion through use of a color-intensity plot overlaid on plan view. The color range associates green with immediate occupancy (IO), yellow to orange with life safety (LS), red with collapse prevention (CP), and has a black cutoff above CP to designate extreme violations of the acceptance criteria. Columns marked with a black outline were observed to have been damaged. From this perspective, all models with masonry infill yield similar predictions for the same columns.

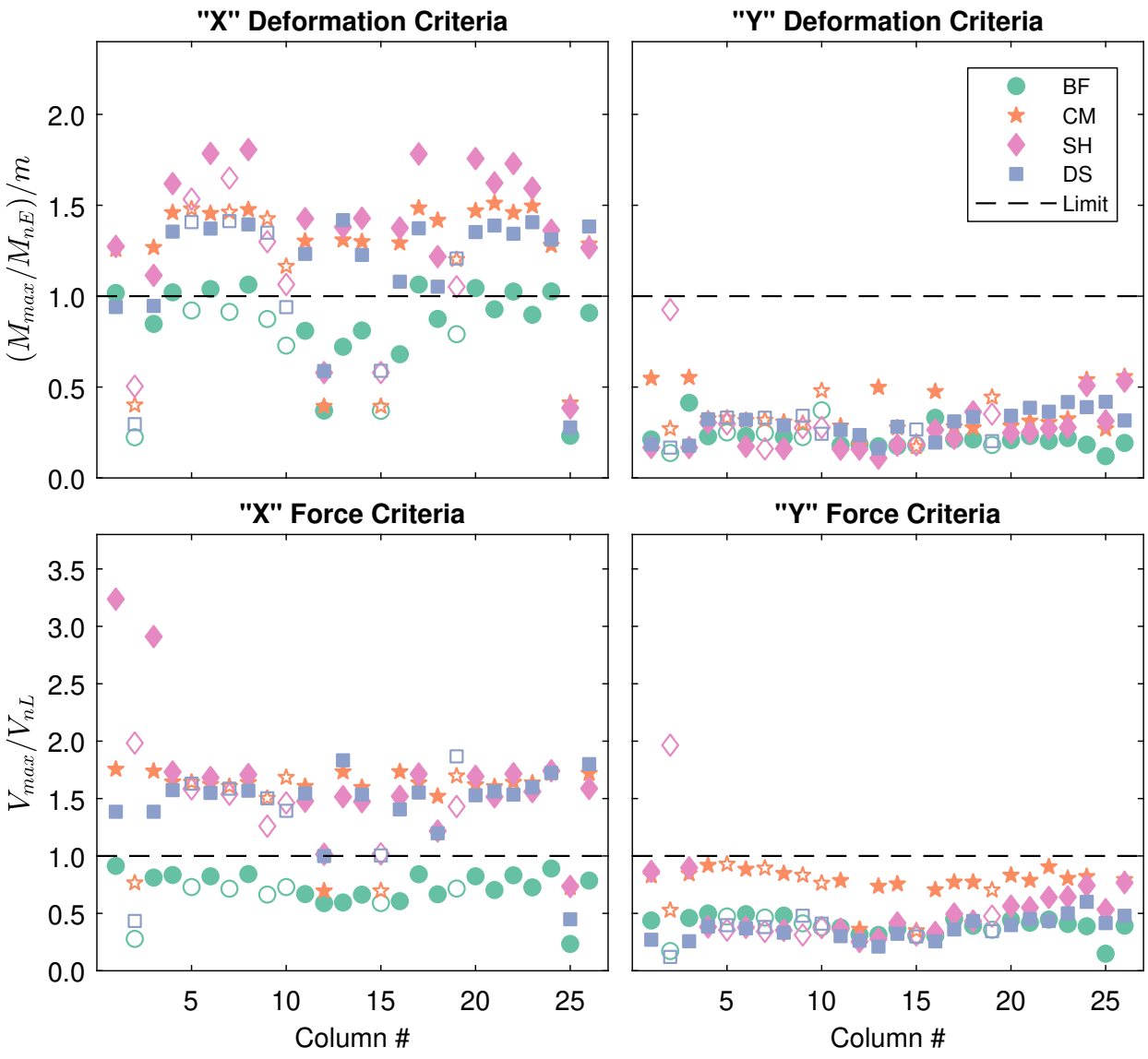

Figure 6.4: Acceptance Criteria for GM: A730 (most-representative GM)

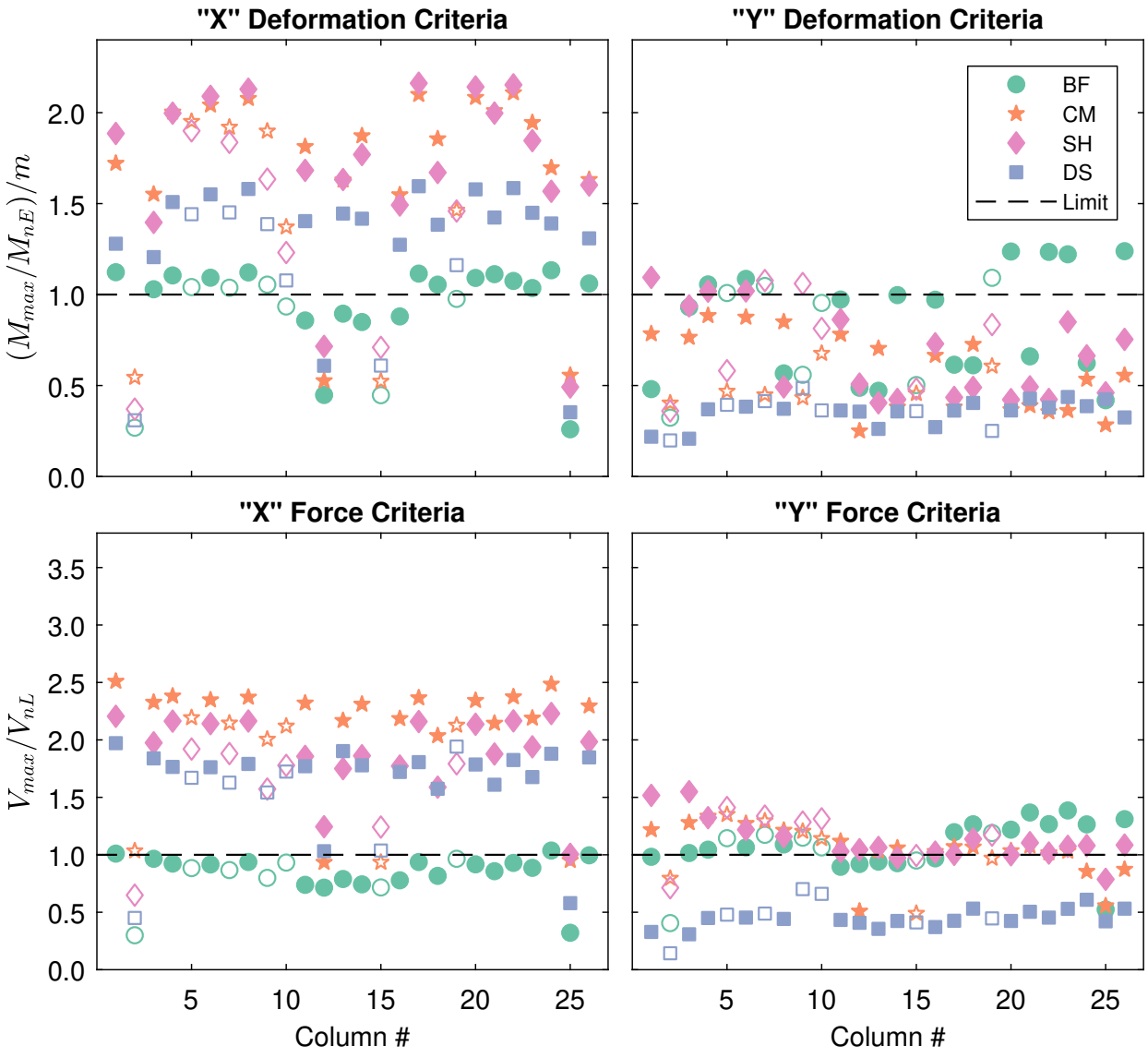

Figure 6.5: Acceptance Criteria for GM: CHY062

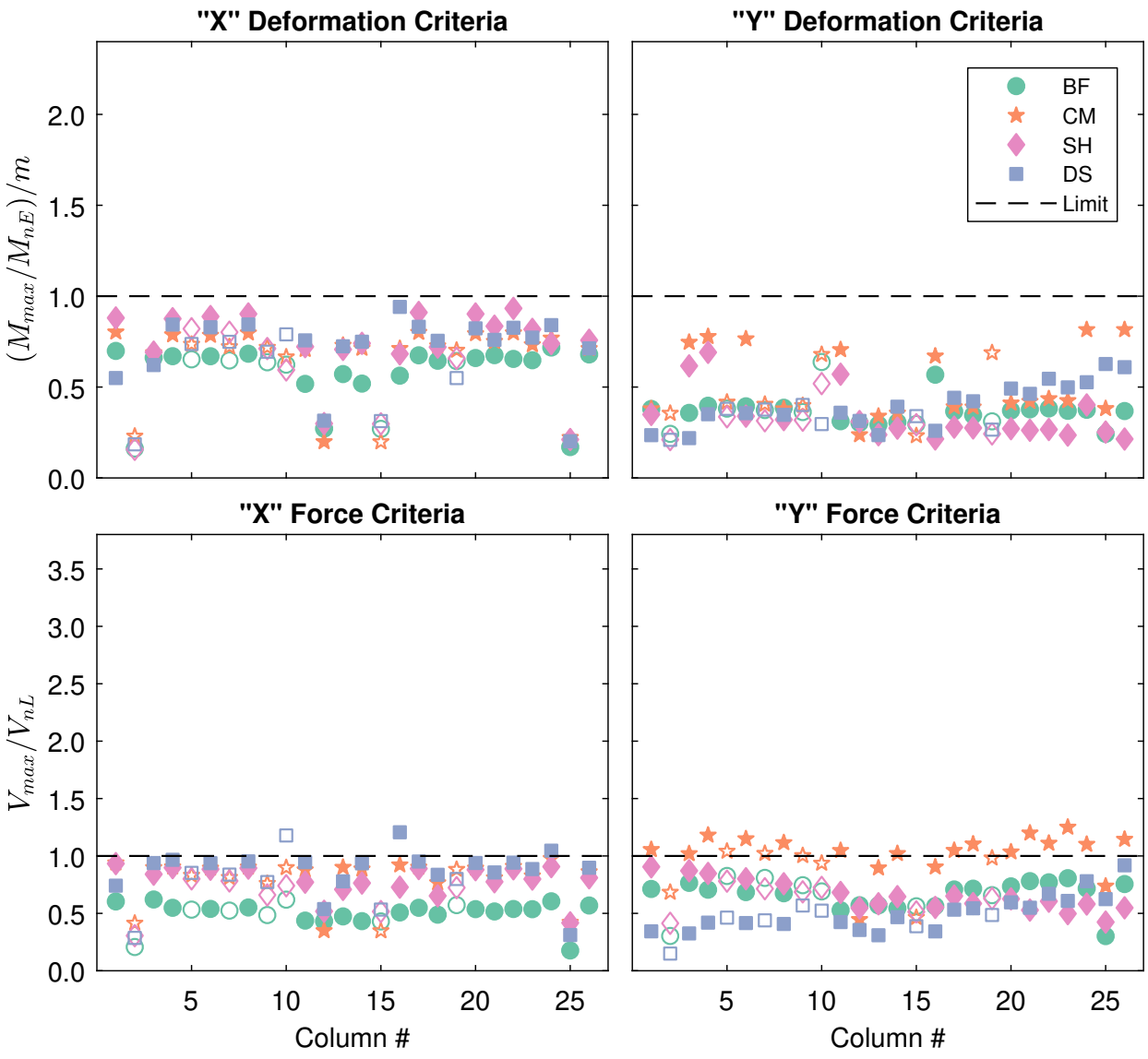

Figure 6.6: Acceptance Criteria for GM: CHY061

Table 6.5: Calculated DCR Values (Flexure and Shear) for GM: A730

Column	**Flexure DCR based on** $(M_{max}/M_{nE})/m_{Table}$								**Shear DCR based on** V_{max}/V_{nL}							
	BF Model		CM Model		SH Model		DS Model		BF Model		CM Model		SH Model		DS Model	
	x	y	x	y	x	y	x	y	x	y	x	y	x	y	x	y
#1	1.02	0.21	1.26	0.55	1.27	0.17	0.94	0.19	0.91	0.44	1.76	0.83	3.24	0.87	1.39	0.27
#2	0.22	0.14	0.40	0.27	0.50	0.93	0.30	0.17	0.28	0.17	0.77	0.53	1.98	1.96	0.43	0.12
#3	0.85	0.41	1.27	0.55	1.11	0.17	0.95	0.18	0.81	0.46	1.74	0.84	2.91	0.90	1.39	0.26
#4	1.02	0.23	1.46	0.33	1.62	0.30	1.36	0.32	0.83	0.50	1.64	0.92	1.73	0.38	1.57	0.39
#5	0.92	0.25	1.48	0.33	1.53	0.30	1.41	0.33	0.73	0.47	1.64	0.93	1.58	0.35	1.63	0.40
#6	1.04	0.23	1.46	0.32	1.79	0.17	1.37	0.32	0.82	0.49	1.62	0.88	1.68	0.38	1.55	0.37
#7	0.91	0.25	1.46	0.32	1.65	0.16	1.41	0.33	0.71	0.46	1.61	0.89	1.54	0.34	1.59	0.38
#8	1.06	0.23	1.48	0.31	1.81	0.16	1.39	0.29	0.84	0.48	1.64	0.85	1.71	0.35	1.57	0.33
#9	0.87	0.22	1.43	0.30	1.30	0.28	1.35	0.34	0.66	0.41	1.50	0.83	1.26	0.31	1.50	0.48
#10	0.73	0.37	1.16	0.48	1.06	0.28	0.94	0.24	0.73	0.38	1.68	0.76	1.46	0.38	1.39	0.41
#11	0.81	0.18	1.30	0.29	1.43	0.16	1.23	0.26	0.67	0.38	1.61	0.79	1.48	0.36	1.54	0.30
#12	0.37	0.18	0.39	0.18	0.58	0.16	0.59	0.24	0.59	0.31	0.70	0.36	1.01	0.25	1.00	0.26
#13	0.72	0.17	1.31	0.50	1.38	0.11	1.42	0.16	0.59	0.31	1.73	0.74	1.52	0.28	1.83	0.21
#14	0.81	0.18	1.30	0.28	1.43	0.18	1.23	0.28	0.66	0.37	1.60	0.76	1.47	0.42	1.53	0.32
#15	0.37	0.18	0.39	0.17	0.58	0.18	0.59	0.27	0.59	0.31	0.70	0.35	1.02	0.31	1.00	0.30
#16	0.68	0.33	1.29	0.48	1.38	0.26	1.08	0.19	0.61	0.30	1.73	0.71	1.52	0.33	1.41	0.26
#17	1.06	0.21	1.49	0.28	1.78	0.22	1.37	0.31	0.84	0.45	1.64	0.77	1.71	0.49	1.55	0.36
#18	0.87	0.21	1.42	0.28	1.22	0.36	1.05	0.33	0.67	0.39	1.52	0.77	1.22	0.43	1.20	0.43
#19	0.79	0.18	1.20	0.44	1.05	0.35	1.21	0.20	0.72	0.36	1.70	0.70	1.43	0.48	1.87	0.34
#20	1.04	0.21	1.47	0.29	1.76	0.25	1.35	0.34	0.82	0.44	1.62	0.83	1.69	0.56	1.53	0.40
#21	0.93	0.23	1.51	0.31	1.62	0.25	1.39	0.39	0.70	0.42	1.60	0.79	1.52	0.55	1.56	0.45
#22	1.03	0.20	1.46	0.30	1.73	0.27	1.34	0.36	0.83	0.45	1.64	0.91	1.72	0.64	1.53	0.43
#23	0.90	0.22	1.50	0.32	1.59	0.28	1.41	0.42	0.73	0.41	1.64	0.80	1.56	0.64	1.60	0.50
#24	1.03	0.18	1.28	0.54	1.36	0.51	1.31	0.39	0.89	0.39	1.72	0.82	1.74	0.74	1.72	0.60
#25	0.23	0.12	0.41	0.27	0.39	0.31	0.28	0.42	0.23	0.15	0.73	0.52	0.73	0.53	0.45	0.42
#26	0.91	0.19	1.29	0.56	1.27	0.53	1.38	0.32	0.79	0.39	1.72	0.79	1.59	0.77	1.80	0.48

Table 6.6: Acceptance Criteria Parameters (Flexure and Shear) for GM: A730

Column	*m*-values based on ASCE-41 [2017] *Table 10-10a*								*J*-values based on $M_{max}/M_{nE} \geq 1.0$							
	BF Model		CM Model		SH Model		DS Model		BF Model		CM Model		SH Model		DS Model	
	x	y	x	y	x	y	x	y	x	y	x	y	x	y	x	y
#1	1.13	2.35	1.12	1.15	1.06	1.07	1.11	1.13	1.15	1.00	1.41	1.00	1.35	1.00	1.04	1.00
#2	2.33	2.38	2.34	2.39	2.27	1.19	2.21	1.18	1.00	1.00	1.00	1.00	1.15	1.10	1.00	1.00
#3	1.13	1.16	1.13	1.15	1.07	1.08	1.11	1.13	1.00	1.00	1.43	1.00	1.19	1.00	1.05	1.00
#4	1.13	2.30	1.13	2.29	1.12	1.14	1.11	1.13	1.15	1.00	1.65	1.00	1.81	1.00	1.50	1.00
#5	1.13	2.34	1.13	2.31	1.13	1.15	1.11	1.13	1.04	1.00	1.67	1.00	1.73	1.00	1.56	1.00
#6	1.13	2.34	1.13	2.29	1.13	2.35	1.11	1.13	1.18	1.00	1.64	1.00	2.02	1.00	1.53	1.00
#7	1.13	2.34	1.13	2.30	1.13	2.35	1.11	1.13	1.03	1.00	1.65	1.00	1.87	1.00	1.57	1.00
#8	1.13	2.35	1.13	2.31	1.13	2.35	1.12	1.14	1.21	1.00	1.67	1.00	2.05	1.00	1.56	1.00
#9	1.13	2.27	1.12	2.25	1.11	1.14	1.08	1.10	1.00	1.00	1.60	1.00	1.45	1.00	1.46	1.00
#10	1.13	1.16	1.12	1.15	1.12	1.14	1.12	1.14	1.00	1.00	1.31	1.00	1.19	1.00	1.05	1.00
#11	1.13	2.35	1.13	2.31	1.13	2.34	1.11	1.13	1.00	1.00	1.47	1.00	1.61	1.00	1.37	1.00
#12	2.19	2.21	2.16	2.18	2.18	2.20	1.84	1.10	1.00	1.00	1.00	1.00	1.26	1.00	1.08	1.00
#13	1.13	2.35	1.13	1.16	1.13	2.35	1.13	1.15	1.00	1.00	1.48	1.00	1.56	1.00	1.60	1.00
#14	1.13	2.35	1.13	2.30	1.13	2.34	1.11	1.13	1.00	1.00	1.47	1.00	1.62	1.00	1.36	1.00
#15	2.18	2.20	2.16	2.18	2.17	2.19	1.85	1.10	1.00	1.00	1.00	1.00	1.26	1.00	1.09	1.00
#16	1.13	1.16	1.13	1.16	1.13	1.16	1.13	1.15	1.00	1.00	1.46	1.00	1.56	1.00	1.22	1.00
#17	1.13	2.35	1.13	2.32	1.13	2.35	1.11	1.14	1.21	1.00	1.68	1.00	2.02	1.00	1.53	1.00
#18	1.12	2.27	1.12	2.24	1.11	1.13	1.08	1.09	1.00	1.00	1.59	1.00	1.35	1.00	1.13	1.00
#19	1.13	2.35	1.13	1.15	1.12	1.15	1.11	1.13	1.00	1.00	1.35	1.00	1.18	1.00	1.34	1.00
#20	1.13	2.34	1.13	2.30	1.13	2.34	1.11	1.13	1.18	1.00	1.66	1.00	1.99	1.00	1.50	1.00
#21	1.13	2.35	1.13	2.34	1.13	2.35	1.11	1.13	1.05	1.00	1.71	1.00	1.84	1.00	1.54	1.00
#22	1.13	2.31	1.13	2.29	1.13	2.31	1.11	1.13	1.16	1.00	1.64	1.00	1.95	1.00	1.49	1.00
#23	1.13	2.31	1.13	2.32	1.13	2.33	1.11	1.13	1.01	1.00	1.69	1.00	1.80	1.00	1.56	1.00
#24	1.13	2.35	1.13	1.15	1.12	1.15	1.13	1.15	1.16	1.00	1.44	1.00	1.53	1.00	1.48	1.00
#25	2.33	2.38	2.34	2.39	2.31	2.36	2.11	1.17	1.00	1.00	1.00	1.00	1.00	1.00	1.00	1.00
#26	1.13	2.35	1.13	1.15	1.13	1.15	1.13	1.15	1.03	1.00	1.45	1.00	1.43	1.00	1.56	1.00

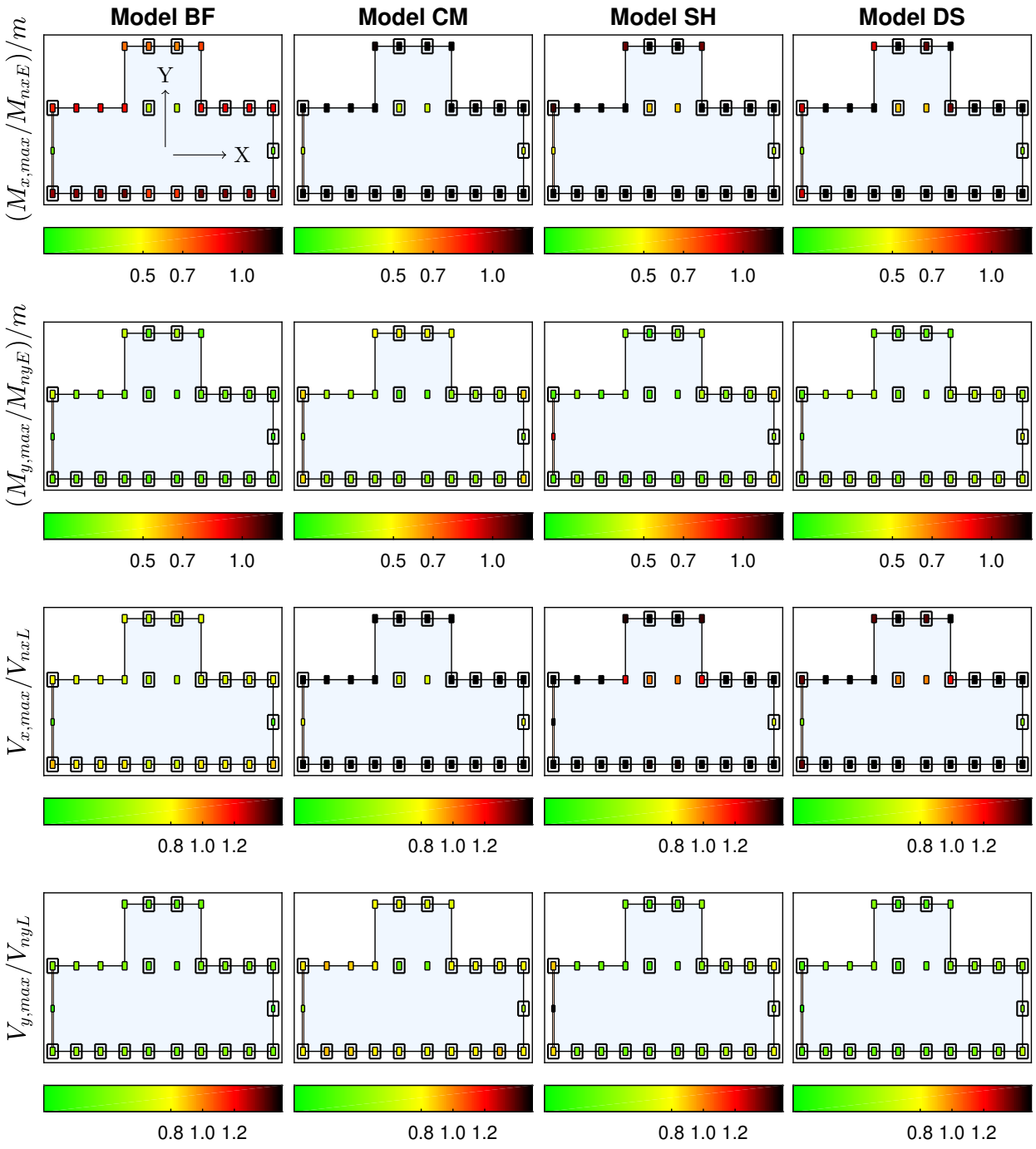

Figure 6.7: Acceptance Criteria for GM: A730 (most-representative GM)

In summary, the results of this evaluation indicate that the ASCE 41-17 linear dynamic procedure (LDP) can predict the damage mechanism experienced by the Nanhau District Office. Several conclusions based on the outcome of this evaluation are as follows:

- Most columns violate the ASCE 41-17 acceptance criteria in the long, X, building direction. This was the primary loading direction and is consistent with the damage state. This is most relevant for the infill models for which the results in Figure 6.7 appear nominally identical.

- Some columns violate the ASCE 41-17 acceptance criteria in the short, Y, building direction. This is not consistent with the observed damage. This prediction can be explained, in part, due to use of a linear-elastic assumption to describe the nonlinear behavior of non-ductile reinforced concrete. Given the high DCR values in the X-direction, one could suppose that columns damaged in this direction would limit extent of engagement in the Y-direction. This is not captured unless component deterioration is included in the model. Additionally, for the case of Model CM, the use of rigid offset elements artificially stiffened the infill out-of-plane direction. It was not possible, under this methodology, to allocate stiffness in only the infill in-plane direction. Better modeling practice would be to assign a beam-column element with variable-direction stiffness in place of rigid offsets.

- The bare-frame (BF) model shows consistently lower DCR values in the X-direction relative to the model variations. This can be attributed entirely to the lack of masonry infill, as the model is otherwise nominally identical, and also that the infill was primarily aligned in the X-direction for the models in which it was included. Regarding the calculated DCRs, this model appears to have a flexure-controlled damage mode. This is inconsistent with the observed damage and thus makes claim that negligence of masonry infill can drastically affect predicted behavior.

- How the engineer includes masonry infill into a building model also affects the pre-

dicted building response. Three methods were selected for this study: one strictly aligned with the language of ASCE 41-17 (model CM) and two designed as reasonable interpretations of the standard (models SH and DS). The trend of the calculated DCRs across the first-story columns, especially in the X-direction, appears similar but scaled between the model variations. Although there is a decent scatter in the results, all models do predict damage, especially in shear for the X-direction. This is consistent with the observed damage.

- Figure 6.7 shows a higher prediction of damaged columns than were observed during building reconnaissance. Columns marked with a black outline were observed to have been damaged. This can be explained under an assumption that ASCE 41-17 LDP aims to be conservative. Over-predicted 'failure' leads the engineer to either establish a retro-fit measure or to conduct a more rigorous nonlinear analysis to better define building response.

- The use of different ground motion records, all from stations with reasonable proximity to the building site, has a substantial affect on the building response. This highlights a need to carefully and clearly identify which motion (or response spectrum) to consider when performing an ASCE 41 analysis.

Chapter 7

EVALUATION OF ASCE 41 TIER 3 NONLINEAR DYNAMIC PROCEDURE

The second phase of the Tier 3 evaluation employed a nonlinear response history analysis through use of the OpenSees software platform. To provide data of value to the professional engineering community, OpenSees models were created to be consistent with modeling approaches typical to engineering practice. Models employed for linear analysis (discussed in Chapter 6) were considered for nonlinear analysis, within the modeling constraints imposed by the OpenSees platform. This chapter discusses the modeling and analysis of three model variations developed from a consistent baseline: 1) without modeled masonry infill, 2) with masonry infill represented by rigid offsets at the base of columns, and 3) with masonry infill modeled as diagonal, compression-only struts. Nonlinear analysis was conducted only for the Nanhau District Office. Nonlinear results were evaluated by comparing the column end rotation against calculated allowable plastic rotation and by the ratio of shear forcing demand against nominal shear capacity. Result evaluation was limited to only the first-story columns based on observed structural damage.

7.1 Overview of ASCE 41 Nonlinear Analysis

Phase 2 of the Tier 3 evaluation employed a nonlinear response history analysis to calculate forcing and deformation demands experienced as a result of selected ground motion records. ASCE 41-17 terminology refers to this method as the Nonlinear Dynamic Procedure (NDP). Similar to the LDP, preliminary work comprised the development of a full system model. Development of the model, however, increased in complexity from those discussed in the linear analysis section given the new inclusion of nonlinearity in element formulations and

inelasticity in material response. ASCE-41 [2017] offers guidelines for the use of generalized load-deformation relationships with which to characterize the nonlinear response. This takes the form of concentrated rotational hinges for which a predefined force-deformation backbone is supplied based on input parameters. Figure 7.1 gives an example of generalized force-deformation curves as sourced from ASCE-41 [2017]. Curve types 1 and 2 pertain to deformation-controlled actions and Type 3 to force-controlled actions. For the purpose of this study, methods were sourced from external literature for the implementation of a more targeted component analysis. Specific examples are discussed in the following sections.

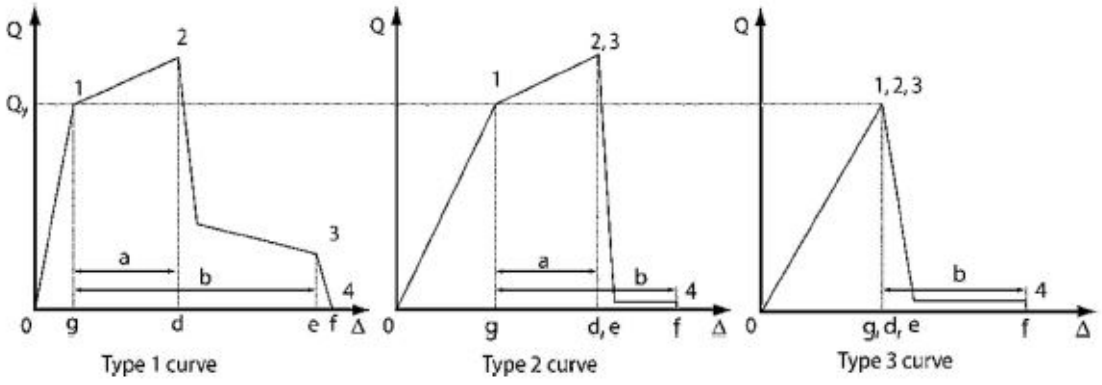

Figure 7.1: ASCE 41 Component Force vs. Deformation Curves [ASCE-41, 2017]

Performance acceptability was evaluated separately for force-controlled and deformation-controlled actions. Force-controlled actions compared forcing demands against lower-bound strength (calculated using specified material strength). This is identical to the linear analysis. Deformation-controlled actions compared recorded component end rotation against allowable plastic rotation as outlined in ASCE-41 [2017] *Table 10-8* per the specified performance level. Column flexure and column shear were again assumed as deformation-controlled and force-controlled, respectively. Material strengths implemented in individual calculations differed based on the action designation. Specified material strengths and the corresponding expected strength modifiers are outlined in Section 3.4. Similar analysis steps were considered to that of the linear analysis:

1. Determine necessary structural components to be modeled and develop a system by which to write them into a numerical model.

2. Define response behavior of elements (beam-column, truss, shear spring) based on structural drawings and nonlinear material models.

3. Assign distribution of force and mass into the model to be representative of the original structure.

4. Perform nonlinear response-history analysis and record results at each analysis step.

5. Process output results and compare to ASCE 41-17 acceptance criteria.

6. Consider additional model behavior beyond the ASCE 41 scope to assess performance of the model on both a global and local scale.

7.2 Modeling

All nonlinear analysis was performed using OpenSees [McKenna et al., 2004]. OpenSees supports serial analyses, parallel analysis in which the same model is subjected to different earthquake motions and different processors are used to conduct each analysis (OpenSeesMP), and analyses of extremely large systems, for which the solution of linear systems of equations are parallelized (OpenSeesSP). This framework was selected as a means to account for the size and complexity of the 3D model as well as the need for multiple sets of modeling decisions. Selection of OpenSees also permitted use of specialized material and element formulations and stable analysis algorithms and convergence testing [Pacific Earthquake Engineering Research Center, 2012].

Scripts were used to define input information that would then be passed into subroutines to calculate parameters necessary for the construction of material models, element formulations, and analysis procedures. A separate routine gathered this collection of information and drafted a text file that outlined all aspects of the model. Post-processing measured where then introduced to source individual files of output data, gather the data, and analyze

following successive OpenSees analysis. Sequencing of these steps was progressed in stages with increasing sophistication and refinement.

7.2.1 Baseline Model

A single, baseline model was developed from general modeling assumptions to govern the appearance and structural response of the system. Subsequent models utilized this baseline as the framework upon which to building in specific variations considered in this study. This is most pertinent in inclusion of partial-height masonry infill. Basis model characteristics are as follows:

- Nodes defining centerline column and beam connectivity match measurements from the construction documents. These nodes mapped the skeletal structure of the building and outline the moment framing system.
- Mass was assigned to all story nodes in the translational degrees of freedom. The application of and magnitude of mass assigned was consistent with the linear analysis.
- All base nodes were fully restrained against translation and rotation. This assumes no foundation or soil flexibility. Construction documents show well-reinforced spread footings at column based, but available soil information was inadequate to enable modeling of foundation flexibility. This was consistent with the linear analysis.
- A rigid diaphragm constraint was assigned to the nodes at each story level. This defined a relationship in which the same lateral drift would be experienced by all nodes at the story level.
- Columns were modeled as 2D line elements using a force-based beam-column element with nonlinear fiber-type section models and the *BeamWithHinges* numerical integration scheme. Figure 7.2 gives an idealization of the typical column model. Observed post-earthquake damage to columns indicated that these elements exhibited inelastic

response, and thus the following characteristics were designed to best outline the known behavior in the model:

- The force-based element employs the assumption of a linear moment field and constant axial load distribution along the element length. An intra-element solution is required to determine end moments and axial loads that result in element nodal displacements and rotations that satisfy compatibility with connecting elements.
- The *BeamWithHinges* integration scheme was used with nonlinear fiber-type section models assigned at integration points at element ends and with elastic section models in the element interior. The *BeamWithHinges* integration scheme assumes that element deformation is concentrated within a 'plastic hinge length' that is defined by the user.

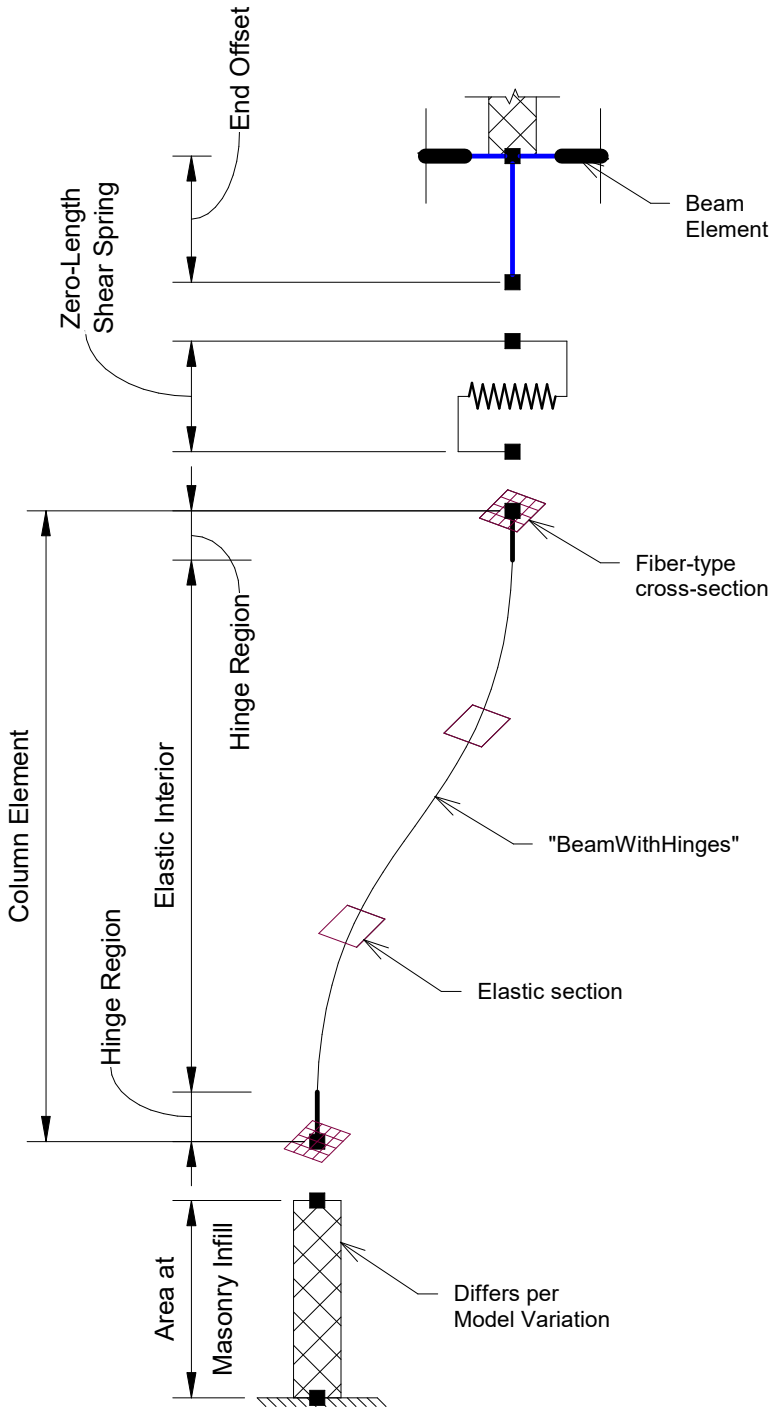

Figure 7.2: Idealization of OpenSees *BeamWithHinges* within Column Assembly

– The fiber-type sections comprised unconfined and confined concrete regions as well as steel fibers with fiber response defined. Figure 7.3 shows an idealized view of the fiber-type section. The material response of unconfined (cover) concrete was defined using the OpenSees *Concrete01* material model. This model represents the nonlinear compressive response with zero tensile strength. Required input parameters include fpc and $epsc0$ as specifications of the maximum compressive strength and the strain at which it occurs and $fpcu$ and $epsU$ as specifications of the residual crushing strength and strain, respectively. The material response of confined (core) concrete was defined using the OpenSees *Concrete02* material model. This model is similar to *Concrete01* but includes linear tensile softening. Additional input parameters include the ratio between unloading slope and the initial slope, λ, the specified tensile strength, ft, and the tensile softening stiffness, Ets. The initial stiffness is the same for both compression and tension. A strength multiplier of $\times 1.3$ was assumed in acknowledgement of confinement strengthening. The material response of steel reinforcement was defined using the OpenSees *Steel02* material model. This model is based on the uniaxial Giuffre-Menegotto-Pinto steel material with yield strength, fy, initial stiffness, $E0$, and specified strain-hardening ratio, b. Other input values: $R0$, $cR1$, and $cR2$, were assigned recommended values from the OpenSees documentation. Figures 7.4 to 7.6 give the OpenSees reference images next to a tabulation of the input parameters.

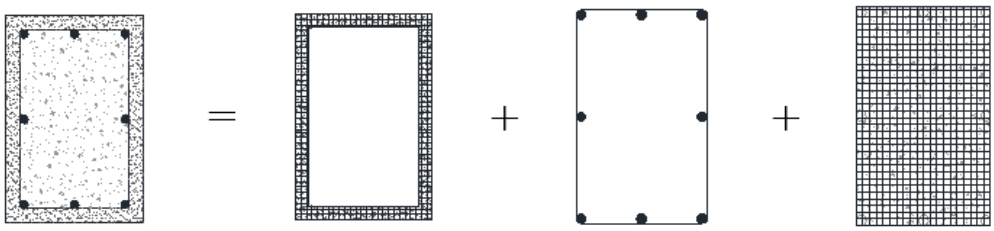

Figure 7.3: Idealization of a Fiber Cross-Section [Furtado et al., 2015]

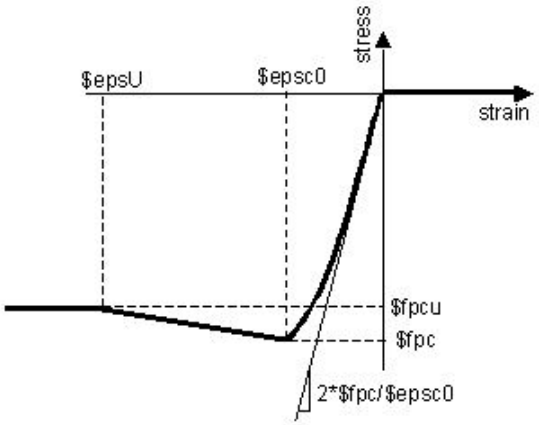

Parameter	Value	Units
fpc	-4.50	ksi
$epsc0$	-0.0020	ϵ
$fpcu$	-0.90	ksi
$epsU$	-0.0030	ϵ

Figure 7.4: OpenSees *Concrete01* and Input Parameters for Cover Concrete

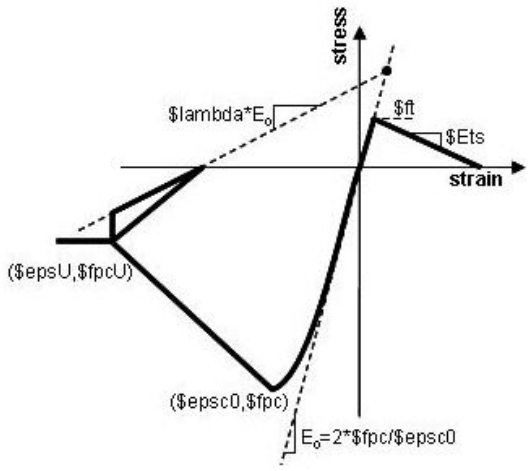

Parameter	Value	Units
fpc	-5.6250	ksi
$epsc0$	-0.0020	ϵ
$fpcu$	-1.1250	ksi
$epsU$	-0.010	ϵ
λ	0.10	
ft	0.7875	ksi
Ets	393.750	ksi

Figure 7.5: OpenSees *Concrete02* and Input Parameters for Core Concrete

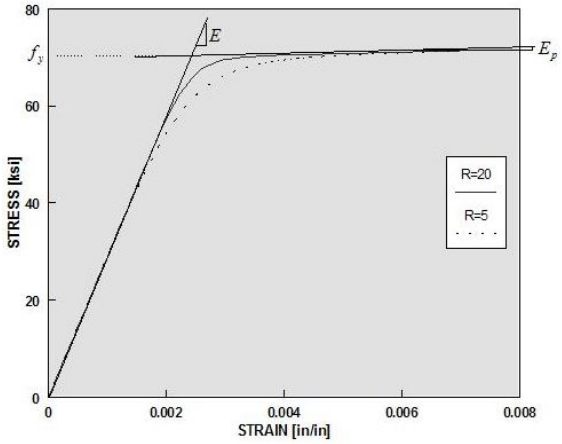

Parameter	Value	Units
fy	50	ksi
$E0$	29000	ksi
b	0.03	
$R0$	18	
$CR1$	0.9250	
$CR2$	0.1500	

Figure 7.6: OpenSees *Steel02* and Input Parameters for Steel Reinforcement

  - Elastic section flexural, axial, and shear stiffness were defined as $0.3EI_{gross}$, EA_{gross}, and GA_{gross}, respectively. The flexural stiffness modifier is with respect to ASCE-41 [2017] *Table 10-5*.

- Beam elements were modeled as 2D line elements using elastic beam-column elements with assigned gross-section properties. Post-earthquake damage to beams was not observed, thus, beams were modeled using *ElasticBeamColumn* elements as a means to simplify the numerical model. Moment demand-to-capacity ratios were computed following building analysis to verify this assumption. Figure 7.2 shows sample connectivity of beam elements with column assembly.

- Beam-column joint regions were defined to be elastic and very stiff. This was implemented by adding 2D elastic beam-column elements with flexural stiffness equal to five times flexural member stiffness to ends of beams and columns extending from frame member-joint interface to the center of the joint. Figure 7.2 shows sample location of element-joint interface elements.

- Shear springs were added at the top of all column elements using zero-length elements. Post-earthquake damaged observed for the columns showed consistent cases of diago-

nal cracking. This is indicative of high shear effects. In order to capture (and control) the shear response experienced by flexural beam-column elements in the model, these separate 'spring' elements were introduced with explicit force-deformation characteristics defined for the two lateral degrees of freedom. The OpenSees 1D *Hysteretic* material model was used to simulate this shear response. This model employs a multilinear envelope and a trilinear unload-reload response to simulate flexure shear and shear critical conditions. For this study, the shear model comprised a trilinear backbone curve with initial response defined by gross-section stiffness out to nominal shear strength, V_n, using Equation 4.4 and lower bound material strength. This is consistent with ASCE-41 [2017] generalized force-deformation curves to describe force-controlled actions. In calculating shear strength, equation parameter N_{UG} was substituted using the static axial load due to gravity, P_g, and the deformation ductility factor, k_{nl}, was set equal to 1.0 based on displacement ductility parameter, m, calculated as $^{M_{UD}}/_{M_{CE}}$ at each time step. Cyclic unloading stiffness was assumed equal to the elastic loading stiffness. Post-peak response was assumed with a 1% degrading slope and a constant residual strength of $0.2V_n$. While simplistic in application, this hysteretic backbone is acceptable to simulate the onset of strength loss (i.e. triggering of shear failure), which was deemed more important for this study than explicit simulation of the post-peak response. Figure 7.7 gives the OpenSees reference image for the *Hysteretic* material as well as an example of the backbone curve as featured in the model. In defining the force-deformation response, the input parameters depend on column details. Figure 7.2 shows an idealized placement of the shear spring above the column element.

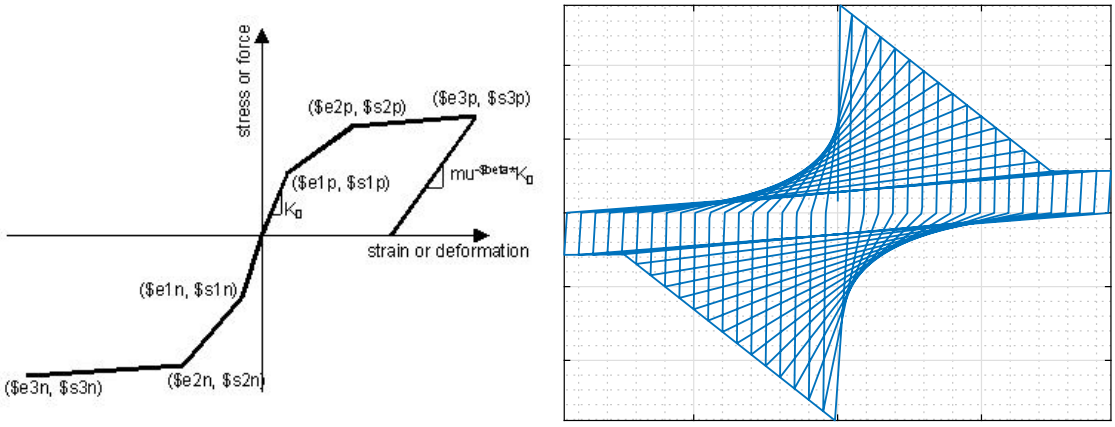

Figure 7.7: OpenSees *Hysteretic* and an Example Shear Spring Model

- Full-height masonry infill (located only on the western wall of the building) was modeled using coupled, single-direction, compression-only truss elements. Element connectivity was assigned between the top of columns and the floor below at the opposite end of the bay. This approach is supported by ASCE-41 [2017] as a simplified representation of full-height infill. Element geometry was defined with thickness equal to that of the masonry infill and effective width, a, was calculated per Equation 6.2. This is consistent with the linear analysis. The strength and cyclic force-deformation response was idealized as 'weak concrete' and characterized using the *Concrete01* material model with zero tensile strength. This approach follows the results of Mohammad Noh et al. [2017] in which this OpenSees modeling was compared with experimental data for infill in RC frames. Figure 7.8 gives the OpenSees reference image next to a tabulation of the input parameters.

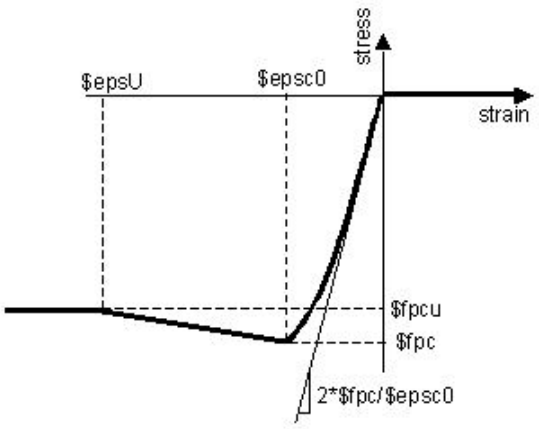

Parameter	Value	Units
fpc	-1.5600	ksi
$epsc0$	-0.0020	ϵ
$fpcu$	-0.3120	ksi
$epsU$	-0.0060	ϵ

Figure 7.8: OpenSees *Concrete01* and Input Parameters for Masonry Infill

7.2.2 Model Variations

The nonlinear analysis sought to best replicate the model variations selected for the linear analysis. Each variation built upon the assumptions discussed for the baseline model, but each differed in the treatment of partial-height masonry infill. Figure 7.2 acknowledges this condition in the variable labeling of column area within the height of masonry infill. The differences that define individual model variations are restricted only to the treatment of this column area. Figure 7.9 gives an idealization of the changes as applied to the aforementioned column assembly. Descriptions of the model variations are as follows:

1. Neglect all presence of masonry infill, (denoted as [BF] for 'bare-frame'). It was assumed that the infill is either already cracked from previous loading conditions no longer acts as a singular component, is poorly connected to the framing elements and thus cannot transfer forces or resist deformations, or otherwise does not engage with the lateral force-resisting system. The column is full story height and no short-column effects are considered.

2. Assign rigid end-zones extending up from the bottom of the column equal to the height of the masonry infill (denoted as [CM] for 'ASCE 41 Compliant'). Column base offsets

were defined to be elastic and very stiff. This was implemented by adding 2D elastic beam-column elements with flexural stiffness equal to five times the column flexural stiffness. All other section parameters reflected gross column properties. Rigid offsets offer a simple means by which to induce a short-column effect by greatly reducing deformability over the offset region. However, it is important to acknowledge that rigid offsets augment the flexural stiffness both in-plane and out-of-plane directions; in a real structure, masonry infill does not confine the out-of-plane direction.

3. Represent infill through use of compression-only diagonal struts (modeled as truss elements) connected to nodes on adjacent columns (denoted as [DS] for 'Diagonal Struts'). This approach adopts usage of a provision for full-height infill and applies it to cases of partial-height infill; element geometry and cyclic force-deformation response are applied similarly. In order to provide a node for strut connectivity at the height of masonry infill, column base offsets were defined consistent with model CM. This approach introduces both a short-column effect as well as an attempt to include masonry contribution in the model.

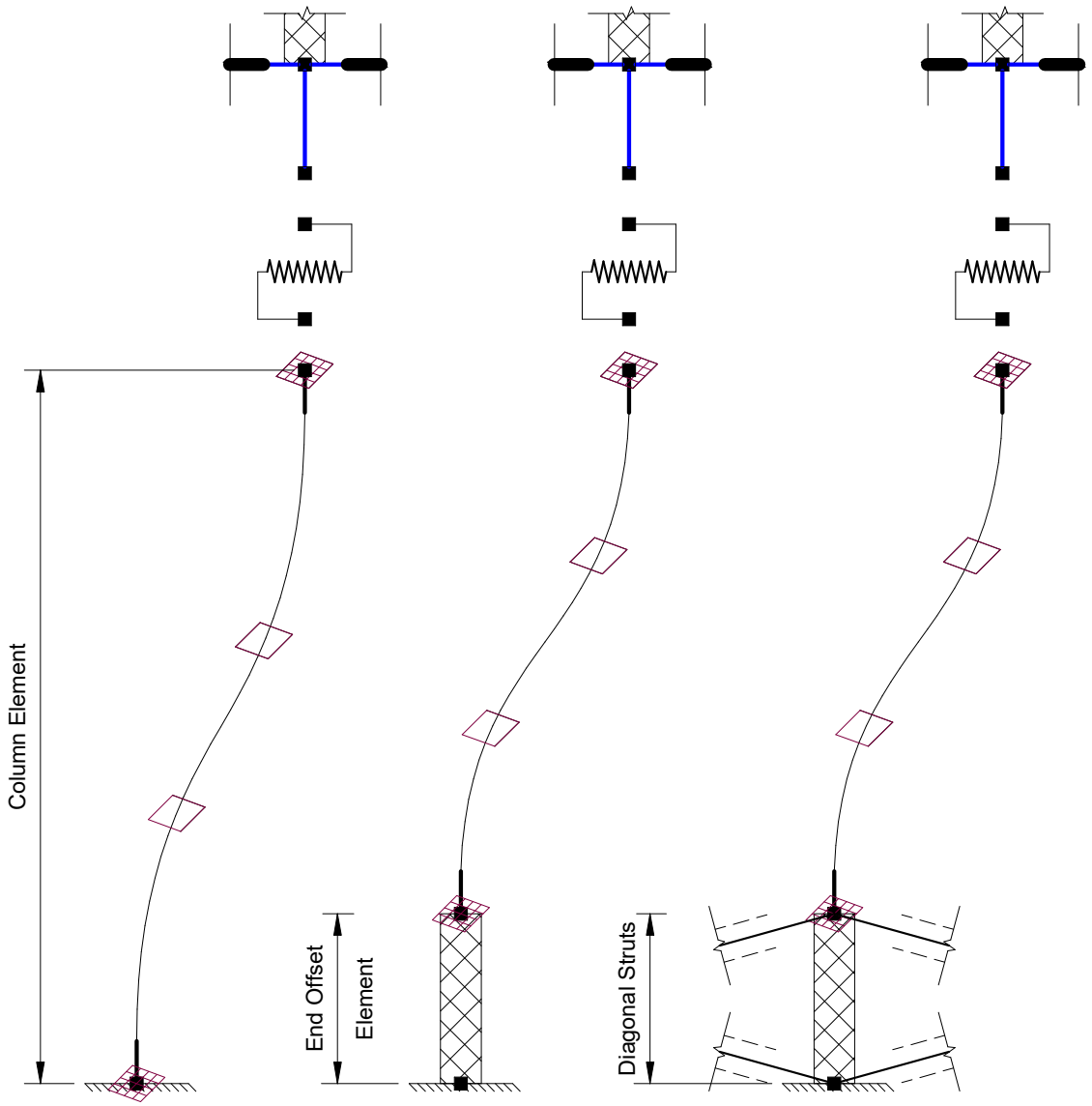

Figure 7.9: Comparison of Column Models between Model Variations BF, CM, and DS, Respectively

7.3 Analysis

Nonlinear analysis was performed in three sequential stages. Eigenvalue analysis considered the original, undamaged condition of the structure to assess the elastic building periods. Gravity loading introduced a simulation of regular-use expected forcing demand on the structural framing. Lateral loading was defined using coupled, single-direction acceleration histories. Nodal and element forces and deformations began recording at start of the dynamic analysis. Figure 7.10 gives a visual perspective of the initial state of the numerical model.

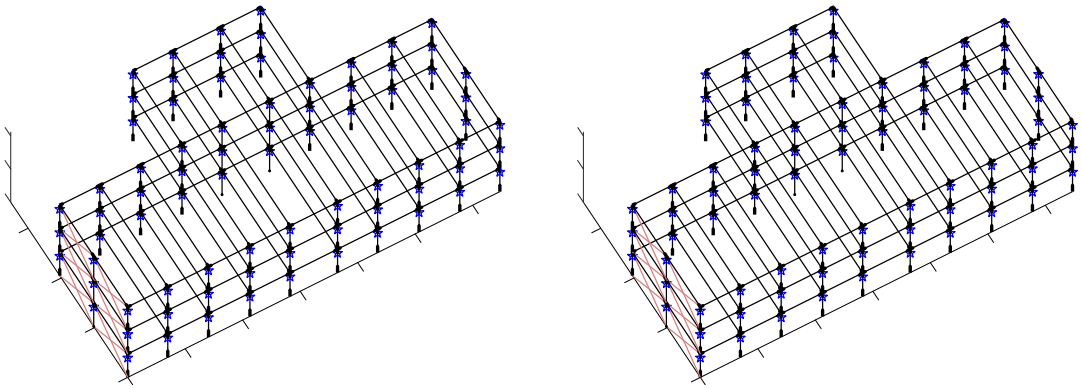

Figure 7.10: Line Model Representations of Numerical Models CM and DS

7.3.1 Eigenvalue Analysis

An eigenvalue analysis was performed prior to gravity and earthquake loading to determine the fundamental period, T_1, of the structure in an initial, undamaged state. This calculation incorporates the distribution of mass and stiffness in the structure to yield distinct natural frequencies. T_1 permits an estimate towards the relative building stiffness per model variations. Table 7.1 gives a comparison on nonlinear results against those from the linear analysis. Take note that the nonlinear models are consistently stiffer than the linear models.

One explanation may be that the plastic hinge regions, under undamaged conditions, maintain gross-section column stiffness. This differs from the uniform application of an effective stiffness modifier as executing in the linear analysis. Furthermore, note that model BF is substantially softer than the masonry variations (which is to be expected), and that T_1 is consistent between models CM and DS. As an estimate of forcing demand from the above ground motions, Table 7.2 gives the corresponding values of spectral acceleration, per T_1, for each ground motion response spectrum. The values in the table reflect the SRSS combination of the EW and NS individual directions. The ground motion recommended most applicable, Station A730, is shown in bold.

Table 7.1: Natural Periods, T [sec], from Modal Analysis

Model	Analysis	T_1	T_2	T_3
BF	NL	0.67	0.59	0.57
	L	0.92	0.73	0.70
CM	NL	0.48	0.44	0.20
	L	0.59	0.49	0.47
DS	NL	0.41	0.40	0.20
	L	0.70	0.42	0.31

Table 7.2: Spectral Acceleration, S_a [g], at T_1

Model	T_1 [sec]	**A730**	CHY062	CHY061
BF	0.67	**0.63**	0.92	0.46
CM	0.47	**0.68**	1.12	0.61
DS	0.41	**0.59**	1.08	0.86

Figure 7.11 show a pictoral representation of the mode shapes corresponding to the first

and third structural periods for models CM and DS. The mode shapes were constructed from relative nodal deformations recorded during eigenvalue analysis. This is a graphical representation of building response to ground motion frequency content that approaches building period. Typically, mode #1 pertains to long-building-direction global deformation, mode #2 to short-building-direction global deformation, and mode #3 to torsional engagement. Note the consistent modal response between the two model variations.

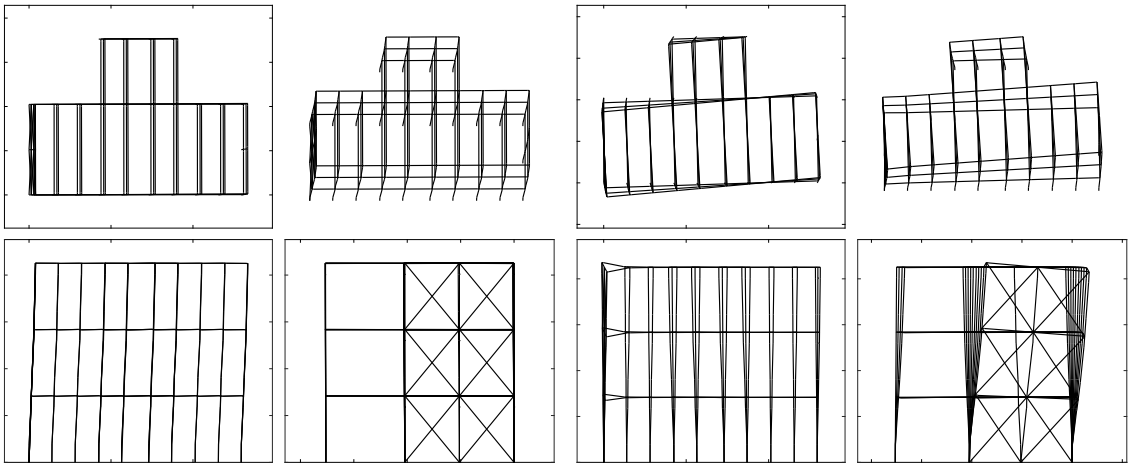

(a) Mode Shape #1 (b) Mode Shape #3

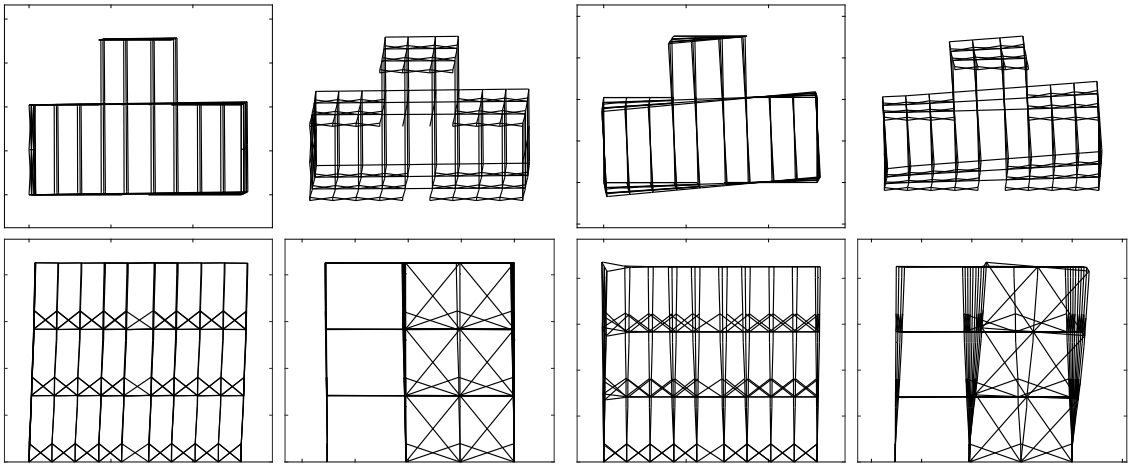

(c) Mode Shape #1 (d) Mode Shape #3

Figure 7.11: Mode Shapes for Modes #1 and #3 for Model Variations CM and DS

7.3.2 Gravity Loading

Gravity loads were assigned consistent with the linear analysis. Lumped values of both DL and LL were extracted from the linear analysis and assigned as concentrated point loads in the nonlinear model. Point loads were applied to the tops of columns at the top-most node of the column assembly. Refer to the beam-column joint centerline in Figure 7.2. Gravity analysis was performed prior lateral forcing using load-control application and ten cumulative steps. Gravity pre-loading best simulates the as-built condition. All results reflect the load combination of $1.1(DL + 0.25LL)$, and no follow up simulation was conducted for the case of $0.9DL$.

7.3.3 Nonlinear Response-History Analysis

Nonlinear response-history analysis was performed using pairs of acceleration records acquired from ground motion recording stations, as presented in Section 3.2. The records were not scaled. A combination of 2.7% modal damping (90% of total damping) and 0.3% Rayleigh damping (10% of total damping) was assumed based on recommendations from the ATC project team. Modal damping was applied constant over the first three models and Rayleigh damping assigned to the current structure stiffness and bound between the first and third modes so as to sufficiently damp out higher mode effects. The analysis time step was initially assumed equal to the recording interval of the acceleration record. At each time step, a Newton-Raphson algorithm was used to find a converged status, with convergence defined by an unbalanced energy error less than $1.0e^{-8}$. If not, the convergence test failed, and the analysis process was modified. Modifications to the analysis scheme progressed as follows: 1) switch the test algorithm to Krylov-Newton, which is more robust but requires more time to solve; 2) systematically reduce the time integration time step; and 3) loosen the convergence test tolerance and increase the number of allowable test iterations. Modifications specified in steps 2 and 3 were returned to initial conditions upon each successful test convergence.

7.4 Acceptance Criteria

As is done for the linear analysis, ASCE 41 posits separate measures by which to evaluate force-controlled and deformation-controlled actions. Force-controlled actions (i.e. column shear) are again compared to a capacity limit calculated using lower bound material strengths. Deformation-controlled actions, however, are now held relative to an allowable plastic rotation limit. Plastic rotation is defined in the context of a concentrated moment-rotation hinge and follows the generalized force-deformation backbone shown in Figure 7.12. ASCE-41 [2017] *Table 10-8* defines the parameters a, b, and c for use of this backbone. The calculation for individual parameters are as follows:

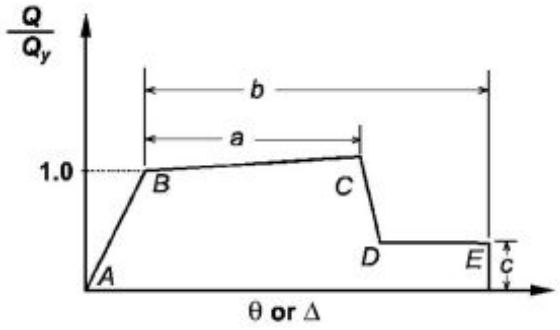

Figure 7.12: Generalized Moment-Rotation Backbone [ASCE-41, 2017]

$$a = \left[0.042 - 0.043\left(\frac{N_{UD}}{A_g f'_{cE}}\right) + 0.63\rho_t - 0.023\frac{V_{yE}}{V_{Col0E}}\right] \geq 0.0 \tag{7.1}$$

$$b = \left[\frac{0.5}{5 + \left(\frac{N_{UD}}{0.8A_g f'_{cE}}\right)\left(\frac{1}{\rho_t}\right)\left(\frac{f'_{cE}}{f_{ytE}}\right)} - 0.01\right] \geq a \tag{7.2}$$

$$c = \left[0.24 + 0.4\left(\frac{N_{UD}}{A_g f'_{cE}}\right) \geq 0.0\right. \tag{7.3}$$

where a (termed θ_a) and b (termed θ_b) are measurements of plastic rotation for Figure 7.12, c is the ratio of residual capacity, N_{UD} is the maximum compressive axial load in the column,

V_{yE} is the plastic shear demand of the column per Equation 4.6, V_{Col0E} is the expected shear capacity from Equation 4.4 but without modification by k_{nl}, the subscript $_E$ indicates expected material strength, and all other variables are as defined earlier in this document.

Individual component demands were tracked at each time step of the response-history analysis. This permitted the continuous tracking of certain parameters, such as the column axial load, N_{UD}, rather than assuming a single, static condition. It also afforded the calculation of column shear capacity, V_n, and the plastic rotation parameters, θ_a and θ_b, at each time step using real-time component information and incorporating axial load amplification. Column internal shear was extracted as the absolute maximum value from either end node. Column end rotation was calculated on the basis of fiber-section curvature multiplied against the plastic hinge length. This, too, was collected as the absolute maximum value between the top and bottom hinge regions, taken at each time step. Column drift, δ/l_u, resulted from the displacement differential between the bottom node of the column and the top node of the shear spring (as the combined two make up the column assembly).

Component acceptability was held relative to DCRs respective to the action designation, whether deformation-controlled (i.e column flexure) or force-controlled (i.e. column shear). The acceptance criteria for flexure, differing from the linear analysis, was now based on allowable column rotational demand, not deformation ductility; the acceptance criteria for shear remained identical to the linear analysis. Due to the selected use of OpenSees *BeamWithHinges* beam-column elements and fiber-type sections, the nonlinear analysis did not incorporate ASCE 41 moment-rotation hinges. Limiting column rotated was thus defined on the basis of desired structure performance level **Collapse Prevention (CP)** to which ASCE-41 [2017] sets a rotation limit of $0.7\theta_b$ based on Equation 7.2. Flexural acceptance (as a deformation-controlled action) was also evaluated on the basis of column drift relative to allowable rotation demand. This consistent with the use of horizontal shear springs that permit large drift upon shear failure initiation. Drift limits were also the standard means to evaluate column deformation in previous edition, ASCE-41 [2014]. Flexure and shear acceptance was thus based on the following demand-to-capacity ratios:

$$Flexure\ (drift) \rightarrow \frac{\delta/l_u}{\theta_b} \leq 0.70 \tag{7.4}$$

$$Flexure\ (rotation) \rightarrow \theta/\theta_b \leq 0.70 \tag{7.5}$$

$$Shear \rightarrow V/V_{CL} \leq 1.0 \tag{7.6}$$

where δ is the cumulative column and shear spring displacement, θ is the recorded column end rotation, θ_b is the calculated rotation limit for CP performance state based on Equation 7.2, V_{CL} represents the lower bound shear capacity, V_n, calculated using specified material strengths, and all other variables are as defined earlier in this document.

7.5 Results

The outcome of the nonlinear analysis attempted to expand upon the results from the linear analysis. Similar use of ASCE-41 [2017] acceptance criteria aimed to draw similarities between the calculated acceptance criteria (namely, the analytical prediction) and the observed damage state. Figures 7.13, 7.14, and 7.15 give plots of the DCR values calculating using the ASCE 41-17 acceptance criteria per the description in Section 7.4. As with the linear analysis, results are provided only for the columns located at the first level of the structure and joint shear was neglected. Violation of the acceptance criteria is marked separately between deformation-controlled flexure and force-controlled shear. For flexure, two lines mark collapse prevention (CP) and life safety (LS) allowable DCRs, while the shear DCR is with respect to unity. Plotting above these lines would be an analytical prediction of damage. The following figures include all three model variations and are provided for each considered ground motion. Note how the values differ with respect to the modeling of the infill, which is a engineer assumption, and also to the input motion, which is attributed to the uncertainty of the 'correct' acceleration record. Column numbering is in reference to Figure 3.9, and filled markers identify the columns where damage was observed in the real structure.

Similar to the linear analysis, specific focus was placed on the results attributed to

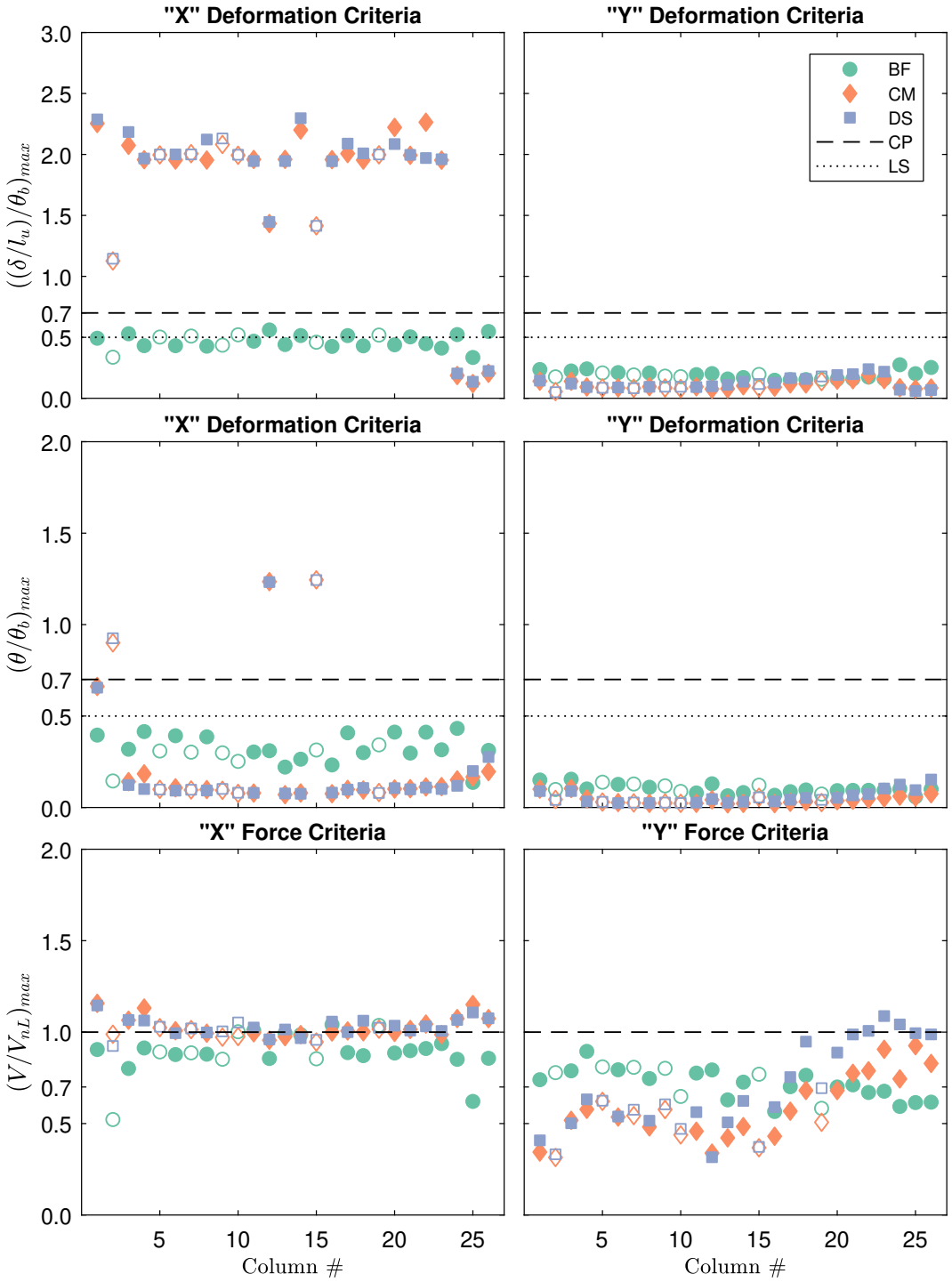

Figure 7.13: Acceptance Criteria for GM: A730 (most-representative GM)

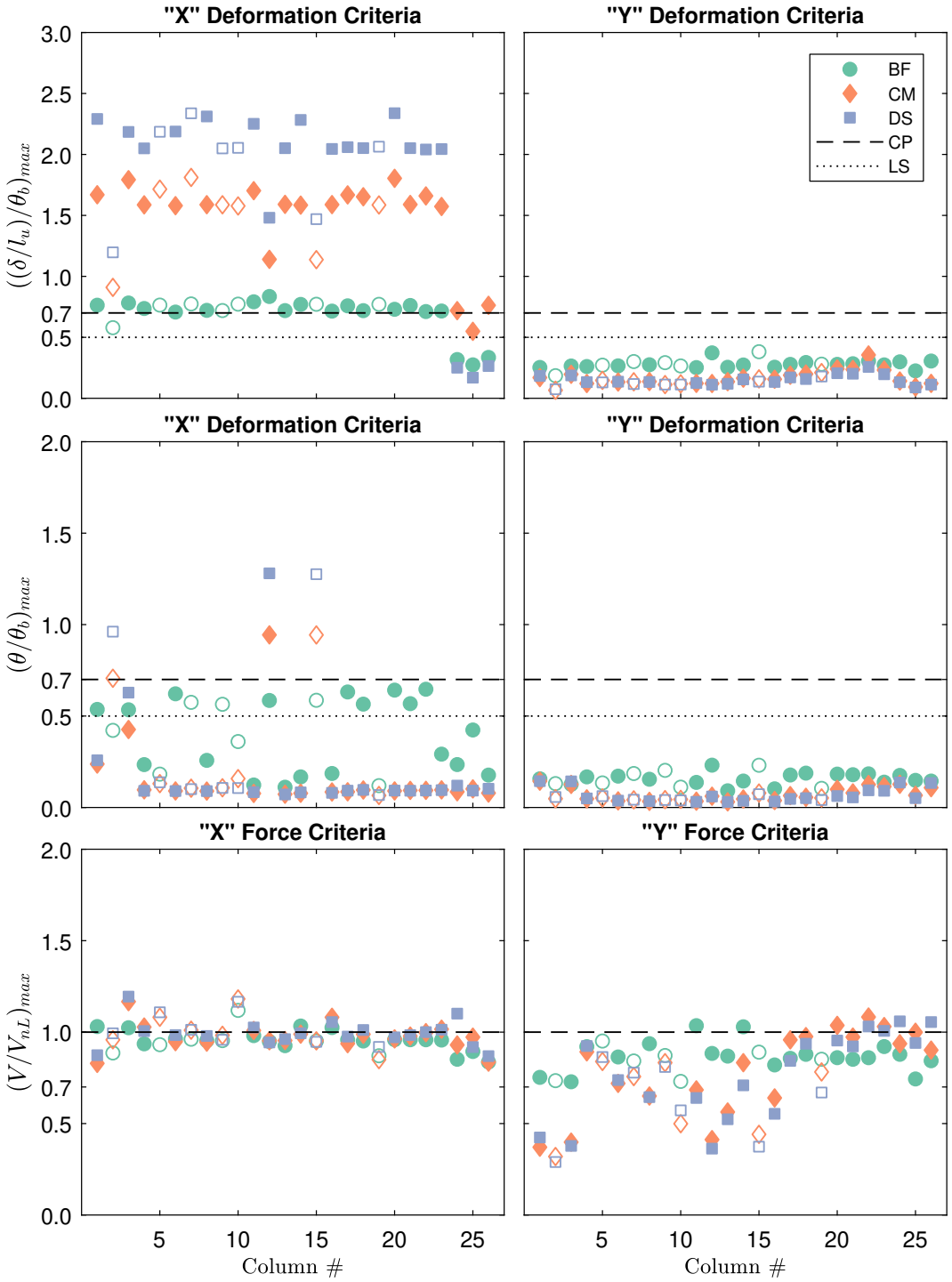

Figure 7.14: Acceptance Criteria for GM: CHY062

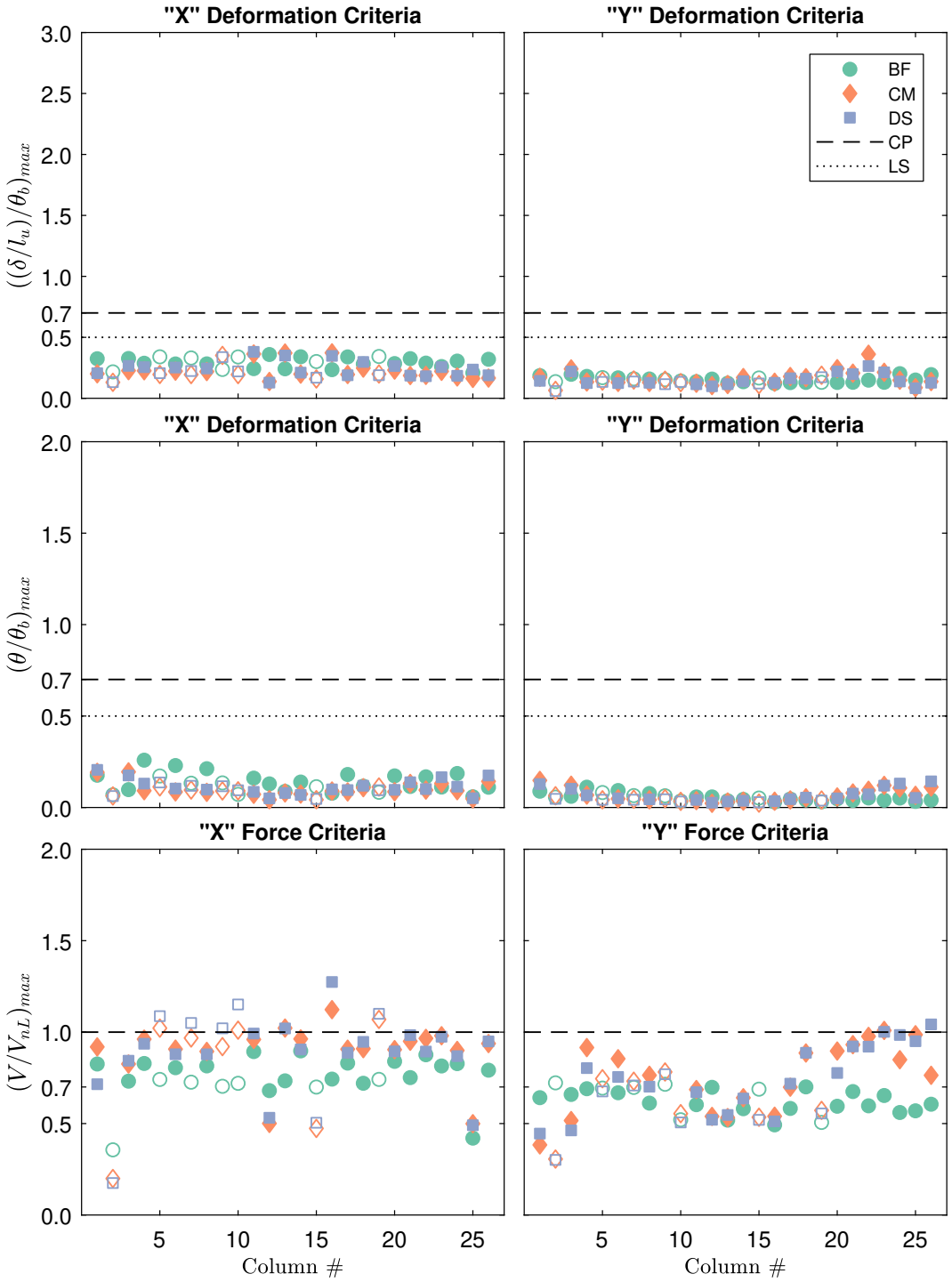

Figure 7.15: Acceptance Criteria for GM: CHY061

ground motion record A730. Table 7.3 provides a tabulation of the values as show in Figure 7.13, and Table 7.4 presents the two rotation parameters, a and b, that describe the moment-rotation backbone curve. Figure 7.16 contextualizes the DCR values for this ground motion through use of a color-intensity plot overlaid on plan view. The color range associates green with immediate occupancy (IO), yellow with life safety (LS), orange to red with collapse prevention (CP), and has a black cutoff above CP to designate extreme violations of the acceptance criteria. Columns marked with a black outline were observed to have been damaged. From this perspective, the two models with masonry infill yield similar predictions for the same columns.

Regarding the ASCE 41-17 acceptance criteria, two observations must be made. For one, the methodology appears to accurately capture the distribution of shear damage observed in the structure. Most all columns in the X-direction indicate force-controlled violations of the acceptance criteria to which the model identified shear failure. For another, the deformation criteria using rotation does not match the extent of damage predicted by the model. Rather, the deformation contained with the shear spring elements does not translate to rotation of the columns. Use of a rotation-based criteria does not match the modeled state. The proposed use of story drift in place of column rotation more accurate describes the extent of deformation in the columns. However, it is important to note that the deformation predicted by the two infill masonry models is not consistent with the real structure. No residual drift was observed at Nanhau District Office. The extreme deformation contained by the shear spring elements is, rather, a construct of the modeling of shear failure.

Acknowledging that the nonlinear models differ from the real structure, ASCE 41-17 acceptance criteria do accurately match the performance of the modeled components. To further assess the behavior of the models, this study sought also explore certain aspects of the model beyond the scope of an ASCE 41 acceptance criteria bases assessment. Full response-history records for the nonlinear analysis permit incite into the global response of the structure as well as into local behavior of individual columns. Global response reflects the acting damage mechanism and provides a full-scale perspective of structural behavior.

Table 7.3: Calculated DCR Values (Flexure and Shear) for GM: A730

Column	**Flexure DCR based on** $((\delta/l_u)/\theta_b)_{max}$						**Shear DCR based on** $(V/V_{nL})_{max}$					
	BF Model		CM Model		DS Model		BF Model		CM Model		DS Model	
	x	y	x	y	x	y	x	y	x	y	x	y
#1	0.47	0.22	2.29	0.14	2.44	0.13	0.91	0.74	1.11	0.34	1.14	0.42
#2	0.32	0.17	1.21	0.05	1.24	0.05	0.52	0.78	0.97	0.31	0.92	0.33
#3	0.51	0.21	2.17	0.14	2.12	0.12	0.78	0.76	1.07	0.51	1.06	0.51
#4	0.43	0.24	2.09	0.09	2.08	0.09	0.91	0.85	1.14	0.56	1.06	0.61
#5	0.48	0.20	2.12	0.09	2.11	0.08	0.89	0.80	1.03	0.60	1.04	0.59
#6	0.42	0.20	2.09	0.09	2.24	0.08	0.88	0.79	1.02	0.53	1.01	0.52
#7	0.49	0.18	2.28	0.08	2.16	0.08	0.88	0.80	1.01	0.51	1.03	0.54
#8	0.42	0.20	2.18	0.09	2.08	0.09	0.89	0.74	0.99	0.46	0.99	0.51
#9	0.43	0.17	2.09	0.08	2.25	0.09	0.86	0.80	0.99	0.56	1.04	0.60
#10	0.50	0.17	2.12	0.08	2.11	0.09	0.98	0.61	1.00	0.42	1.07	0.45
#11	0.46	0.19	2.17	0.09	2.06	0.09	1.01	0.76	1.00	0.44	1.02	0.56
#12	0.54	0.20	1.53	0.08	1.53	0.10	0.85	0.79	0.96	0.34	0.96	0.31
#13	0.44	0.16	2.09	0.08	2.06	0.11	1.00	0.61	0.99	0.40	1.00	0.50
#14	0.49	0.16	2.27	0.10	2.27	0.13	0.99	0.72	1.00	0.48	0.96	0.62
#15	0.45	0.19	1.51	0.08	1.51	0.12	0.86	0.77	0.94	0.37	0.95	0.37
#16	0.41	0.15	2.09	0.09	2.06	0.13	1.04	0.56	1.00	0.41	1.04	0.58
#17	0.49	0.15	2.12	0.12	2.11	0.16	0.89	0.70	1.00	0.57	0.98	0.75
#18	0.42	0.15	2.09	0.12	2.10	0.15	0.87	0.76	1.00	0.68	1.06	0.92
#19	0.50	0.15	2.12	0.14	2.11	0.17	1.03	0.58	1.04	0.51	1.01	0.67
#20	0.42	0.15	2.30	0.15	2.42	0.18	0.89	0.70	1.00	0.66	0.98	0.89
#21	0.48	0.16	2.11	0.15	2.11	0.19	0.90	0.71	1.01	0.77	1.02	0.97
#22	0.43	0.17	2.42	0.19	2.09	0.23	0.91	0.67	1.04	0.76	0.98	1.01
#23	0.39	0.16	2.08	0.15	2.08	0.21	0.94	0.68	1.00	0.90	1.02	1.06
#24	0.55	0.28	0.19	0.09	0.21	0.07	0.84	0.60	1.08	0.74	1.07	1.06
#25	0.36	0.21	0.12	0.08	0.14	0.06	0.59	0.60	1.11	0.93	1.07	1.00
#26	0.58	0.26	0.20	0.09	0.23	0.07	0.86	0.62	1.07	0.82	1.10	0.98

Table 7.4: Calculated Rotation Parameters from ASCE 41-17 Table 10-8 for GM: A730

Column	**Max θ_a [rad] from Equation 7.1**						**Max θ_b [rad] from Equation 7.2**					
	BF Model		CM Model		DS Model		BF Model		CM Model		DS Model	
	x	y	x	y	x	y	x	y	x	y	x	y
#1	0.022	0.022	0.018	0.020	0.018	0.020	0.022	0.029	0.021	0.029	0.021	0.029
#2	0.024	0.024	0.025	0.024	0.025	0.024	0.026	0.039	0.026	0.039	0.026	0.039
#3	0.023	0.022	0.018	0.020	0.018	0.020	0.023	0.029	0.021	0.029	0.021	0.029
#4	0.023	0.020	0.018	0.018	0.018	0.018	0.023	0.029	0.021	0.029	0.021	0.029
#5	0.022	0.020	0.017	0.017	0.017	0.017	0.022	0.029	0.021	0.029	0.021	0.029
#6	0.022	0.020	0.017	0.018	0.017	0.018	0.022	0.029	0.021	0.029	0.021	0.029
#7	0.022	0.019	0.017	0.017	0.017	0.017	0.022	0.029	0.021	0.029	0.021	0.029
#8	0.022	0.019	0.017	0.017	0.017	0.017	0.022	0.029	0.021	0.029	0.021	0.029
#9	0.021	0.018	0.016	0.016	0.016	0.016	0.021	0.029	0.021	0.029	0.021	0.029
#10	0.021	0.021	0.016	0.019	0.016	0.018	0.021	0.029	0.021	0.029	0.021	0.029
#11	0.019	0.018	0.013	0.016	0.013	0.016	0.021	0.029	0.021	0.029	0.021	0.029
#12	0.020	0.017	0.020	0.017	0.020	0.017	0.020	0.027	0.020	0.027	0.020	0.028
#13	0.020	0.019	0.015	0.018	0.015	0.017	0.021	0.029	0.021	0.029	0.021	0.029
#14	0.019	0.018	0.013	0.016	0.013	0.016	0.021	0.029	0.021	0.029	0.021	0.029
#15	0.020	0.017	0.020	0.017	0.020	0.017	0.021	0.029	0.021	0.029	0.021	0.029
#16	0.021	0.020	0.014	0.017	0.014	0.017	0.021	0.029	0.021	0.029	0.021	0.029
#17	0.022	0.020	0.017	0.017	0.017	0.017	0.022	0.029	0.021	0.029	0.021	0.029
#18	0.021	0.019	0.016	0.017	0.016	0.017	0.021	0.029	0.021	0.029	0.021	0.029
#19	0.021	0.020	0.016	0.018	0.016	0.018	0.021	0.029	0.021	0.029	0.021	0.029
#20	0.022	0.020	0.017	0.017	0.017	0.017	0.022	0.029	0.021	0.029	0.021	0.029
#21	0.022	0.020	0.018	0.018	0.018	0.018	0.022	0.029	0.021	0.029	0.021	0.029
#22	0.022	0.020	0.017	0.018	0.017	0.018	0.022	0.029	0.021	0.029	0.021	0.029
#23	0.023	0.021	0.018	0.019	0.018	0.019	0.023	0.029	0.021	0.029	0.021	0.029
#24	0.023	0.022	0.018	0.020	0.018	0.020	0.023	0.029	0.021	0.029	0.021	0.029
#25	0.024	0.024	0.018	0.021	0.018	0.021	0.026	0.039	0.026	0.039	0.026	0.039
#26	0.023	0.022	0.018	0.020	0.018	0.020	0.023	0.029	0.021	0.029	0.021	0.029

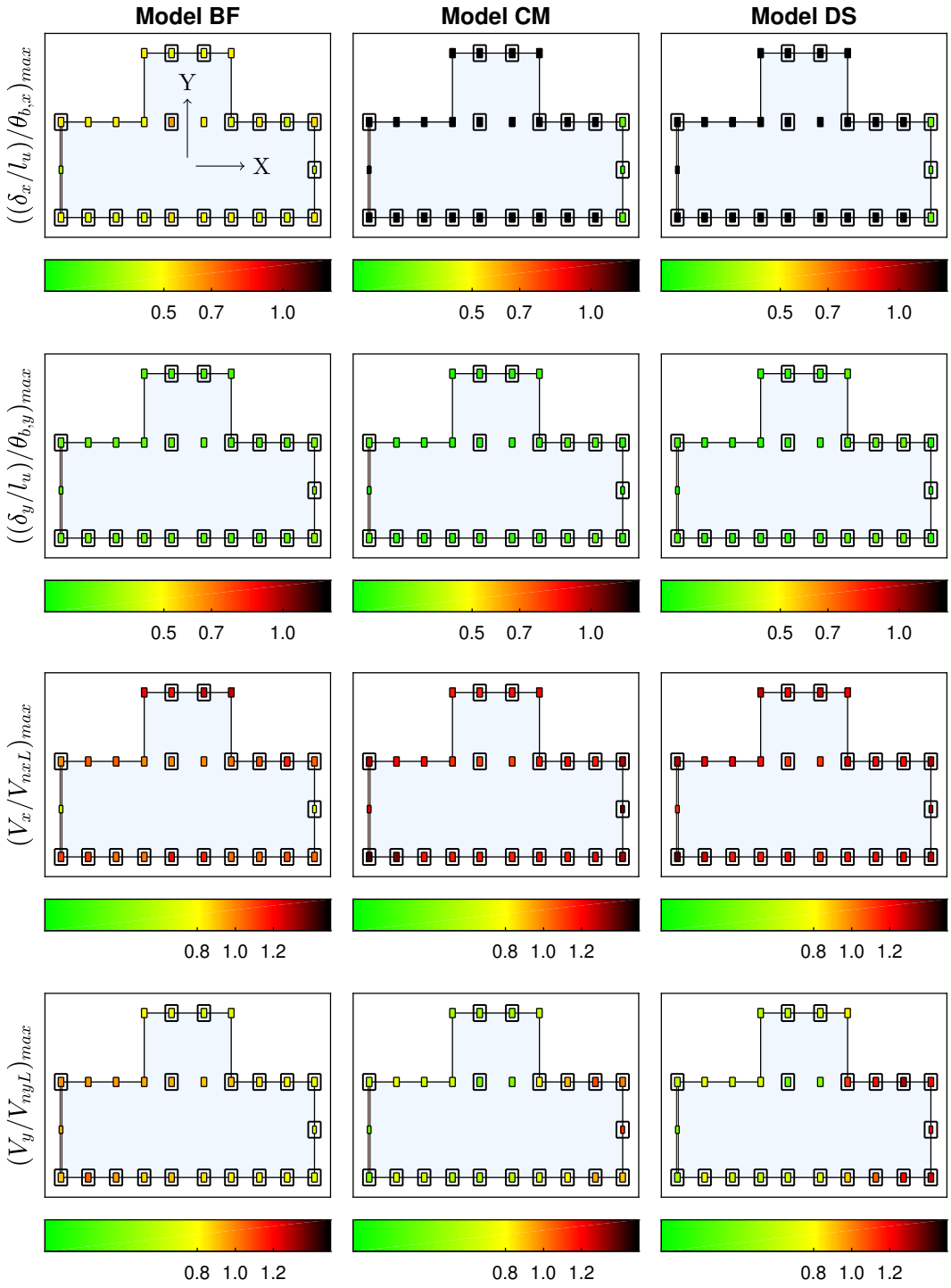

Figure 7.16: Acceptance Criteria for GM: A730 (most representative GM)

Local response highlights the behavior of individual components of the model and checks validity of initial model assumptions.

Global response, as recorded from the individual models, is described in the following figures. Figure 7.17 presents the plots of the base shear as a function of interstory drift for all three models. Both masonry models highlight permanent, plastic deformation as a result of first-story drift. Upper level story drift does not show significant nonlinear behavior. In contrast, the bare-frame model appears to remain linear throughout the duration of the ground motion. Whereas the concentration of damage mode within the first story is consistent with the damage mechanism observed, the Nanhau Distric Office did not display indicators of residual drift as described by the nonlinear analysis. Drift of the numerical models is linked to the method by which shear failure was modeled. Once nominal shear capacity, V_n, was exceeded by a column, the shear spring controlled all further response. This behavior was largely drift controlled and resulted permitted large deformations as the springs progressively softened until a stable, residual capacity. Accordingly, the predicted drift demands are a construct of the shear spring implementation. Figures 7.18 and 7.19 decompose the first-story drift into the individual element contributions: flexural column and shear spring. This is shown both as total drift as well as cumulative drift participation. These plots reaffirm plastic drift for the masonry models in the X-direction, but now identify that near all deformation demand is contained within the shear springs. The bare-frame model continues to show primarily flexural behavior.

Local response was investigated for both damaged (D) and undamaged (N) pairs of columns. Four columns were selected, two of each type, and are plotted in the same figure for comparison. These columns were #'s 6, 22, 5, and 7. The damage columns selected are ones for which photos were available from the reconnaissance, so as to see the extent of damage relative to the modeled behavior. Columns 6 and 22 were shown in Figures 3.7b (left side) and 3.8b. Again, column numbering is in reference to Figure 3.9. Figure 7.20 plots the shear spring response as a function of the column drift (cumulative column and spring). This result is consistent with the acceptance criteria (DCR around 1.0) and with

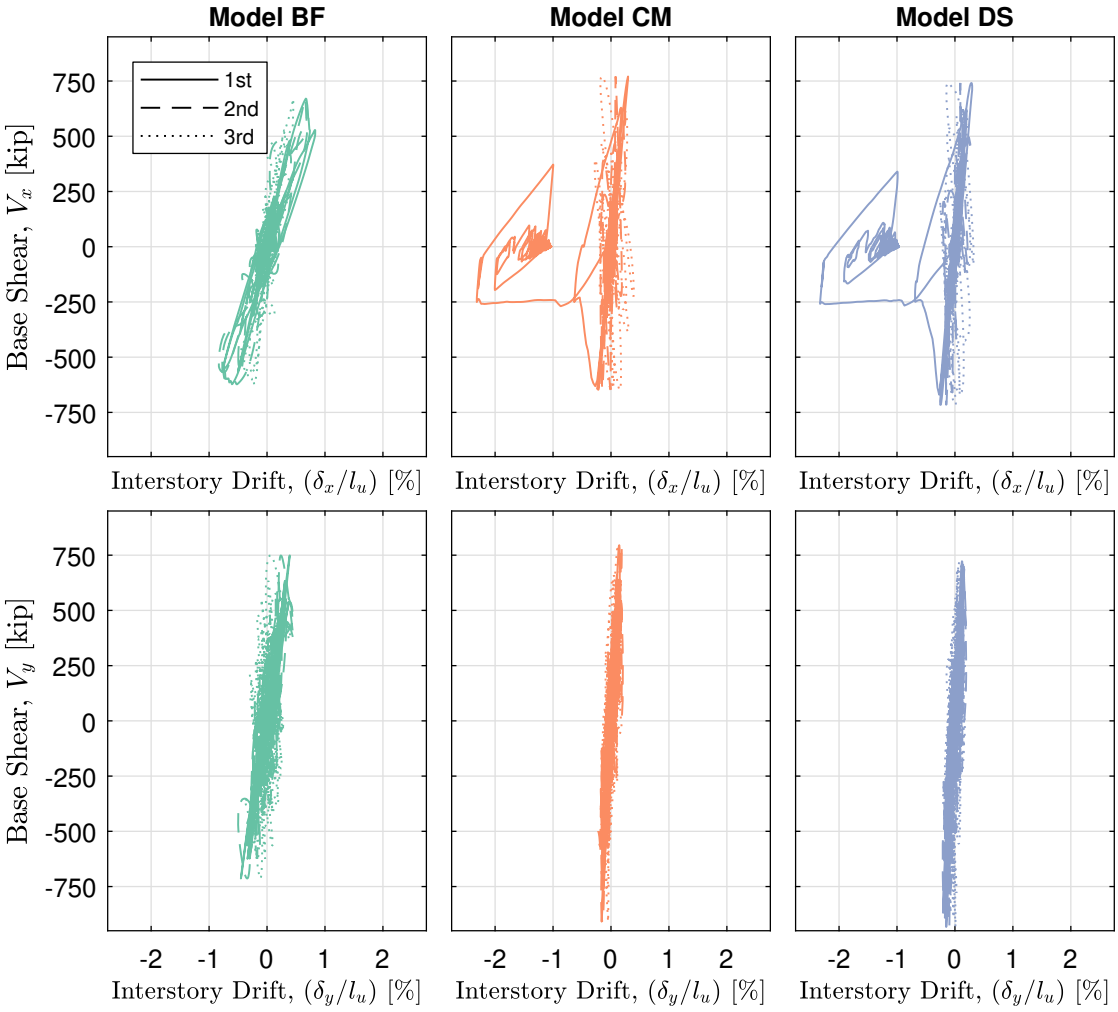

Figure 7.17: Base Shear vs. Interstory Drift

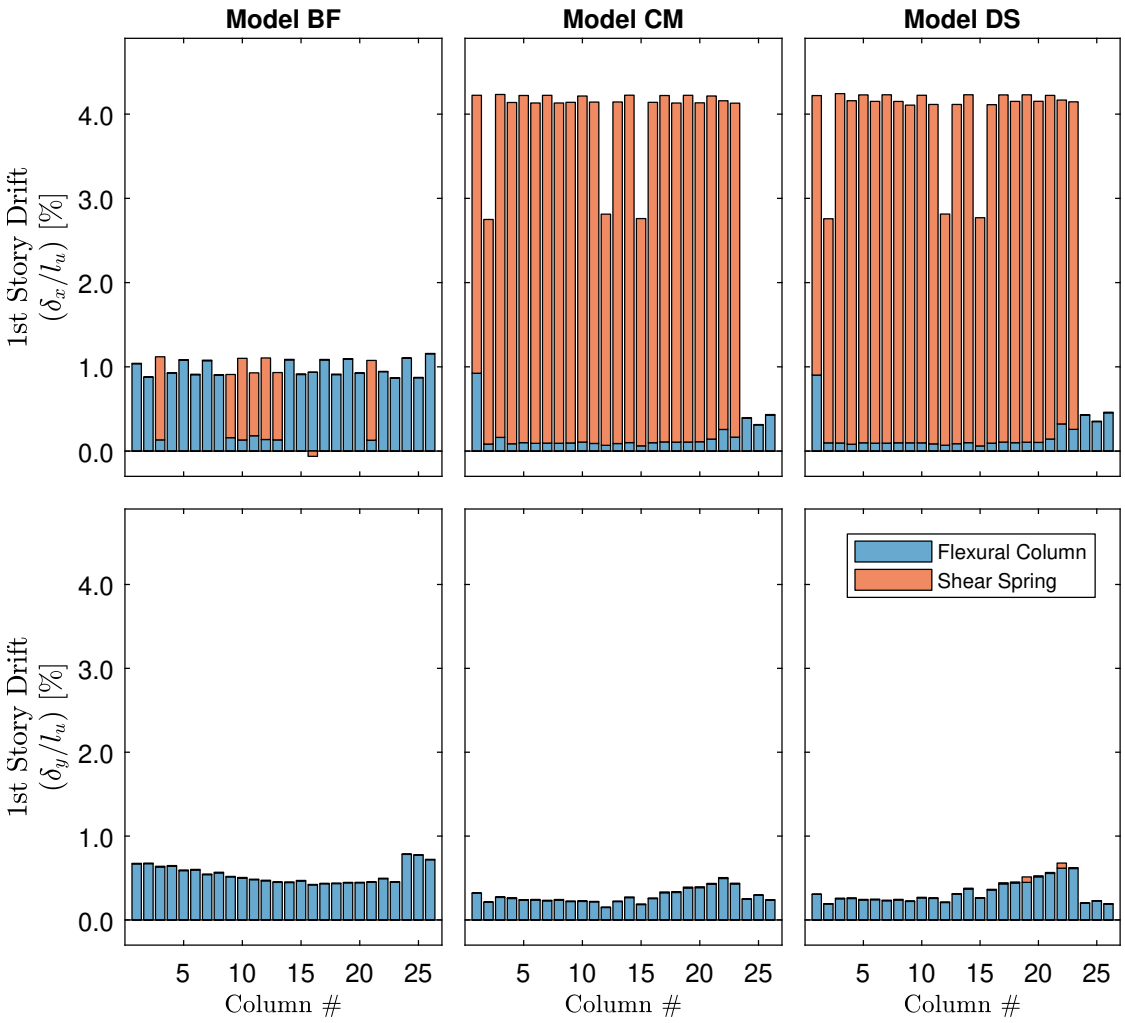

Figure 7.18: 1st Story Drift, Element Engagement

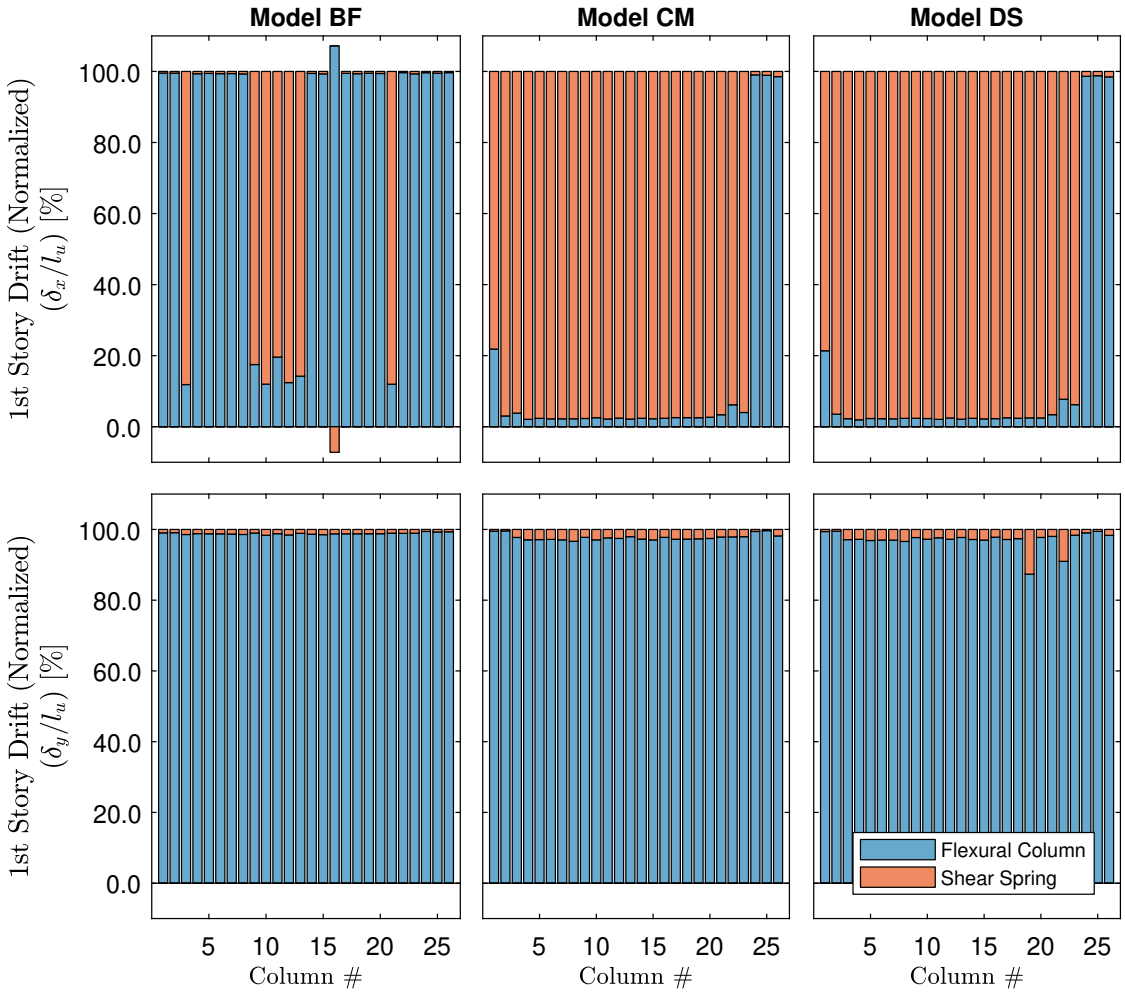

Figure 7.19: 1st Story Drift (Normalized), Element Engagement

the drift plots shown earlier. The springs in models CM and DS initiate shear failure and trigger loss of shear stiffness, accumulating large deformations in the X-direction. The bare-frame model does not feature shear spring engagement. While results for columns 5 and 7 in models CM and DS are not consistent with an undamaged observation, the modeled element behavior is as expected based on the input demands. Figures 7.21 and 7.22 revisits component story drift, but with time-history plots for both the flexural column and shear spring deformations. Models CM and DS show large, plastic deformation of the shear springs and minimal engagement by the flexural columns in the X-direction. Only the bare-frame model features Y-direction drift, and it is primarily flexural. Figures 7.23 and7.24 highlight column flexural behavior. Models CM and DS show little flexural engagement in either direction. The bare-frame model clearly engaged in flexure-controlled behavior. For the models that included provisions for the partial-height infill, shear spring engagement controlled the column behavior in simulation of a non-ductile shear failure.

In summary, the results of this evaluation indicate that the ASCE 41-17 nonlinear dynamic procedure (NPD) can accurately represent the damage mechanism experienced by the Nanhau District Office. Several conclusions based on the outcome of this evaluation are as follows:

- Most columns violate the ASCE 41-17 acceptance criteria in the long, X, building direction. This was the primary loading direction and is consistent with the damage state. This holds true to the results of the linear analysis.

- Few columns violate the ASCE 41-17 acceptance criteria in the short, Y, building direction. This is consistent with the observed damage. It also affirms the claim from the linear analysis that the violation of acceptance criteria in the Y-direction for the linear analysis was was the result of linear-elastic assumptions imposed on typically nonlinear behavior.

- The extent of predicted drift demand (and associated limiting rotational demand) for the models with masonry infill is a function of the modeling provisions to identify shear

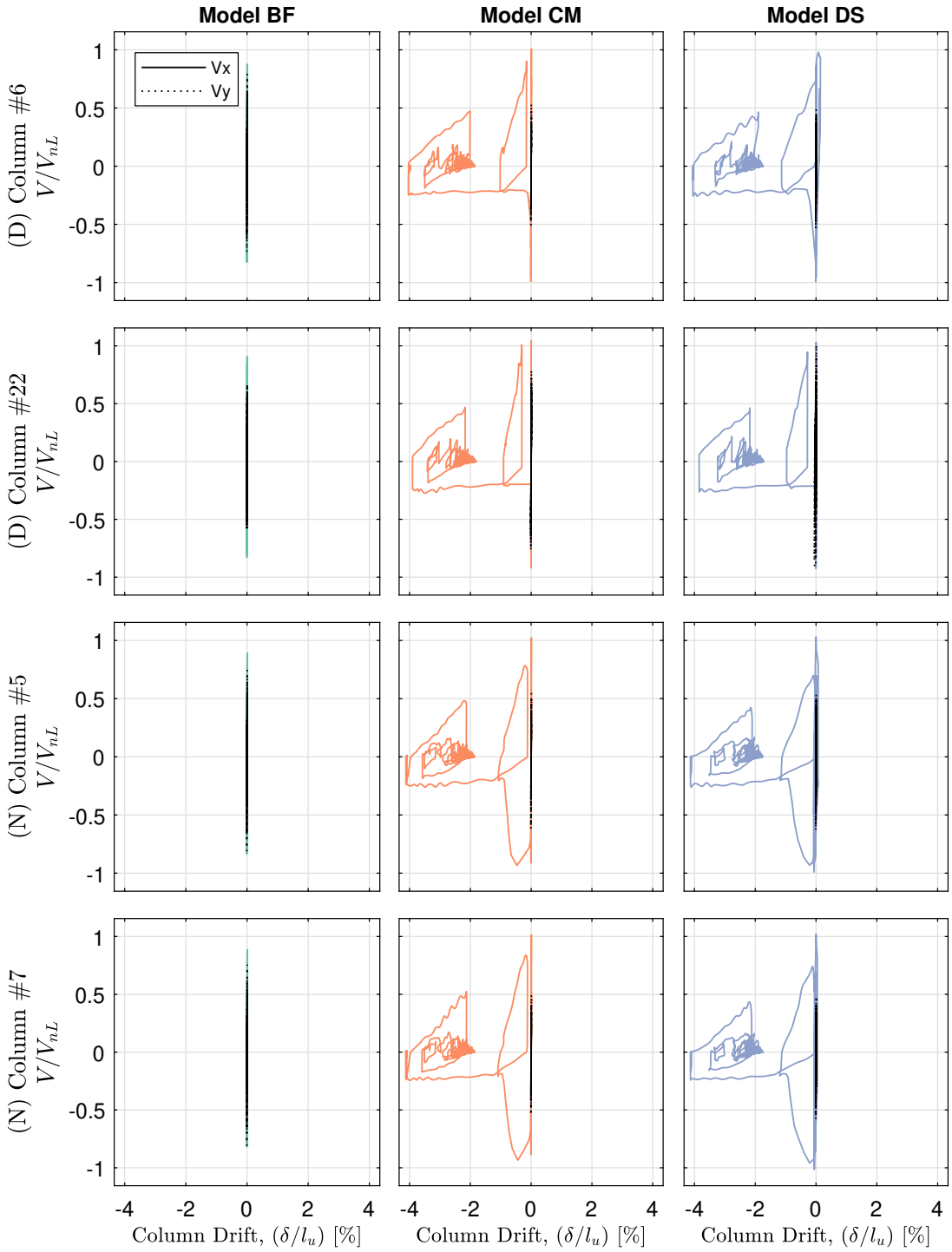

Figure 7.20: Hysteretic Response of Shear Spring above Column

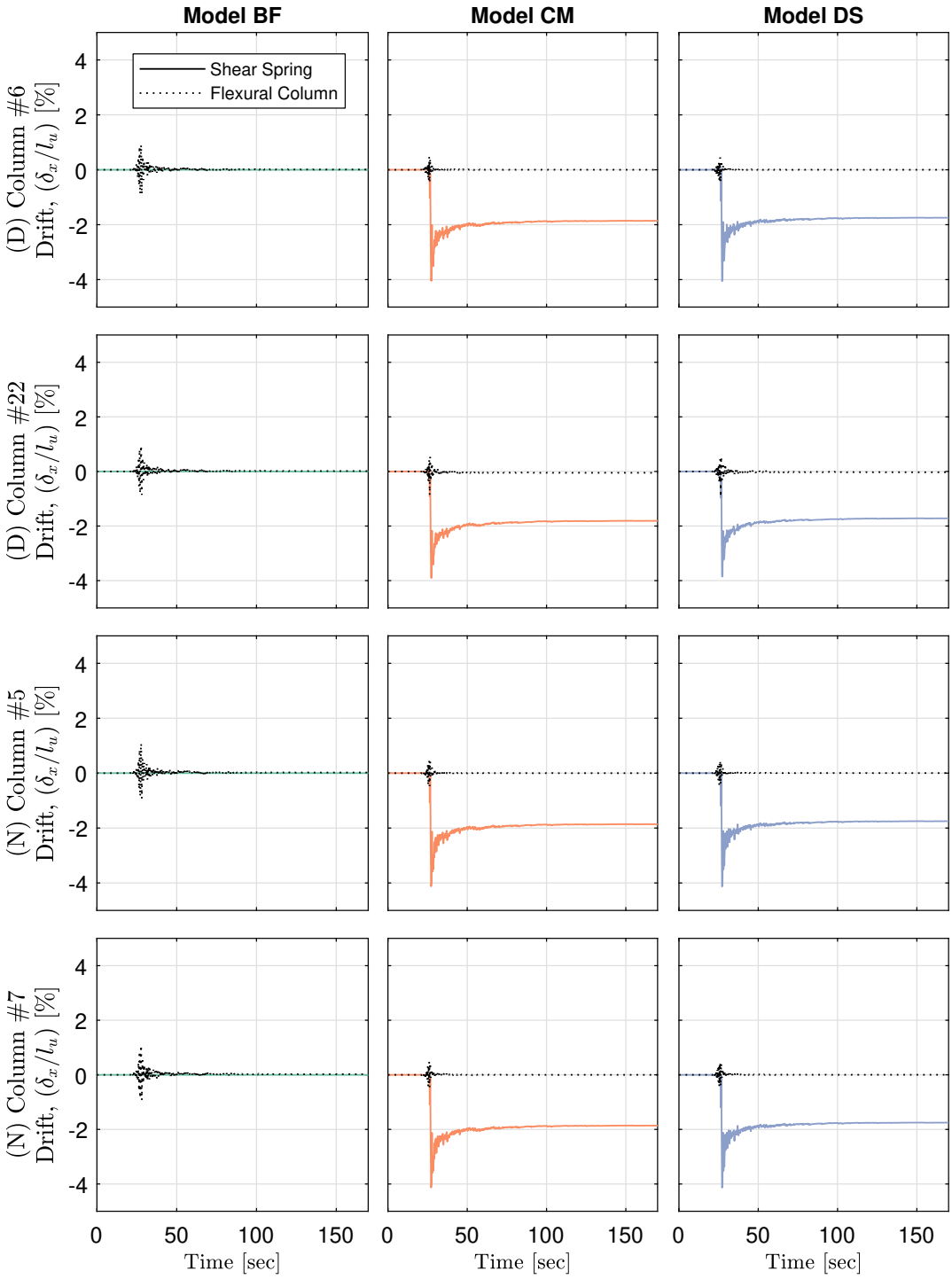

Figure 7.21: Column Drift Time-History

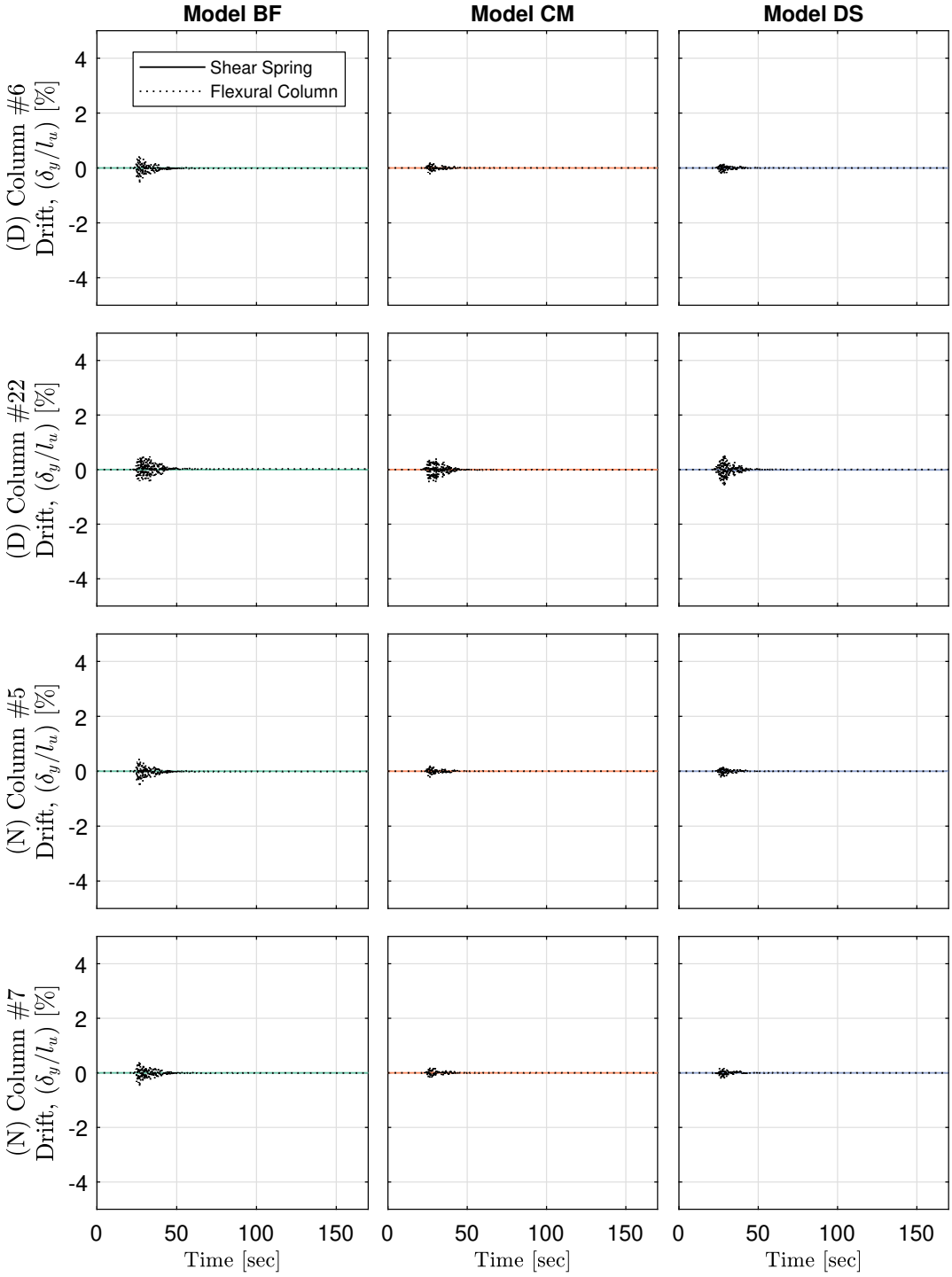

Figure 7.22: Column Drift Time-History

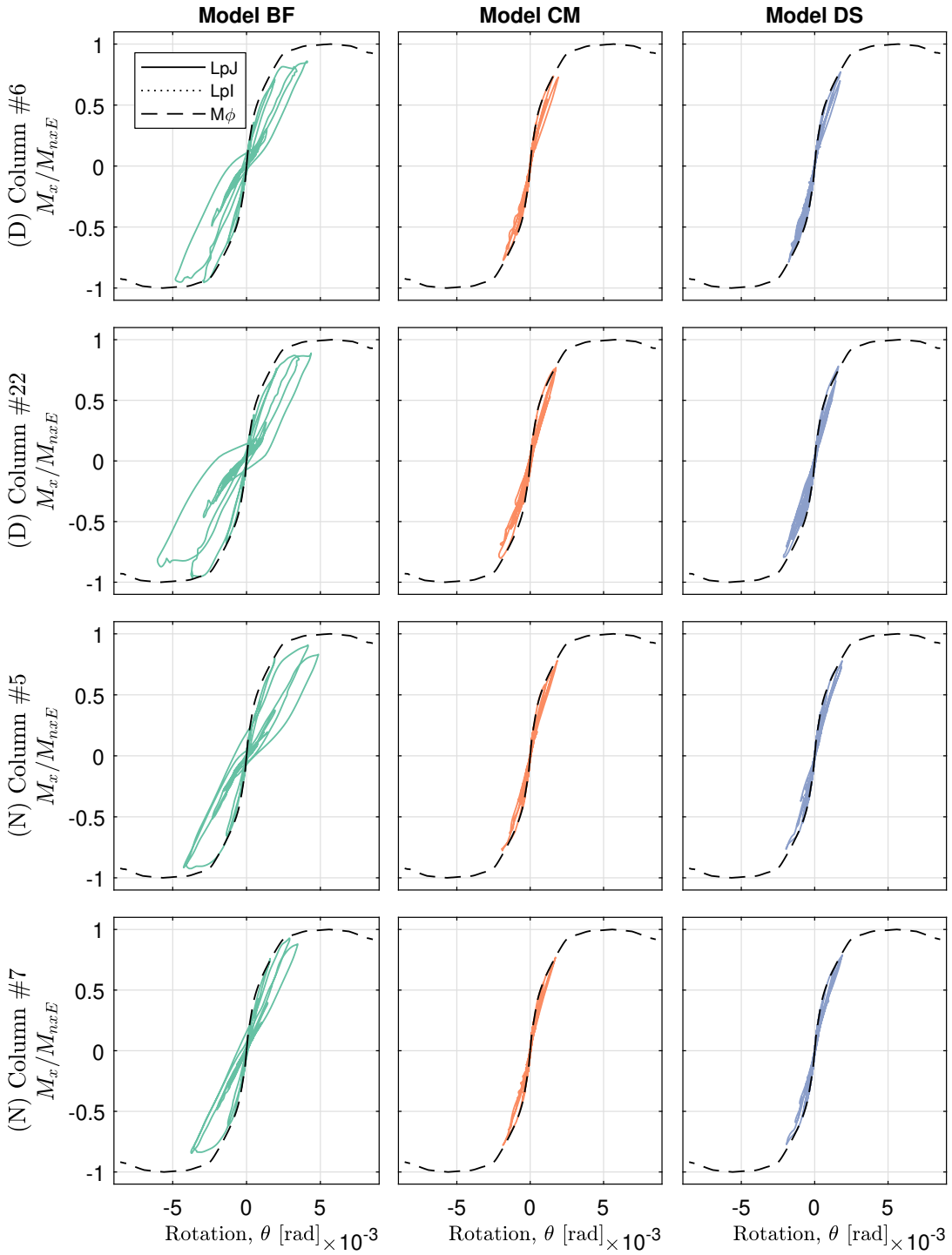

Figure 7.23: Column Fiber-Section Moment-Rotation Time-History

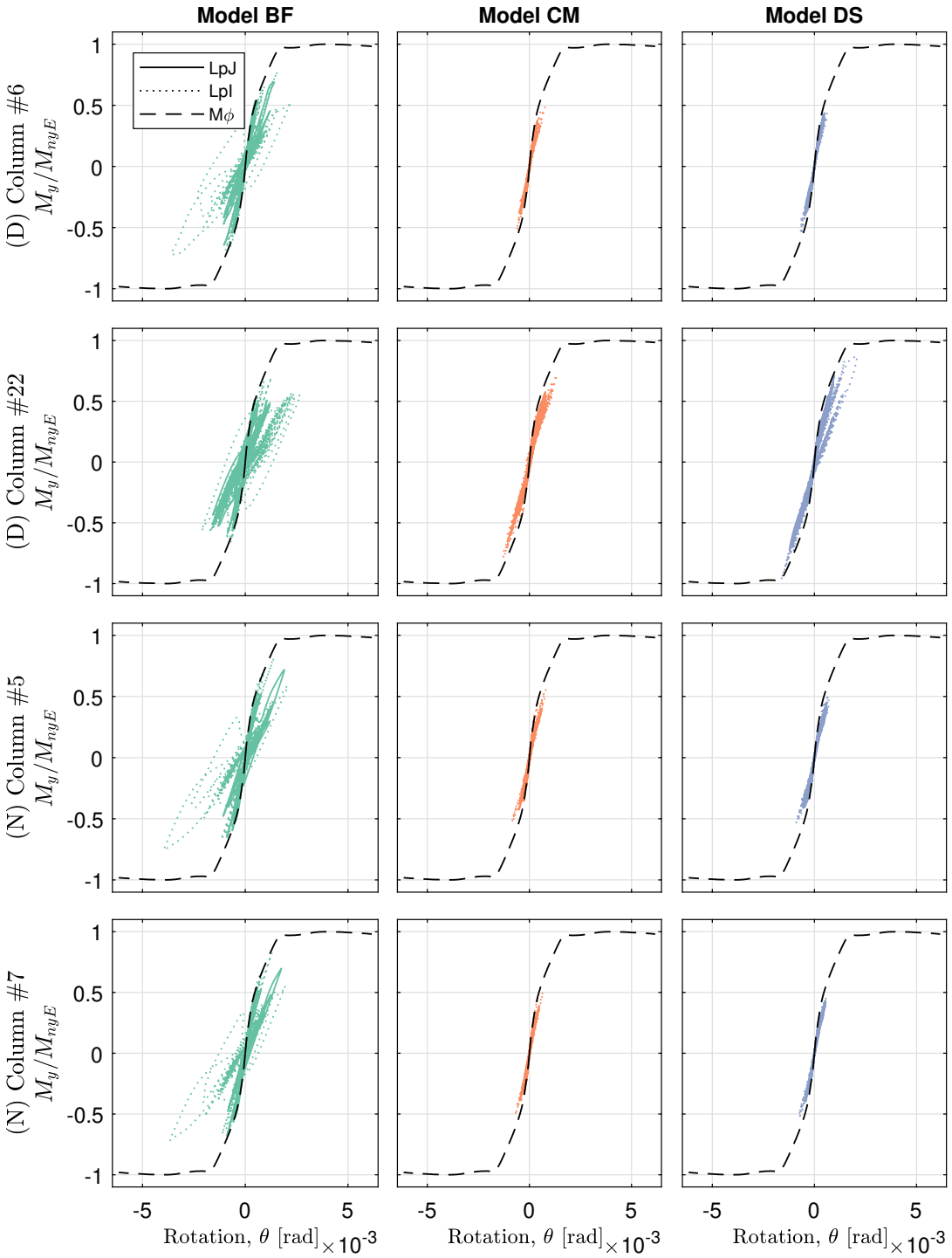

Figure 7.24: Column Fiber-Section Moment-Rotation Time-History

failure. The real structure did not show residual drifting, whereas the results of this study give predictions of large deformation.

- The method by which shear failure is included into the model has a substantial affect on both the global and local behavior. This study included simple, hysteretic models with preset backbone curves. Spring behavior was defined as stiff, linear-elastic prior to exceedance of a pre-calculated capacity. Once triggered, the shear springs proceeded to define the subsequent response of the column for the remainder of the motion. This approach could be improved by introducing an element through which to track flexure and shear interaction at each time step. This would allow for a flexible backbone and more calibrated response.

- The shear demand-to-capacity ratios appear to be capped around a value of 1.0. This is the result of having established shear springs that limited the development of shear demand once the capacity was exceeded. A reason why some columns show shear $DCR > 1.0$ is that the capacity, V_n of the shear springs had to be calculated in advance and thus does not account for axial load amplification.

- Use of column drift provides a more accurate assessment of deformation-controlled behavior given the use of horizontal shear springs that initiate shear failure. Engagement of the shear springs permits large deformations within the spring element with little deformation demand passed on to flexural columns. Substituting drift, δ/l_u, as the demand parameter yields criteria condition consistent with the behavior of the individual elements. This is most relevant for cases of shear-critical (and possible flexure-shear) columns.

- The modeling approaches for representing masonry infill (stiff offset elements and diagonal struts) show less variation than was observed in the linear analysis. This indicates that a simplistic, short-column offset approach may be sufficient in representing partial-height masonry infill for nonlinear analysis.

- The bare-frame (BF) model shows behavior that conforms with a flexure-controlled response. This model experienced little to no engagement of the shear springs and drift response captured primarily by the flexural columns. This was expected for having no consideration of partial-height infill (nor short-column effect) and thus continues the claim that negligence of the masonry infill can drastically affect predicted behavior.

Chapter 8

SUMMARY, CONCLUSIONS, AND RECOMMENDATIONS FOR FUTURE WORK

The objective of this study was to use reconnaissance data from the 2016 Meinong earthquake to assess the application and accuracy of current procedures for evaluating the earthquake vulnerability of existing structures. The work focused on older low to mid-rise RC buildings for which moment framing was the primary lateral force-resisting system. The work comprised two phases. The first phase considered 'screening' processes as outlined in the ASCE 41 standard as well as in the new ATC 78-7 report. These screening procedures are limited in depth, with the objective of quickly identifying potential vulnerabilities in the structural system based on simple calculation and common irregularities. ATC-78 [2018] employs a ranking system to compare estimates of collapse risk across multiple buildings. The second phase of this work focused on a single building from the reconnaissance data. ASCE-41 [2017] Tier 3 linear and nonlinear dynamic procedures were applied to the Nanhau District Office to evaluate the expected response and earthquake vulnerability. Analysis results were compared with building damage resulting from strong ground shaking due to the 2016 Meinong earthquake. The following sections summarize observations for each of the evaluation measures considered and propose improvements resulting from this work. It is acknowledged that there are opportunities for advancement beyond the scope of this work; thus, this chapter gives recommendations for future work.

8.1 Evaluation of ASCE 41 Tier 1

A review of reconnaissance data from the Meinong earthquake supported selection of sixteen buildings for application of an ASCE 41 Tier evaluation. For these buildings, on-site or near-

site earthquake data as well as data characterizing the extent of post-earthquake damage was available. This information was used to assess the ASCE 41 Tier 1 screening procedure. The combination of structural drawings, ground motion records, and post-earthquake observations provided a unique opportunity to assess the accuracy of the Tier 1 screening. Each building was evaluated using the standard checklists for RC moment frame structures (type C1). This approach proved to be a quick and relatively efficient method for surveying the various structures. However, for multiple structures, apparent contradictions between the compliance checks and the damage state of individual components were observed.

8.1.1 Summary of Strengths

- The Tier 1 evaluation identified columns as potentially vulnerable components, which was consistent with the observed damage.
- The following items were consistently identified as noncompliant on the standard checklists: column shear stress, strong-column-weak-beam, column-tie spacing, and joint reinforcing. Many of which are associated with non-ductile seismic performance.
- As is desirable for a preliminary investigation, basing decisions on quick checks and visible irregularities provides for fast and easy assessment across many structures. For all of the damaged buildings, the outcome of this evaluation indicates that the observed structural damage would be likely. This outcome motivates the need for further, more rigorous, investigation or the design of a retrofit measure.

8.1.2 Summary of Weaknesses

- Results indicate the evaluation procedure under-estimates column shear demand and over-estimates column shear strength for the case of shear failure or shear-controlled response. This was commonly identified for columns that exhibited post-earthquake diagonal cracking.

- The shear stress in columns calculation assumes that the base shear distributes up the height of the structure. In cases of soft-story mechanisms, all shear demand may be concentrated within a single story. Columns must then resist the plastic shear demand resulting from column hinging.

- For many buildings, column demand-capacity was predicted < 1.0 but damage consistent with shear failure or shear-controlled response was observed. Column shear strength equations employed in other codes and presented in the literature were found to produced demand-capacity ratios more consistent with observed damage.

8.1.3 Recommendations for Improvement

- Add a provision to consider plastic shear demand in cases of soft-story vulnerabilities and short-column effects. Calculate column shear strength per ASCE-41 [2014], but with parameter $k_{nl} = 0.70$, which is the lower bound within the specified range of 1.0 to 0.70. Calculations of shear demand-capacity using $k_{nl} = 0.70$ resulted > 1.0 across many of the damaged columns in many of the buildings. This is more consistent with the observed damage, and is a minor modification to the procedure as-written.

- Consider the impact of masonry infill as a stiffening component for underlying and adjacent framing members. This is especially pertinent in the case of partial-height infill for which ASCE 41 provides no guidance beyond the designation of a reduced column height.

- A strong-column-weak-beam (SCWB) moment ratio of 1.2 is not sufficient to inhibit a first-story mechanism. This is especially true in the case of partial-height infill where it is theorized that infill acts to stiffen the beam and affect the flexural response. This condition is not considered in the procedure as-written.

8.2 Evaluation of ATC 78-7

The ATC 78-7 procedure was conducted as a follow-up to the ASCE 41 Tier 1 evaluation. While both procedures are intended to provide an enhanced understanding of the system response to strong ground motion. To quantity seismic vulnerability, this new procedure links estimated building response to the most likely damage mechanism on the basis of plastic analysis. The ATC 78-7 assessment process was applied to the Nanhau District Office and the Xingfu Building; though, Xingfu fell outside the conditions for application of this methodology due to large torsional irregularities. This approach proved to be reasonably efficient at processing the two buildings, though longer than ASCE 41 Tier 1. The outcome of the procedure resulted in estimates of building performance that appear consistent with the magnitude of post-earthquake damage. However, the predicted damage mechanism for Nanhau, distributed beam yielding, differed observed damage mode, soft-story.

8.2.1 Summary of Strengths

- The ATC 78-7 procedure represents an advancement beyond the ASCE 41 Tier 1 screening as it considers plastic behavior and damage modes to improve assessment of collapse risk. It is, however, constrained to the 'collapse prevention' performance state.
- The step-wise organization and structural-system-specific chapters help direct the evaluation, such that, while more rigorous than the ASCE 41 Tier 1 procedure, the process remains relatively quick.
- The use of a building rating system enables prioritization of retrofit across a suite of evaluated structures. This is viewed as a significant strength in comparison with the ASCE standard.

8.2.2 Summary of Weaknesses

- The calculation of the effective building period, T_e, assumes that the lateral force-resisting system is sufficiently ductile to undergo stable softening (cracking, yielding, rotation, etc.)without strength loss out to the point of collapse initiation. This is not an appropriate assumption for systems vulnerable to brittle failure modes.

- The calculation of too long of an effective building period, T_e, when applied to a typical design response spectrum, results in a correspondingly small spectral acceleration. Under-estimating the input demand leads to artificially lower calculated deflections and an unconservative estimate of deformation demand-capacity and building performance.

8.2.3 Recommendations for Improvement

- For Nanhau, the method fails to predict a soft-story mechanism, resulting from column shear failure, and instead predicts a 'distributed beam yielding' mechanism. This issue could be addressed by reducing the calculated column shear strength, V_n, using the ASCE 41 equation and $k_{nl} = 0.70$. This is the same recommendation given for the Tier 1 evaluation.

- Revision to fully consider the impact of partial-height infill. While the provision requires consideration of partial-height infill as a reduction of column effective height, and thus an increased column shear demand for a soft-story mechanism, the procedure neglects the impact of infill masonry on the underlying beam stiffness and the additive stiffening to the global system. Increased stiffness would reduce, Te, and likely increase spectral acceleration and earthquake demand into the calculations of deformation demand-capacity.

8.3 Evaluation of ASCE 41 Tier 3 Linear Dynamic Procedure

The ASCE 41-17 Tier 3 linear dynamic procedure (LDP) was assessed by comparing the calculated acceptance criteria with observed, post-earthquake damage for the Nanhau District

Office. Dynamic loading was defined by bi-directional ground motion acceleration histories acquired from recording stations near the building site. Four linear models were developed: a bare-frame (BF) baseline model, and the bare-frame model plus modeled partial-height infill using three different approaches. For all models, linear time-history analyses were conducted and absolute maximum forcing demands were extracted for each component action. Several ground motion histories were considered to gauge the impact of uncertainty in demand on predicted response. Evaluation of analysis results focused on first-story columns, as this was where significant damage was observed. Demand-capacity ratios were calculated for the ASCE 41-17 methodology considering both deformation-controlled (flexure) and force-controlled (shear) component actions. The results were then compared with the observed damage to assess the accuracy with which the LDP 'predicted' the known damage state.

8.3.1 Summary of Strengths

- The LDP predicted the damage mechanism observed for the Nanhau District Office. For most first-story columns, DCRs exceeded 1.0 in 'violation' of the ASCE 41-17 acceptance criteria and indicated column 'failure.'
- Predicted damage was primarily aligned with the long, X, building direction, which is consistent with the observed damage state.
- The different modeling approaches for the masonry infill yielded nominally identical outcomes relative to the acceptance criteria. Different modeled resulted in different DCR values, though the DCRs for most first-story columns exceeding 1.0. As such, the ASCE 41-17 approach to simply insert a short-column effect at locations of partial-height masonry infill is sufficient for a LDP.

8.3.2 Summary of Weaknesses

- Linear analysis predicted some damage in the short, Y, building direction. This is not consistent with the observed damage. It is assumed to be an outset of a linear-elastic

assumption imposed on nonlinear behavior. Nonlinear analysis may limit the extent of Y-direction behavior through X-direction deterioration.

- The diagonal strut approach with masonry material properties is a good method, but requires use of nonlinear analysis in SAP2000 to create the a compression-only truss condition.

8.3.3 Recommendations for Improvement

- Reevaluate the use of different material properties (expected vs. nominal) for deformation-controlled and force-controlled actions for the same component. Currently ASCE 41-17 defines different material strengths based on this action designation, even within the same component. As this study considered flexure to be deformation-controlled and shear to be force-controlled, two different material strengths were used to describe the same column. This is confusing; a preferred approach would be to introduce a strength reduction factor for less-ductile or less-desirable response modes.

- Clarify the definition of the shear equation parameter k_{nl} in ASCE 41-17 Equation 10-3. This variable is described as a shear strength reduction factor based on expected deformation ductility. Clarify 1) that this is based on flexural deformation and 2) that $k_{nl} < 1.0$ should be used even if the DCR for flexure < 1.0.

8.4 Evaluation of ASCE 41 Tier 3 Nonlinear Dynamic Procedure

The ASCE 41-17 Tier 3 nonlinear dynamic procedure (NDP) was used to assess the Nanhau District Office beyond constraints of the previous linear analysis. Nonlinear analysis employed use of open-source software OpenSees; this software enables script-based model development. Dynamic loading was defined by bi-directional ground motion acceleration histories acquired from recording stations near the building site. Three models were developed: a bare-frame (BF) baseline model, and the bare-frame model plus modeled partial-height infill using two different approaches. These models employed similar base assumptions to

their linear counterparts. All columns were defined using beam-column elements to simulate inelastic flexural response over specified plastic hinge regions. Fiber-type sections permitted moment-axial interaction to dynamically recalculate the flexural capacity. Hysteretic shear springs were attached at the top of all columns to define the column shear response. These column modeling decisions fell outside the scope of ASCE 41-17 provisions: no allowance was thus made to modify the flexural behavior based on shear-vulnerable conditions, nor was flexural behavior defined using the proscribed moment-rotation hinge model. Evaluation of analysis results focused on first-story columns, as this was where significant damage was observed. Analysis output was evaluated using ASCE 41-17 acceptance criteria calculated across the entire time-history, with conclusions based on the maximum DCR at any time step considering both deformation-controlled (flexure) and force-controlled (shear) component actions. The results were then compared with the observed damage to assess the accuracy with which the NDP 'predicted' the known damage state. Further inquiry was made into assessing model behavior using recorded results outside the scope of the ASCE 41-17 methodology.

8.4.1 Summary of Strengths

- The NDP predicted the location of observed damage as well as the column shear damage/failure mechanism for the Nanhau District Office. Under collapse prevention (CP) performance state, most columns violate the ASCE 41-17 acceptance criteria in the long, X, building direction, and only a few violate in the short, Y, building direction. This is consistent with the observed damage.

- A reduction in the number of columns that were predicted to violate the acceptance criteria in the Y-direction supports the claim that the linear analysis results are artificially skewed by the assumption of of linear-elastic response.

- Substituting column drift, δ/l_u, in place of column plastic rotation, θ, provided more accurate assessment of hinge rotation-based acceptance criteria for the case of defining column shear response with a hysteretic spring-type model.

- The modeling approaches for representing masonry infill (stiff offset elements and diagonal struts) yield results that are nominally identical. This indicates that a simple, short-column offset approach may be sufficient in representing partial-height masonry infill for nonlinear analysis.

8.4.2 Summary of Weaknesses

- The use of beam-column elements with concentrated inelasticity within hinge regions and fiber-type sections represent modeling decisions outside of the scope of the ASCE 41 standard. These decisions made it unnecessary to calculate moment-rotation models and also no reduction of flexural capacity was defined to address shear-critical behavior. Accordingly, these guidelines within ASCE 41 were not replicated in the evaluation.

- The spring models developed to define the column shear response produced too controlling of an impact on the model response. The purpose of these models was to identify the point of shear failure and trigger degrading shear strength. However, once triggered, all deformation localized to the column shear springs. This resulted in predictions of large first-story drifts of which no residual drift was noticed at the Nanhau District Office.

- The engagement of the shear springs locked large deformation within the spring elements. This resulted in limited deformation demand being passed into the flexural columns. Thus, ASCE 41-17 rotation-based acceptance criteria did not predict column damage as per the site observations.

8.4.3 Recommendations for Improvement

- Improvements or guidelines are recommended for inclusion of a shear-failure indicator into the nonlinear model. The selected use of a simple, hysteretic model for which shear failure triggered a degrading response shifted all deformation demand out of the flexure-controlled column element and into the column shear spring. This produced

predictions of large first-story drift that were not observed in the post-earthquake reconnaissance. This approach could be improved by introducing an improved element in which flexure and shear interaction is simulated and for which deformation capacity and the role of strength loss are accurately simulated.

- ASCE 41-17 may want to consider an option for deformation-demand to be evaluated using total column drift (flexure + shear deformations) rather than column hinge rotation. The use of column hinge rotation became a poor indicator for cases in which all lateral deformation localized in the column shear springs and minimal rotation demand was read by the column elements.

- The typical ASCE 41-17 model employs moment-rotation hinges and does not simulate the impact of variable axial load on the column flexural capacity. Rather, the methodology defines a moment-rotation hinge response envelope to be developed in advance of the numerical analysis using column-axial load due to gravity load; this ignores the increase in flexural capacity, and shear demand, associated with axial load amplification. Fiber-type section models could be used to simulate axial-moment interactions. However, this would require additional model development to simulate reduced flexural deformation capacity due to high shear demand, as is currently the method in ASCE 41-17.

8.5 Recommendations for Future Work

The following items were not included in this study, but are recommended as a continuation of the work conducted or to advance the linear and nonlinear modeling approaches, as described in earlier chapters:

- Further the ASCE-41 [2017] Tier 3 evaluation to consider the Xingfu Building, which collapsed during the Meinong earthquake. This requires, among other things, identification of the likely collapse mechanism as well as sourcing more representative ground motion records through collaboration with a geotechnical engineer, as was done for the

Nanhau District Office.

- Advance the nonlinear modeling to include use of the OpenSees *Limit State Material* model developed by Elwood [2004]. This model works in combination with column elements that employ fiber-type section models to enable simulation of onset of strength loss due to reduced shear capacity at large flexuralductility demands. Thus, the model enables simulation of the impact of axial and shear load on flexual response. Modification of the Elwood [2004] implementation in OpenSees is required to reflect the ASCE-41 [2017] definition of column shear capacity.

- Compare the results of this study with results generated using the lumped plasticity moment-rotation (i.e. columns without fiber-type sections or fiber-hinge models) models that are the basis of ASCE-41 [2017].

- Investigate and model the known additional construction at the Nanhau District Office for which no information was provided in the structural plans. This includes a new structure localed in the north-west recess of the building and an exterior stair located at plan north of the building. This would better reflect the state of the structure at time of the earthquake, though response of the model is likely to change with respect to these new features.

REFERENCES

ACI-318 (2014). *Building Code Requirements for Structural Concrete and Commentary*. American Concrete Institute, aci 318-14 edition.

ASCE-31 (2004). *Seismic Evaluation of Existing Buildings*. American Society of Civil Engineers, asce/sei 31-03 edition.

ASCE-41 (2014). *Seismic Evaluation and Retrofit of Existing Buildings*. American Society of Civil Engineers, asce/sei 41-13 edition.

ASCE-41 (2017). *Seismic Evaluation and Retrofit of Existing Buildings*. American Society of Civil Engineers, asce/sei 41-17 edition.

ASCE-7 (2013). *Minimum Design Loads for Buildings and Other Structures*. American Society of Civil Engineers, asce/sei 7-10 edition.

ATC-78 (2018). "Seismic evaluation of older concrete frame, frame-wall, and bearing wall buildings for collapse potential." *Report No. 07*, The Applied Technology Council, Redwood City, CA. Prepared for: Federal Emergency Management Agency.

Burton, H. and Deierlein, G. (2014). "Simulation of seismic collapse in nonductile reinforced concrete frame buildings with masonry infills." *Journal of Structural Engineering*, 140.

Computers and Structures, Inc. (2018). *SAP2000 v20*. Walnut Creek, CA. http://www.csiamerica.com/products/sap2000.

Elwood, K. and P. Moehle, J. (2005). "Drift capacity of reinforced concrete columns with light transverse reinforcement." *Earthquake Spectra - EARTHQ SPECTRA*, 21.

Elwood, K. J. (2004). "Modelling failures in existing reinforced concrete columns." *Canadian Journal of Civil Engineering*, 31(5), 846–859.

FEMA-356 (2000). *Prestandard and Commentary for the Seismic Rehabilitation of Buildings*. Federal Emergency Management Agency, Washington, D.C.

Furtado, A., Rodrigues, H., and Arêde, A. (2015). "Numerical modelling of rc columns subjected to biaxial horizontal loading and variable axial load." *American Journal of Civil Engineering and Architecture*, 3.

Galeotti, F. and Lehman, D. E. (2017). "Assessment of the asce 41-13 tier 1 evaluation." *Report No. 01*, The University of Washington, Seattle, WA.

Ghannoum, W. and Matamoros, A. (2014). "Nonlinear modeling parameters and acceptance criteria for concrete columns." *ACI Special Publication 297, Seismic Assessment of Existing Reinforced Concrete Buildings*, 1–24.

Heintz, Jon A., e. a. (2017). "Recommended modeling parameters and acceptance criteria for nonlinear analysis in support of seismic evaluation, retrofit, and design." *Report No. NIST GCR 17-917-45*, The Applied Technology Council, Redwood City, CA. Prepared for: U.S. Department of Commerce Engineering Laboratory National Institute of Standards and Technology (NIST).

Hua, J., Eberhard, M. O., Lowes, L. N., and Gu, X. (2018). "Modes, mechanisms and likelihood of seismic shear failure in rectangular reinforced concrete columns.

McKenna, F., L. Fenves, G., and Scott, M. (2004). *OpenSees: Open System for Earthquake Engineering Simulation*. Pacific Earthquake Engineering Research Center, University of California, Berkeley. http://opensees.berkeley.edu/wiki/index.php/Main_Page.

Mohammad Noh, N., Liberatore, L., Mollaioli, F., and Tesfamariam, S. (2017). "Modelling of masonry infilled rc frames subjected to cyclic loads: State of the art review and modelling with opensees." *Engineering Structures*, 150, 599–621.

Pacific Earthquake Engineering Research Center (2012). *OpenSees Wiki*. University of California, Berkeley. http://opensees.berkeley.edu.

Scott, M. and L. Fenves, G. (2006). "Plastic hinge integration methods for force-based beam–column elements." *Journal of Structural Engineering-ASCE - J STRUCT ENG-ASCE*, 132.

Tarque, N., Candido, L., Camata, G., and Spacone, E. (2015). "Masonry infilled frame structures: State-of-the-art review of numerical modelling." *Earthquakes and Structures*, 8, 733–759.

TMS-402 (2011). *Building Code Requirements and Specification for Masonry Structures*. The Masonry Society, tms 402/602-11 edition.

U.S. Geological Survey (2018). *Earthquake Hazards Program*. Reston, VA. https://earthquake.usgs.gov/earthquakes/eventpage/us20004y6h/executive.